

UNIVERSITÄTSKLINIKUM HAMBURG-EPPENDORF

Zentrum für Molekulare Neurobiologie Hamburg (ZMNH),

Prof. Dr. Matthias Kneussel

**Characterization of Interactions between the Neural Cell Adhesion
Molecule L1 and Nuclear Proteins**

Dissertation

zur Erlangung des PhD

an der Medizinischen Fakultät der Universität Hamburg

vorgelegt von:

María Girbés Mínguez/ aus Valencia, Spanien

Hamburg 2020

Angenommen von der

Medizinischen Fakultät der Universität Hamburg am: 17.08.2020

Veröffentlicht mit Genehmigung der

Medizinischen Fakultät der Universität Hamburg.

Prüfungsausschuss, der/die Vorsitzende: Prof. Dr Dr. Melitta Schachner

Prüfungsausschuss, zweite/r Gutachter/in: Prof. Dr. Udo Bartsch

TABLE OF CONTENTS

1. Introduction	9
1. 1. Cell adhesion molecules.....	9
1. 2. The cell adhesion molecule L1	10
1. 2. 1. Proteolytic processing of L1.....	12
1. 2. 2. Nuclear L1 fragments.....	12
1. 2. 3. Nuclear L1 binding partners.....	13
1. 3. DBHS proteins: SFPO, NonO, PSCP1.....	15
1. 4. MeCP2 and Rett syndrome	16
1. 5. Aim	19
2. Materials and Methods	21
2. 1. Animals.....	21
2. 1. 1. Generation of L1-deficient mice	21
2. 1. 2. Generation mutated L1 mice (L1 ^{RA})	21
2. 2. Suppliers of chemicals, kits, reagents, and laboratory equipment.....	22
2. 3. Antibodies	23
2. 3. 1. Primary antibodies	23
2. 3. 2. Secondary antibodies.....	24
2. 4. Bacteria	25
2. 5. Bacterial vectors.....	25
2. 6. Cell lines	26
2. 7. Commercial peptides and recombinant proteins	26
2. 8. Oligonucleotides	26
2. 9. Viruses (AAV: Adeno-associated virus 1)	27
2. 10. Buffers, solutions, chemicals and media.	28
2. 10. 1. Buffers, solutions and chemicals used for agarose gel electrophoresis.	28
2. 10. 2. Buffers, solutions and chemicals used for protein production.....	28
2. 10. 3. Media and chemicals used for bacterial cultures.	29
2. 10. 4. Buffers, solutions and media used in cell culture.	30
2. 10. 5. Reagents and buffers used for SDS-PAGE and WB analyses.....	32
2. 10. 6. Reagents and buffers used for extraction of nuclear proteins.....	34
2. 10. 7. Solutions and reagents used for immunostainings.....	35
2. 10. 8. Buffers, solutions and chemicals used for ELISA.....	36
2. 10. 9. Buffers, solutions and chemicals used during AAV injection of mice.....	37
2. 11. Molecular biology methods and cloning strategies	38

2. 11. 1.	Reverse transcription	38
2. 11. 2.	Polymerase chain reaction (PCR)	38
2. 11. 3.	PCR product clean-up.....	39
2. 11. 4.	Agarose gel electrophoresis.....	39
2. 11. 5.	In-Fusion cloning method and Primer design	40
2. 11. 6.	LIC Cloning and basis of Primer design	41
2. 11. 7.	Transformation of E. coli and plasmid isolation	42
2. 11. 8.	Determination of DNA concentration and purity	43
2. 11. 9.	DNA sequencing.....	43
2. 11. 10.	Expression and purification of recombinant proteins	43
2. 11. 11.	In vitro cell-free protein synthesis	45
2. 11. 12.	Genotyping of mice.....	45
2. 11. 13.	Design of shRNAs	47
2. 12.	Biochemical methods.....	49
2. 12. 1.	Preparation of brain and cerebellar extracts and cell lysates	49
2. 12. 2.	Determination of protein concentration	49
2. 12. 3.	SDS – Page gel electrophoresis	49
2. 12. 4.	Coomassie staining of polyacrylamide gels	50
2. 12. 5.	Western Blot Analysis	50
2. 12. 6.	Quantification of relative protein concentrations.....	50
2. 12. 7.	ELISA.....	51
2. 12. 8.	Label-free binding assay (BIND).....	51
2. 12. 9.	Co-immunoprecipitation using nuclear protein extracts from mouse brains	52
2. 12. 10.	Co-immunoprecipitation using in vitro expressed proteins	52
2. 12. 11.	RNA isolation from cell lysates.....	53
2. 13.	Cell culture methods and assays.....	54
2. 13. 1.	Preparation of coverslips	54
2. 13. 2.	Culture of mouse primary cerebellar granule cells.....	54
2. 13. 3.	Culture of mouse primary cortical neurons.....	55
2. 13. 4.	Culture and differentiation of mouse neural stem cells.....	55
2. 13. 5.	Stimulation of L1-signalling.....	56
2. 13. 6.	Cell transduction using AAVs	56
2. 13. 7.	Neurite outgrowth assay.....	57
2. 14.	Immunostainings and histology.....	57
2. 14. 1.	Immunocytochemistry	57
2. 14. 2.	Perfusion of the mouse brain	57

2. 14. 3.	Immunohistochemistry	58
2. 14. 4.	Proximity ligation assay	59
2. 14. 5.	Confocal microscopy	59
2. 14. 6.	Analysis of PLA signal	60
2. 14. 7.	Analysis of co-localization	61
2. 15.	Transduction in vivo using AAVs	62
2. 15. 1.	Intracerebroventricular injection of perinatal mice	62
2. 15. 2.	Direct cerebellar cortical injection of perinatal mice	62
2. 16.	Statistical analysis	63
3.	Results.....	65
3. 1.	interaction between L1 and the DBHS proteins NonO, SFPQ and PSCP1.....	65
3. 1. 1.	L1-ICD directly binds to NonO and SFPQ, but not to PSCP1	65
3. 1. 2.	L1 and the DBHS proteins are found in close proximity in cerebellar granule cells	66
3. 1. 3.	SFPQ and NonO interact with L1 in the cellular context, and these interactions are enhanced by stimulation of L1 signalling.....	68
3. 2.	Interaction between L1 and MeCP2	72
3. 2. 1.	MeCP2 directly binds to L1 intracellular domain.....	72
3. 2. 2.	MeCP2 binds to the L1 fragments L1-70 and L1-30.....	75
3. 2. 3.	L1 and MeCP2 are in close proximity in neural cells and tissue	78
3. 2. 4.	L1 - MeCP2 interaction is enhanced after stimulation of L1 signalling.....	79
3. 2. 5.	L1 and MeCP2 co-localize in the mouse hippocampus.....	80
3. 2. 6.	L1 and MeCP2 co-localize in the cytoplasm of mouse Neural Stem Cells	82
3. 2. 7.	MeCP2 regulates the production of L1 fragments via up-regulation of Myelin Basic Protein in the mouse cortex and cerebellum	84
3. 2. 8.	MeCP2 knocked-down cerebellar granule cells show longer neurites.....	92
3. 2. 9.	MeCP2 regulates neurite outgrowth in cerebellar neurons via Myelin Basic Protein	94
3. 2. 10.	MeCP2 dosage alters soma size of cerebellar granule cells	96
4.	Discussion.....	99
4. 1.	L1 binds to the DBHS proteins NonO and SFPQ, but not to PSCP1	99
4. 2.	Narrowing down binding sites in L1 and NonO/SFPQ that mediate their interactions.....	101
4. 3.	L1 binds to MeCP2 via its intracellular domain	103
4. 4.	MeCP2 binds to the L1 fragments L1-70 and L1-30.....	103
4. 5.	L1 binding to MeCP2 is enhanced after stimulation of L1-signalling.....	104
4. 6.	L1-MeCP2 interaction increases during neuronal differentiation	104
4. 7.	MeCP2 influences the generation of L1-70	108
4. 8.	MeCP2 expression influences L1-dependent neurite outgrowth.....	109

4. 9.	Neuronal morphology and MeCP2	110
4. 10.	L1-MeCP2 interaction: implications for neurological disorders	111
4. 11.	L1 and its nuclear binding partners: relationships and gene regulatory functions	113
4. 12.	Conclusions	116
5.	Summary/ Zusammenfassung	117
6.	Abbreviations	121
7.	Bibliography	124
8.	Acknowledgements	139
9.	Curriculum Vitae	141
10.	Appendix: vector maps	142
11.	Eidesstattliche Erklärung	148

1. INTRODUCTION

1. 1. CELL ADHESION MOLECULES

During the development of organisms, the processes of cell proliferation, migration and differentiation are important in order to achieve the formation of complex structures like tissues and organs. These processes are modulated by the interaction between cells, and between cells and their microenvironment. Cell adhesion molecules (CAMs) are mediators of these interactions, being very important during development and for the maintenance of healthy tissues in mature organisms (Wai Wong et al., 2012).

CAMs interact with each other (homophilic interactions) and with other molecules (heterophilic interactions), within one cell (cis interactions), or on neighbouring cells or the extracellular matrix (trans interactions), to affect their position and interactions with other cells, resulting in contact-mediated or chemical attraction or repulsion affecting neuronal migration, axon guidance and fasciculation (Maness & Schachner, 2007). CAMs are divided into four superfamilies: immunoglobulin superfamily of cell adhesion molecules (IgCAMs), cadherins, integrins, and the superfamily of C-type lectin-like domain proteins (CTLDs). IgCAMs, cadherins and integrins are involved in neural processes, while CTLDs have important immunological functions. The L1 subfamily within the IgCAMs, depicted in Figure 1.1, includes L1, CHL1 (close homolog of L1, also known as CALL), neurofascin and NrCAM (Maness & Schachner, 2007).

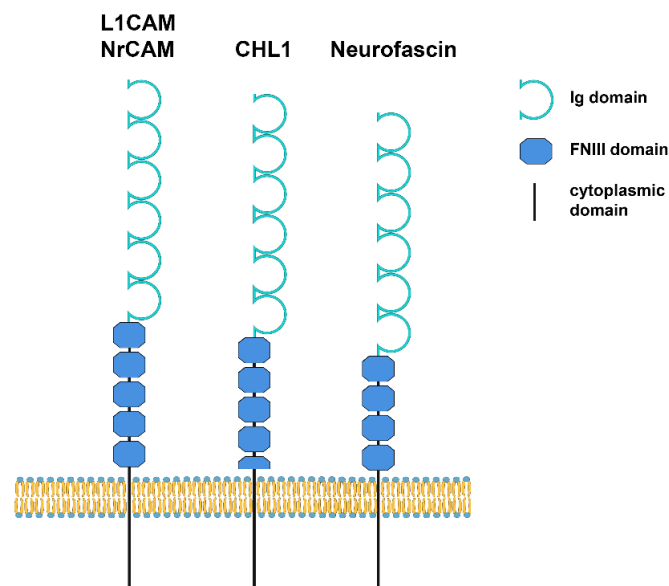


Figure 1. 1. L1 family of cell adhesion molecules. *Ig domain: Immunoglobulin like domain, FNIII domain: Fibronectin type III domain. Original figure.*

1. 2. THE CELL ADHESION MOLECULE L1

The cell adhesion molecule L1 (L1) is considered a key player in the development of the nervous system since its discovery in 1984 (Rathjen & Schachner, 1984). During development, L1 is expressed in postmitotic neurons, oligodendrocytes, and Schwann cells, and during adulthood L1 is found on neurons in the brain. It is also present in other tissues, like the endothelium, and the urinary and reproductive tracts (Samatov et al., 2016).

L1 is comprised of an extracellular region, which contains six immunoglobulin-like domains and five fibronectin type III repeats, a transmembrane domain, and a highly conserved intracellular domain of ~110 residues (Maness & Schachner, 2007). L1 can bind homophilically to other L1 molecules, or heterophilically to other neural cell adhesion molecules, such as integrins, CD24, neurocan and neuophilin (Brümmendorf et al., 1998). The intracellular domain contains the sequence FIGQ/AY, which mediates the binding to ankyrin or to other cytoskeletal proteins like actin, spectrin, and ezrin-radixin-moesin (ERM) (Dickson et al., 2002), and thereby enables the coupling to the subcortical actin cytoskeleton (Bennett & Baines, 2001). L1 performs cis binding in the plasma membrane to other L1 molecules, or to neuropilin-1 (NP-1), which is a component of the semaphorin 3A (Sema3A) receptor complex, through the sequence FASNKL located in the first immunoglobulin-like domain (Castellani, 2002). The binding of L1 to neuropilin-1 affects the responsiveness of growth cones to Sema3A (Castellani, 2002; Maness & Schachner, 2007; Wei & Ryu, 2012). In addition, L1 can bind in trans to shedded L1 fragments (Holm et al., 1995), or to full-length L1 influencing axon fasciculation, branching (Schäfer & Frotscher, 2012), extension, and guidance (Azemi et al., 2011; Lagenaur & Lemmon, 1987). In addition, L1 can bind to other cell adhesion molecules such as axonin-1 and contactin, affecting neurite outgrowth (Kuhn et al., 1991; Lieberoth et al., 2009).

Alternative splicing of the neuronal isoform of L1, containing exons 2 and 27, includes the sequence 'RSLE' in the intracellular domain, and enables L1 endocytosis via the AP2-clathrin adaptor (Kamiguchi et al., 1998). Non-neuronal isoforms of L1 are expressed in cell types like Schwann cells, hematopoietic cells (Balaian et al., 2000), and epithelial cells (Nolte et al., 1999).

The molecular mass of L1 is ~200 kD, differing between cell types depending on distinct glycosylations occurring in up to 22 different sites in the extracellular domain, and these have been found to affect L1 homophilic and heterophilic interactions (Kleene et al., 2001; Wei & Ryu, 2012). Additional posttranslational modifications affect L1 function, such as ubiquitination, which facilitates lysosomal degradation and could control its re-appearance at the cell surface influencing neurite outgrowth and cell adhesion (Schäfer et al., 2010),

SUMOylation, which is required for proteolytic processing events (Lutz et al., 2012; Lutz, Wolters-Eisfeld, et al., 2014), or phosphorylation, which prevents L1 binding to AP-2 and clathrin-mediated internalization of L1 (Schaefer et al., 2002).

The L1 gene is located on the X chromosome, and there is a large number of neurological disorders in humans which have been linked to mutations of the L1 gene, and are known as L1-syndrome. Several conditions are associated with L1-mutations, such as hydrocephalus, MASA syndrome (mental retardation, aphasia, shuffling gate, adducted thumbs), corpus callosum hypoplasia, spastic paraplegia (Jouet et al., 1994), foetal alcohol syndrome (Arevalo et al., 2008), and possibly other X-linked neurological disorders. Severe consequences are associated with mutations of the extracellular regions of L1, of importance for adhesion and signalling, and most often milder symptoms occur with mutations in the intracellular domain, which could alter signalling or cytoskeleton interactions (Yamasaki et al., 1997).

L1 knockout mice have been extensively studied in order to understand the molecular basis of L1-syndrome (Dahme et al., 1997; Fransen, 1998). L1-deficient mice showed altered corticospinal tract (Jakeman et al., 2006), abnormal pyramidal decussation, decreased axonal association with non-myelinating Schwann cells, ventricular dilatation, hypoplasia of the cerebellar vermis, and hydrocephalus in C57BL/6background (K. Itoh et al., 2004). Dendritic abnormalities were found in the cortex of these mice, and they have a smaller hippocampus, corpus callosum and cerebellum (Demyanenko et al., 2001; Rolf et al., 2001). This further indicates the important role that L1 plays in the development of the nervous system.

During the initial study of L1-functions in the nervous system, several antibodies have been developed to detect this protein. Besides allowing L1-detection, these antibodies have been shown to be neutral to L1 function, but also to trigger or inhibit L1 signalling cascades and functions: antibody 555 is neutral, antibody 557 stimulates L1 functions (Appel et al., 1995) and antibody 324 inhibits some L1 functions (Mechtersheimer et al., 2001). Furthermore, recombinant L1-Fc (fusion of the extracellular domain of L1 with the fragment crystallizable region of human IgG) can promote L1-mediated neuronal survival and neurogenesis (Appel et al., 1995; S. Chen et al., 1999), due to the simulation of L1 homophilic interactions, which stimulate L1-dependent cellular responses (Kiefel et al., 2012; Mechtersheimer et al., 2001).

Research in cancer biology has determined L1 is a major factor during the progression of human cancers. L1 expression is associated with poor prognosis, tumour progression and metastasis to lymph nodes in nearly all cancers (Altevogt et al., 2016). In contrast, the expression of L1 in children with neuroblastoma has been shown to be a marker of good prognosis (Wachowiak et al., 2007). It has been argued that L1 can have a static function as a cell adhesion molecule promoting cell adhesion, but conversely promote motility driving cell

migration in metastasis of cancers (Kiefel et al., 2012). Hence the potential of L1 as a target for cancer therapy, makes of great importance understanding L1 functions at the molecular level (Samatov et al., 2016).

1. 2. 1. *PROTEOLYTIC PROCESSING OF L1*

L1 can undergo ectodomain shedding, an important mechanism for regulating the function of cell surface proteins. It has been reported that L1 can be cleaved in the extracellular domain by serine proteases such as plasmin, trypsin, and PC5A (Kalus et al., 2003; Nayeem et al., 1999; Sadoul et al., 1988), generating an 80 kD transmembrane, and a soluble extracellular 140 kD fragment. In addition, members of the ADAM family, like ADAM10 (Gutwein et al., 2003; Mechtersheimer et al., 2001) can cleave L1 as well, resulting in a soluble 180 kD fragment, found in tumour cell lines and the developing mouse brain, and 50 kD and 32 kD membrane-bound fragments from membrane-proximal shedding. The 32 kD fragment can be further processed by presenilin/ γ -secretase resulting in a 28 kD fragment (Riedle et al., 2009), which induces nuclear signalling and modulates gene expression.

1. 2. 2. *NUCLEAR L1 FRAGMENTS*

Previous results by our research group showed that L1-specific stimulation with antibody 557 and triggering of L1 signalling, lead to cleavage of full-length L1 at the plasma membrane by myelin basic protein (MBP), and generation of a SUMOylated transmembrane 70 kD fragment (L1-70). This fragment contains the intracellular domain of L1, transmembrane domain, and part of the extracellular domain (Lutz, 2013).

The L1-70 fragment was shown to travel from the plasma membrane to an endosomal compartment, and to be released into the cytoplasm and transported into the nucleus depending on the Lys¹¹⁴⁷ nuclear localization signal, by importin and chromatin-modifying protein 1 (Lutz et al., 2012). L1-70 has important neural functions: it enhances L1-mediated neurite outgrowth and neuronal survival in vitro (Lutz, Loers, et al., 2014), regulates synaptic plasticity (Kraus, Kleene, Henis, et al., 2018), promotes Schwann cell process formation and myelination of axons by Schwann cells, and improves functional recovery after injury (Lutz et al., 2016).

It has been recently discovered that the LXXLL and FXXLF motifs in the extracellular and transmembrane domains of this L1 fragment, mediate the interaction with the nuclear oestrogen receptors α (ER α) and β (ER β), peroxisome proliferator-activated receptor γ (PPAR γ) and retinoid X receptor β (RXR β) (Kraus, Kleene, Henis, et al., 2018). Mutations of

the LXXLL motif in the transmembrane domain and of the FXXLF motif in the intracellular domain disturb the interaction of the L1 fragment with these nuclear receptors. Mouse embryos virally transduced with L1 carrying this mutation suffer from impaired motor coordination, learning and memory, and synaptic connectivity problems in adult cerebellum. These impairments are similar to those observed in L1-deficient mice, indicating that L1 interaction with nuclear receptors is associated with synaptic contact formation and plasticity.

Furthermore, the levels of these fragments are correlated with brain development, regeneration after spinal cord injury, and degeneration in an Alzheimer's disease mouse model (Lutz, 2013). It is likely that proteolytic processing of L1 is involved in L1-dependent cellular responses to acute and chronic damage to the nervous system.

In addition, stimulation of cerebellar neurons with antibody 557 results in generation and nuclear import of a smaller fragment of L1, with an apparent molecular weight of 30 kD (L1-30). This fragment is generated by cleavage of SUMOylated L1-70 by cathepsin E on the intracellular domain at E₁₁₆₇. This soluble fragment is released into the cytoplasm, and the relocation of the L1 fragment into the nucleus is dependent on the nuclear localization signal on Lys₁₁₄₇. L1-30 was shown to be important for L1-induced neuronal migration, Schwann cell migration and myelination (Lutz, Wolters-Eisfeld, et al., 2014). It is hypothesized that this fragment could play a role in tumorigenesis, since the expression of L1 correlates with an increase in cell migration in most tumour entities, and this increase in L1 expression might lead to enhanced L1-30 production (Lutz, Wolters-Eisfeld, et al., 2014), leading to increased metastatic spread and worse outcomes (Kiefel et al., 2012).

The presence of both L1 fragments in the nucleus suggests that they might interact with DNA or other nuclear regulatory proteins affecting gene expression.

1. 2. 3. NUCLEAR L1 BINDING PARTNERS

Considering that the L1 fragments L1-70 and L1-30 can be found in the nucleus of neurons, they could interact with nuclear proteins such as transcription factors affecting gene expression. The identification of potential L1-binding partners in the nucleus could help our understanding of L1-signalling functions, and the mechanism by which this fragments affect L1-dependent processes such as neurite outgrowth, neuronal survival, neuronal migration, Schwann cell myelination and migration, and regeneration after injury.

Using the recombinant intracellular domain of L1 for affinity chromatography, potential L1 binding partners were identified by mass spectrometry in a nuclear extract of early postnatal mouse brain: SFPQ (also known as polypyrimidine tract binding associated-splicing factor or

PSF), NonO (also known as 54 kD nuclear RNA- and DNA-binding protein or p54nrb), paraspeckle component 1 (PSPC1), DNA topoisomerase I, importin- β , methyl-CpG-binding protein 2 (MeCP2), WD-repeat protein 5 (WDR5), the heterogeneous nuclear ribonucleoproteins hnRNP-A1, -A2/B1 and -A3, histone H1.4, nucleoporin 93 kD (Nup93), heat shock cognate protein 71 kD (Hsc70) and synaptotagmin 1.

After obtaining these results, the DBHS proteins (SFPQ, NonO and PSPC1) and MeCP2 seemed promising candidates, due to their implications in neuronal development and function.

Table 1.1. Mass spectrometry of protein band regions isolated from a nuclear brain extract by affinity chromatography with immobilized L1-ICD. Nominal molecular weight (MW) is given in kDa. Observed tryptic peptide masses (m/z submitted) and masses (MH⁺ matched), database sequence and position (start/end) of the matching tryptic peptides of the indicated murine proteins are shown. Peptides with methionine sulfoxide (MSO) deriving from oxidization of methionine and peptides with one (1) missing trypsin cleavage are indicated.

name	MW [kDa]	m/z submitted	MH ⁺ matched	modification	start	end	database sequence	band(s) [kDa]
SFPQ_mouse	72	1807.8	1807.9		291	306	LFVGNLPADITEDEFK	95, 90, 80
		1252.6	1252.7		312	322	YGEPGEVFINK	95, 90
		1064.4	1063.4	MSO: 349	342	350	AELDDTPMR	80
		1284.6	1283.6	MSO: 38	33	44	SPPPGMGLNQNR	70
		1267.6	1267.6		33	44	SPPPGMGLNQNR	80
		1126.6	1125.5	MSO: 570, 571/1	566	573	REEEMMIR	95, 70
		1760.6	1759.8	MSO: 349/1	335	350	ALAEIAKAELDDTPMR	90
IMB1_mouse	98	1226.0	1225.6		43	54	VLANPGNSQVAR	95
		1632.8	1632.7	MSO: 754	750	762	SDFDMVDYLNELR	95
		2156.2	2157.0		660	679	NYAEYQVCLAAVGLVGDLCR	80
TOP1_mouse	91	1284.7	1283.6		606	617	ELTAPDENVPAK	80
		1112.4	1112.6		255	264	AEEVATFFAK	80
		1228.6	1229.6	1	391	402	DAKVPSPPPGHK	95, 70
		1228.6	1229.6	1	394	404	VPSPPPGHKVK	95, 70
		1040.4	1039.6		478	486	AVALYFIDK	80
PSPC1_mouse	59	1310.4	1310.6		104	114	YGEPSEVFINR	60
		1649.6	1649.7		264	277	FAQPGTFEFYASR	60, 45, 40
		1192.6	1191.5		508	519	GSQGGNFEGPNK	50
		1090.4	1089.5	1	251	258	TQQYHKER	60
		1290.6	1289.7		198	209	GFVEFAAKPPAR	40
MeCP2_mouse	52	1955.8	1955.9		145	162	VGDTSLDPNDFDFTVTGR	45, 40
		1121.6	1122.6		295	304	SVHETVLPIK	45
		1326.6	1326.7	1	134	144	SKVELIAYFEK	45
		1310.4	1309.7		137	147	YDVYLINPQGK	60
SYT1_mouse	48	1584.6	1584.8		201	213	TLNPVFNEQFTFK	35
		1412.6	1412.7		376	388	VFVGYNSTGAELR	35
		1346.6	1345.6	MSO: 226	223	233	TLVMAVYDFDR	35
		1713.6	1712.9	1			KTLNPVFNEQFTFK	35
		1296.4	1296.6	MSO: 302	302	313	MDVGGLSDPYVK	35
NONO_mouse	54	1192.5	1191.6		145	155	FACHSASLTVR	50
		1696.8	1695.7		259	272	FAQPGSFYEYAMR	50
		1192.5	1191.6	1	66	75	KPGEKFTQR	50
		1144.6	1143.6	1	102	111	AGEVFIHKDK	45
WDR5_mouse	37	1560.6	1559.8		208	221	TLIDDDNPPVSFVK	35
		1596.6	1595.7		53	67	FSPNGEWLASSADK	35
NUP93_mouse	94	1412.6	1412.7		719	730	LVPLNQESVEER	50
HSC7C_mouse	71	1666.6	1665.8	MSO: 61	57	71	NQVAMNPTNTVFDAK	50
ROA1_mouse	34	1784.8	1784.9		16	31	LFIGGLSFETTDESLR	35
		1596.6	1596.8	MSO: 186/1	180	194	ALSKQEMASASSQR	35
ROA2_mouse	37	1188.6	1188.6		138	147	IDTIEIITDR	35
ROA3_mouse	40	1713.6	1713.7		168	182	GFAFVTFDDHDTVDK	35
		1120.6	1121.5		205	214	QEMQSAGSQR	40
H14_mouse	22	1228.6	1228.7		35	46	TSGPPVSELITK	95, 70, 60

1. 3. DBHS PROTEINS: SFPQ, NonO, PSPC1

The DBHS proteins play important roles in transcriptional regulation, acting as dynamic mediators of protein-protein, and protein-nucleic acid interactions (Knott et al., 2016). Their basic structure is characterized by a highly conserved core of ~300 amino acids named the 'DBHS' region, which consists of several tandem N-terminal RNA recognition motifs (RRMs), a NonA/paraspeckle domain (NOPS) and a C-terminal coiled-coil domain (B. Dong et al., 1993). The RRM is one of the most abundant and well characterized nucleic acid binding domains, and the RRM-coding sequence is present in 0.5-1.0% of human genes (Daubner et al., 2013).

There are three members of the DBHS family in humans: splicing factor proline/glutamine rich (SFPQ), Non-POU domain-containing octamer-binding protein (NonO) and paraspeckle protein component 1 (PSPC1). These proteins have a nuclear localization signal at their C-terminus, and are well known for being nuclear factors, although there is increasing evidence of the DBHS proteins having cytoplasmic and cell surface functions in some cell types (Furukawa et al., 2015).

One of the most important features of the DBHS proteins is their reciprocal interaction, producing homo/heterodimers, and their dimerization state can depend on the relative abundance of each protein. Different dimers have cell-specific functions, as these proteins can functionally compensate for each other in some biological scenarios. Lack of NonO can be compensated in DNA repair by an upregulation of PSPC1, forming a functional heterodimer with SFPQ (S. Li et al., 2014). Still, SFPQ and NonO do not compensate for the loss of PSPC1 in DNA repair functions (X. Gao et al., 2014), and PSPC1 and SFPQ are not capable to compensate for the loss of NonO in human intellectual disability (Mircsof et al., 2015).

The DBHS proteins play roles in transcriptional repression, activation, initiation, elongation and termination, and they can associate with a wide range of transcription factors, as well as bind to DNA and RNA (Knott et al., 2016; Shav-Tal & Zipori, 2002). During transcriptional repression, SFPQ binds directly to gene promoters, recruiting epigenetic silencers like paired amphipathic helix protein Sin3A (Sin3A) and histone deacetylase (HDAC) (X. Dong et al., 2005). SFPQ/NonO can suppress transcription by sequestering activators from target promoters, and NonO represses genes responsible of the cyclic adenosine 3',5'-monophosphate (cAMP) pathway (Ong et al., 2011). The DBHS are involved in double-stranded DNA break repair, assisting in homology directed repair of nonhomologous end joining. They contribute to maintaining transcript stability, coating nascent transcripts for stabilization (Fox et al., 2002), and they are essential for the formation and integrity of paraspeckles (Clemson et al., 2009), which are ribonucleoprotein bodies located in the cell

nuclei, defined by the colocalization of SFPQ/ NonO/ PSPC1 together with the long coding RNA nuclear paraspeckle assembly transcript 1 (NEAT1). The paraspeckles segregate a subset of nuclear proteins, including the DBHS proteins, depleting their nuclear availability and affecting the target genes of these proteins (Ha et al., 2011). Transcriptional activation seems to be driven by NonO (Knott et al., 2016), which binds and processes nascent RNA transcripts, but also interacts with the transcriptional machinery. PSPC1 can act as putative heterodimer with SFPQ, activating genes in neuronal development (Knott et al., 2016). All DBHS can act as both activators and repressors of the androgen receptor (Mathur et al., 2001). The lack of the SFPQ ortholog in zebrafish causes impaired neurite outgrowth, impaired motor development (Thomas-Jinu et al., 2017), and failure in neuronal differentiation (Jiang et al., 1996).

Mutations in NonO have been identified in patients with intellectual disability (Reinstein et al., 2016), and a similar phenotype is observed in NonO-deficient mice (Mircsof et al., 2015). NonO-deficient mice show a smaller cerebellum, flattened nose, and an anxiety phenotype, and while humans with mutations in NonO show a similar phenotype, their symptoms include a thickened corpus callosum and macrocephaly (Mircsof et al., 2015). Intellectual deficits caused by mutations in NonO could be linked with dysregulated expression of synaptic transcripts, since inhibitory deficits due to the downregulation of GABA have been found (Mircsof et al., 2015).

1. 4. MECP2 AND RETT SYNDROME

MeCP2 is a protein encoded by the MeCP2 gene (MECP2), located on the X chromosome. Mutations of this protein in humans produce Rett Syndrome (RTT), one of the main causes of mental disability in young girls (Baldovino et al., 2016). Two protein coding transcripts exist, producing the two isoforms MeCP2- α (long) and MeCP2- β (short) (Kriaucionis, 2004). It has been observed that specific deactivation of MeCP2- β did not influence normal neural development, while loss of MeCP2- α led to RTT (M. Itoh et al., 2012). In addition, it has been found that the N-terminal domains of MeCP2- α and - β modulate the ability of the methyl-CpG binding domain to bind to DNA, with MeCP2- α having higher binding affinity for DNA than - β (Martínez de Paz et al., 2019).

Regarding expression, MeCP2 is present in almost every tissue, but it is especially abundant in the nervous system (*The Human Protein Atlas: WWW.PROTEINATLAS.ORG*, 2020). This protein has six biochemically distinct domains, and two of them are vital for its function: the methyl-CpG binding domain (MBD), which selectively binds 5MeCyt, and the transcriptional

repressor domain (TRD), which via cofactor binding attracts histone deacetylase to the DNA, and leads to repression of transcription (Nan et al., 1997). The MBD is the only structured domain (α -helix), being 60% of MeCP2 unstructured (Adams et al., 2007). The properties of MeCP2 can be conditioned by post translational modifications: phosphorylation, acetylation, SUMOylation and ubiquitination (Abuhatzira et al., 2007; Ehrhart et al., 2016; Gonzales et al., 2012; Stefanelli et al., 2016; Zhang et al., 2018).

Concerning Rett Syndrome (RTT), it is most often caused by *de novo* mutations of MECP2, however, not all mutations in this gene cause RTT phenotype (Brown et al., 2016). MECP2 is inactivated in one X-chromosome in females, and the degree of inactivation of the healthy MECP2 compared to the mutant, contributes to the difference in phenotypes for RTT (Cheung, 2013). This disease is most often observed in females (Ehrhart et al., 2016), and hemizygous males with a severe mutation are in general not viable, although different non-lethal mutations can cause severe congenital encephalopathy (RTT-like syndrome) in males (Bienvenu & Chelly, 2006).

The typical development of RTT starts with an asymptomatic first phase lasting 6 to 18 months, followed by a second phase of onset, consisting of decreased, arrested, and delayed development of motor and communication skills (Percy, 2011), stereotypic movements, and loss of purposeful movement (Samaco & Neul, 2011). Next follows a third phase of stagnation, lasting from 2 to 10 years, which can include some recovery. Finally, the fourth phase typically reduces mobility once more, while communication and cognition are preserved. Women experiencing this disease often show severe intellectual disability, microcephaly and seizures (Ehrhart et al., 2016).

As for MeCP2 functions, it mainly binds to methylated cytosine residues in the DNA (5MeCyt), adjacently enriched with A/T bases. MeCP2 binds with less affinity to hydroxymethylated DNA (5OHMeCyt) (Hansen et al., 2010), which is considered a marker of active genes in neurons (Chahrour et al., 2008). Mutations of MeCP2 causing RTT disrupt core MeCP2 functions: MeCP2 co-repressor recruitment (Lyst et al., 2013; Matarazzo et al., 2004), chromatin compaction (Della Ragione et al., 2016), and activity dependent transcription activation (Chahrour et al., 2008).

Mutations of MeCP2 in the MBD lead to the loss of 5MeCyt binding activity, and are known to cause RTT (Yang et al., 2016). MeCP2 influences translation by enhancing the AKT/mTOR signalling pathway (Zhang et al., 2018). In addition, it forms a complex with YB1 affecting alternative splicing of downstream gene products (Young et al., 2005). In addition, various miRNAs and long non-coding RNAs are regulated by MeCP2 (Long et al., 2011).

Methylated DNA present in CpG islands, is often present in promotor regions in most human genes (60%), and wrapped around histones preventing their access by transcription factors. As MeCP2 binds to methylated DNA, it attracts co-repressor complexes containing SIN31, nuclear receptor co-repressor 1 (NCOR1) and nuclear receptor co-repressor 2 (NCOR2 or SMRT), recruiting histone deacetylase (HDAC), and leading to chromatin condensation around methylated DNA (Gonzales et al., 2012; Lyst et al., 2013). Lack of MeCP2 causes acetylation of H3 and H1 histones, leading to chromatin decondensation and activation of transcription (Ghosh et al., 2010; Skene et al., 2010). Recent research has found evidence of MeCP2 producing transcriptional repression in human mature neuronal cells, but transcription activation in embryonic stem cells (Y. Li et al., 2013) by recruiting cAMP response element-binding protein 1 (CREB) as a cofactor to target gene promoters, such as brain-derived neurotrophic factor (BDNF), essential for neuronal development and function (Sampathkumar et al., 2016). The expression of MeCP2 target genes is affected in RTT patients, and in mouse and in vitro models of RTT (Jordan et al., 2007; Tudor et al., 2002).

Additionally, MeCP2 is responsible for transcription triggered by neural activity. After membrane depolarization Ca^{2+} -influx leads to phosphorylation of MeCP2, its detachment from DNA, and this leads to chromatin decondensation and transcription (W. G. Chen et al., 2003; Zhou et al., 2006). Blocking of MeCP2 phosphorylation produces RTT symptoms (Bedogni et al., 2014). Phosphorylation of MeCP2 is dependent on dopamine, serotonin and norepinephrine pathways (Hutchinson et al., 2012). Reduced levels of catecholamines were found post-mortem in RTT patients (Brücke et al., 1987; Lekman et al., 1989), which could cause an imbalance in excitatory/inhibitory neural activity (imbalance in GABAergic, glutamatergic and dopaminergic pathways).

MeCP2-deficient mice or mice containing severe mutations in MECP2, show symptoms similar to humans with RTT (N. P. Belichenko et al., 2008; P. V. Belichenko et al., 2009; I.-T. J. Wang et al., 2013). Similar findings were observed in MeCP2 overexpression mouse model (Lu et al., 2016) probably explained by the correct function of MeCP2 being dose dependent. Alterations include arrested neural development after 6 weeks with a smaller brain and reduced neuronal size, problems in movement and breathing, and shortened lifespan (Guy et al., 2001).

MeCP2-deficient neural precursor cells are not different in expression patterns to wild-type controls, (both mRNA and protein), proliferation and differentiation, but this changes during the maturation of precursor cells (Livide et al., 2015). MeCP2-deficient mice show reduced neuronal differentiation, synaptic deficits, decreased dendritic complexity and immature synaptic spine morphology. These findings indicate that MeCP2 is probably more important

for maintaining neuronal function and formation of synapses than for neurogenesis (Kishi & Macklis, 2004).

1. 5. AIM

The aim of this PhD project was to study the interactions between L1, and the potential binding partners NonO, SFPQ, PSPC1, and MeCP2.

In order to achieve this goal, the research was organized as follows:

1. Analysis of the interaction between the intracellular domain of L1 and the L1 fragments, and the binding partners in biochemical assays, and in cellular and tissue contexts.
2. Narrowing down the binding site in L1: identification of the L1-fragment/s interacting with MeCP2.
3. Study the distribution of the binding partners and L1 in differentiating mouse neural cells and early postnatal brain.
4. Examine the potential regulatory role of MeCP2 in the generation of L1-70.
5. Identification of functional consequences of MeCP2 knockdown or overexpression on L1-dependent neurite outgrowth.

2. MATERIALS AND METHODS

2. 1. ANIMALS

2. 1. 1. GENERATION OF L1-DEFICIENT MICE

L1-deficient mice ($L1^{-/y}$) were generated by inserting a tetracycline controlled transactivator inside of the second exon of the X chromosome-linked L1 gene (Rolf et al., 2001). Heterozygous females ($L1^{+/-}$) and wild-type males on a mixed genetic background (129SVJ x C57BL/6J) were used for breeding and obtaining $L1^{-/y}$ male mice and $L1^{+/-}$ male age-matched littermates (Guseva et al., 2009). Animals were housed at standard laboratory conditions with food and water supply *ad libitum* and with an artificial 12 h light/dark cycle. All procedures used were approved by the responsible authorities of the State of Hamburg (Behörde für Wissenschaft und Gesundheit, Amt für Gesundheit und Verbraucherschutz, Lebensmittelsicherheit und Veterinärmedizin; animal permit numbers ORG_679 Morph, A 005/2019 and N 056/2019) and in agreement to the guidelines set by the European Union and Germany. The experiments were conducted and evaluated following the ARRIVE guidelines for animal research (Kilkenny et al., 2010).

2. 1. 2. GENERATION MUTATED L1 MICE ($L1^{RA}$)

A single guide RNA (sgRNA) was chosen after submitting the targeting region, exon 15 of the murine L1, to the CRISPOR design tool (Haeussler et al., 2016). The template for transcription with the targeting sequence (GTTAATGGCAGTGACCCGAA) was generated by PCR using Q5TM DNA Polymerase (New England Biolabs). Transcription was performed using the HiScribeTM T7 High Yield RNA Synthesis Kit (New England Biolabs, E2040S) with subsequent purification of the transcript with the MEGAClearTM Transcription Clean-Up Kit (ThermoFisher Scientific, AM1908), both according to the manufacturer's instructions. A repair oligonucleotide (donor DNA synthesized by Sigma-Aldrich) designed to knock-in the p.R682A substitution, a restriction site for screening (*AciI*) and a further silent mutation for a degenerated PAM sequence had the following sequence:

```
5'AGGTGCCAGGAAATCAGACCTCTACTACCCTCAAGCTGTCCCCCTATGTCCACT
ACACATTTGCGGTCAGTCCATTAACAAATATGGTCCTGGAGAACCCAGCCCTGT
CTCTGAGACTG -3'.
```

Electroporation into 1-cell stage embryos derived from superovulated C57BL/6JHtg mice was performed using 600 ng/ μ l sgRNA, 1 μ g/ μ l donor DNA and 500 ng/ μ l Cas9 protein (Alt-R® S.p. Cas9 Nuclease V3, IDT 1081058) in Opti-MEM TM (Gibco) with the help of the NEPA

21 electroporator (Nepa Gene). Settings were as described by Remy et al. (2017) (Remy et al., 2017). Electroporated embryos were implanted into B6CBF1 foster mothers in the two-cell stage after cultivation in KSOM (potassium-supplemented simplex optimized medium) overnight.

The resulting offspring was analysed by PCR using the Thermo Scientific Phire Animal Tissue Direct PCR Kit and the primers *L1-RA fw* and *L1-RA rev* followed by *Acil* digestion.

Correct integration of the repair construct was verified by sequence analysis. Two independent lineages (termed line x and y throughout the manuscript) with L1 c.[2044C>G;2045G>C] mutation (p.R682A) were obtained and further bred at the UKE animal facility. All experiments were performed in accordance with the local guidelines for animal care and protection.

2. 2. SUPPLIERS OF CHEMICALS, KITS, REAGENTS, AND LABORATORY EQUIPMENT

All chemicals, reagents and kits were purchased from the following companies: Abcam (Cambridge, UK), Abnova (Taipei, Taiwan), Addgene Inc. (Teddington, UK), Applied Biosystems (Foster City, CA, USA), BioLegend (Fell, Germany), BIOMOL (Hamburg, Germany), Bio-Rad Laboratories (Munich, Germany), Bio&SELL, Nürnberg, Germany), Biozol (Eching, Germany), Carl Roth (Karlsruhe, Germany), Corning (Wiesbaden, Germany), Creative BioMart (Shirely, NY, USA), Dako/Agilent Technologies (Santa Clara, CA, USA), Dianova (Hamburg, Germany), DWK Life Sciences (Millville, NJ USA), Enzo Life Sciences (Farmingdale, NY, USA), Eppendorf AG (Hamburg, Germany), GenWay Biotech (San Diego, CA, USA), Hamilton Company (Reno, NE, USA), INVIVO BioTech Service (Hennigsdorf, Germany), Jackson ImmunoResearch (West Grove, PA, UK), LifeTechnologies (Darmstadt, Germany), Macherey-Nagel (Düren, Germany), Merck Chemicals (Darmstadt, Germany), Mundipharma (Limburg, Germany), New England Biolabs (Ipswich, MA, USA), Nunc (Roskilde, Denmark), PAA Laboratories (Cölbe, Germany), PAN Biotech (Aidenbach, Germany), Santa Cruz Biotechnologies (Dallas, TX, USA), Roche Diagnostics (Mannheim, Germany), SERVA Electrophoresis (Heidelberg, Germany), Schafer-N (Copenhagen, Denmark), Sigma-Aldrich (Taufkirchen, Germany), T. H. Geyer (Hamburg, Germany), Thermo Fisher Scientific (Waltham, MA, USA), VWR International GmbH (Darmstadt, Germany), Wheaton (Millville, USA).

2. 3. ANTIBODIES

2. 3. 1. PRIMARY ANTIBODIES

The primary antibodies used in this work are listed in Table 2.1.

Abbreviations: ELISA – enzyme-linked immunosorbent assay, IF – immunofluorescence, IP – immunoprecipitation, PLA – proximity ligation assay, WB – Western Blot.

Table 2. 1. Primary antibodies.

Antibody	Dilution
α Tubulin (TU-02) #sc-8035 (Santa Cruz Biotechnology)	WB 1:500
Actin (C-2) #sc-8432 (Santa Cruz Biotechnology)	WB 1:500
6X His tag® antibody (HRP) #ab1187 (Abcam)	WB 1:5,000 ELISA 1:10,000
β III-tubulin (TU-20) #sc-51670 (Santa Cruz Biotechnology)	IF 1:100
CD171 (L1CAM) #838101 (BioLegend)	WB 1:2,000 ELISA 1:200
CHL1 (C-18) #sc-34986 (Santa Cruz Biotechnology)	ELISA 1:200
GAPDH (6C5) #sc-32233 (Santa Cruz Biotechnology)	WB 1:500
Anti-Green Fluorescent Protein Antibody #AB16901 (Merk Millipore)	IF 1:500
MAP2 #GTX133110 (GeneTex)	WB 1:1,000
MeCP2 D4F3 XP Rabbit mAb #3456 (Cell Signalling Technologies)	WB 1:1,000 IF 1:200 PLA 1:20 IP 1 μ g
MeCP2 Polyclonal Antibody #PA5-12234 (Thermo Fisher Scientific)	IP 2 μ g
Mouse IgG # 012-000-003 (Dianova)	IP 2 μ g

Antibody	Dilution
NCAM-L1 (C-2): #sc-514360 (Santa Cruz Biotechnology)	WB 1:500 PLA 1:10 IF 1:100
Tau (A-10) #sc-390476 (Santa Cruz Biotechnology)	IF 1:100
p54/nrb (H-85) #sc-67016 (Santa Cruz Biotechnology)	PLA 1:10 WB: 1:500
PSF (H-80) #sc-28730 (Santa Cruz Biotechnology)	PLA 1:10 WB: 1:500
PSPC1 (T-20) #sc-84577 (Santa Cruz Biotechnology)	PLA 1:10 WB: 1:500
Rabbit IgG #011-000-003 (Dianova)	IP 1 µg

2. 3. 2. SECONDARY ANTIBODIES

The secondary antibodies used in this work are listed in Table 2.2.

Table 2. 2. Secondary antibodies.

Antibody	Dilution
Cy3-conjugated goat anti-rabbit (Jackson ImmunoResearch)	IF 1:200
Cy5-conjugated goat anti-mouse (Jackson ImmunoResearch)	IF 1:200
HRP-conjugated donkey anti-goat (Jackson ImmunoResearch)	WB 1:10,000
HRP-conjugated goat anti-mouse IgG (Jackson ImmunoResearch)	WB 1:10,000
HRP-conjugated goat anti-rabbit IgG (Jackson ImmunoResearch)	WB 1:10,000

2. 4. BACTERIA

The bacterial strains used in this work are detailed in Table 2.3.

Table 2. 3. Bacteria strains used in this work.

Strain	Company and genotype
<i>E. coli</i> M15 pREP4	(Qiagen) F ⁻ , Φ 80 Δ lacM15, <i>thi</i> , <i>lac</i> ⁻ , <i>mtl</i> ⁻ , <i>recA</i> ⁺ , KmR
<i>E. coli</i> One Shot™ BL21 Star™ (DE3) Chemically Competent	(Thermo Fisher Scientific) F ⁻ , <i>ompT</i> , <i>hsdS_B</i> , (<i>r_B</i> ⁻ , <i>m_B</i> ⁻) <i>gal</i> , <i>dcm</i> , <i>rne131</i> (DE3)
<i>E. coli</i> One Shot™ TOP10 Chemically Competent	(Thermo Fisher Scientific) F ⁻ , <i>mcrA</i> , Δ (<i>mrr-hsdRMS-mcrBC</i>), ϕ 80 <i>lacZ</i> Δ M15, Δ <i>lacX74</i> , <i>recA1</i> , <i>araD139</i> , Δ (<i>ara</i> - <i>leu</i>)7697, <i>galU</i> , <i>galK</i> , <i>rpsL</i> (Str R), <i>endA1</i> , <i>nupG</i>

2. 5. BACTERIAL VECTORS

The bacterial vectors used during this thesis are:

MECP2 cDNA ORF Clone in Cloning Vector pUC19 Vector – Cat # MG53595-U (SinoBiological).

pLATE52 – Cat # K1281 (Thermo Fisher Scientific).

pSP64 Poly(A) Vector – Cat # P1241 (Promega).

pQE-30 – Cat # 32903 (Qiagen).

The vector maps can be found in the appendix.

2. 6. CELL LINES

The following cell lines were used during this thesis:

Human embryonic kidney 293 (HEK293) cells (CRL-1573, American Type Culture Collection).

Neural stem cells isolated from the cerebral cortex of 14-day-old C57BL/6J mouse embryos, kindly provided by Prof. Dr. Udo Bartsch, Department of Ophthalmology, University Medical Center Hamburg-Eppendorf, Hamburg, Germany.

2. 7. COMMERCIAL PEPTIDES AND RECOMBINANT PROTEINS

The following recombinant proteins were used:

MeCP2 (human) recombinant protein Cat # H00004204-P01 (Abnova).

MeCP2 human protein Cat # GWB-BSP531 (Genway).

The following peptides comprising parts of the intracellular domain of L1 were obtained from Schafer-N:

1 - H-CFIKRSKGGKYSVKDKEDTQVDSEARPMKDETGE-OH.

2 - H-CRPMKDETGEYRSLESDNEEKAFGSSQPSLNGDIK-OH.

3A - H-CDIKPLGSDDSLADYGGSD-OH.

3B - H - CSVQVQFNEDGSFIGQYSGK-OH.

4 – H - CSGKKEKEAAGGNDSSGATSPINPAVALE-OH.

2. 8. OLIGONUCLEOTIDES

All the oligonucleotides used were obtained from Metabion International.

L1arm2: 5'–GGA ATT TGG AGT TCC AAA CAA GGT GAT C-3'.

L1 -5UP2: 5'–AGA GGC CAC ACG TAC CGC AGC ATC-3'.

tTA-up3: 5'–TAC ATG CCA ATA CAA TGT AGG CTG C-3'.

L1-RA fw: 5'–TGA GGA CAA GGA AAT GGC TCC-3'.

L1-RA rev: 5'–GCT GTA GCA AGG ACA AGG AAC-3'.

pSP64 MeCP2- α for: 5'-CTT GGG CTG CAG GTC ATG GCC GCC GCT GC-3'.

pSP64 MeCP2- α rev: 5'-GGA TCC TCT AGA GTC TCA GCT AAC TCT CTC GGT CAC GGG C-3'.

pSP64 MeCP2- β for: 5' -GCT TGG GCT GCA GGT CAT GGT AGC TGG GAT GTT AGG GCT CA-3'.

pSP64 MeCP2- β rev: 5'-GGA TCC TCT AGA GTC TCA GCT AAC TCT CTC GGT CAC G-3'.

MeCP2v2ALI_for: 5'-GGT TGG GAA TTG CAA ATG GTA GCT GGG ATG TTA G-3'.

MeCP2v2ALI_rev: 5'-GGA GAT GGG AAG TCA TTA TCA GCT AAC TCT CTC GGT C-3'.

2. 9. VIRUSES (AAV: ADENO-ASSOCIATED VIRUS 1)

All the viruses used during this work were produced by Dr. Ingke Braren (Vector Facility, Universitätsklinikum Hamburg-Eppendorf, Germany), and are listed in Table 2.4.

Table 2. 4. Viruses used in this work.

Name	Titer [vg/ml]
ssAAV1-CMV wild-type L1 (VC406)	$6.02 \cdot 10^{11}$
ssAAV1-CMV L1R/A (VC406)	$2.52 \cdot 10^{11}$
ssAAV1-CMV-L1 E/Q (VC406)	$1.34 \cdot 10^{10}$
AAV1-scCMV-GFP U6-MecP2 (VC424)	$7.15 \cdot 10^{13}$
AAV1-scCMV-GFP U6-scrbl (VC424)	$7.60 \cdot 10^{13}$
AAV1-CMV-GFP MeCP2 (VC473)	$1.5 \cdot 10^{11}$

2. 10. BUFFERS, SOLUTIONS, CHEMICALS AND MEDIA.

2. 10. 1. BUFFERS, SOLUTIONS AND CHEMICALS USED FOR AGAROSE GEL ELECTROPHORESIS.

50xTAE	2 M Tris 1 M acetic acid 50 mM EDTA pH 8.0
Agarose gel solution with Roti-GelStain	0.75- 3% agarose standard (Carl Roth) 1xTAE 0.05 µl/ml Roti-GelStain (Carl Roth)
DNA Ladders	1 kb Plus DNA Ladder (Thermo Fisher Scientific) 100 bp Plus DNA Ladder (Thermo Fisher Scientific)
6x Loading Dye	(Thermo Fisher Scientific)

2. 10. 2. BUFFERS, SOLUTIONS AND CHEMICALS USED FOR PROTEIN PRODUCTION.

Lysis buffer	50 mM NaH ₂ PO ₄ 300 mM NaCl 10 mM Imidazole 20 mM β-mercaptoethanol 1x cOmplete EDTA-free Protease Inhibitor Cocktail (Roche) pH 8.0
Washing buffer 1	50 mM NaH ₂ PO ₄ 300 mM NaCl 10 mM Imidazole 0.1% Triton pH 8.0

Washing buffer 2	50 mM NaH ₂ PO ₄ 600mM NaCl 20mM Imidazole 0.1% Triton pH 8.0
Washing buffer 3	50 mM NaH ₂ PO ₄ 600 mM NaCl 40 mM Imidazole 0.1% Triton pH 8.0
Elution buffer	50 mM NaH ₂ PO ₄ 300 mM NaCl 250 mM Imidazol

2. 10. 3. MEDIA AND CHEMICALS USED FOR BACTERIAL CULTURES.

LB medium (lysogeny broth)	10 g/l bacto-tryptone pH 7.4 10 g/l NaCl 5 g/l yeast extract
LB medium with ampicillin	100 mg/l ampicillin LB medium
Agar plates with ampicillin	20 g/l agar 100 mg/l ampicillin LB medium
S.O.C. medium	(Thermo Fisher Scientific)

2. 10. 4. **BUFFERS, SOLUTIONS AND MEDIA USED IN CELL CULTURE.**

Maintenance medium for HEK293 cells	DMEM, high glucose (PAN Biotech) 10% (v/v) FBS (PAN Biotech) 2% (v/v) Penicillin/Streptomycin (PAN Biotech)
Washing solution for HEK293 cells	PBS (Phosphate buffered saline) without Ca^{2+} and Mg^{2+} (PAN Biotech)
Freezing solution for HEK293 cells	70% DMEM, high glucose 20% (v/v) FBS 10% (v/v) DMSO (Sigma-Aldrich)
Culture medium for HEK293 cells	DMEM, high glucose
Coating solution for primary neurons	Poly-L-lysine (PLL) (Sigma-Aldrich) 0.01% in ddH ₂ O
Cell washing for primary neurons	HBSS: Hank's balanced salt solution without Ca^{2+} and Mg^{2+} containing 0.35 g/l NaHCO_4 and phenol red (Sigma-Aldrich)
Digestion solution for HEK293 cells	Trypsin-EDTA: 0.05% trypsin/ 0.02% EDTA (Sigma-Aldrich) in PBS without Ca^{2+} and Mg^{2+} (Sigma-Aldrich)
Culture medium for cerebellar granule cells	Medium X-1: Neurobasal A (Thermo Fisher Scientific), containing: 1% penicillin/streptomycin 0.1% BSA (Sigma-Aldrich) 10 $\mu\text{g/ml}$ insulin (Sigma-Aldrich) 4 nM L-thyroxine (Sigma-Aldrich) 100 $\mu\text{g/ml}$ transferrin holo (Merck) 30 nM sodium-selenite (Sigma-Aldrich) 1x B27 supplement (Invitrogen) 2 mM L-glutamine

	1 mM sodium pyruvate (Thermo Fisher Scientific) with or without 5% foetal horse serum (PAN Biotech)
Dissociation solution for cerebellar granule cells	10 mg Dnase I (Sigma-Aldrich) 50 mg glucose 20 ml Neurobasal A
Trypsin/DNase solution (cerebellar granule cells)	0.3 g trypsin (Sigma-Aldrich) 30 mg DNase I 300 µl 80 mM magnesium chloride (MgCl ₂) 30 ml HBSS
Culture medium for cortical neurons	Neurobasal medium (Thermo Fisher Scientific) 2 mM L-glutamine (PAN Biotech) 1% penicillin/streptomycin 1x B27 supplement 7% horse serum (PAN Biotech)
Digestion solution for cortical neurons	0.5% trypsin in HBSS
Stopping solution for cortical neurons	10% BSA 10% trypsin inhibitor (Sigma-Aldrich) in HBSS, pH 7.4
Culture medium basic stock for neural stem cells	DMEM/F12 (Thermo Fisher Scientific) 1% penicillin/streptomycin 2 mM L-glutamine 5 mM HEPES (Sigma-Aldrich) 0.3 % glucose 3mM NaHCO ₃ (Sigma-Aldrich)
Culture medium for maintenance for neural stem cells	Culture medium basic with: 1% B27 1% N2 supplement (Thermo Fisher Scientific) 10 ng/ml EGF (ImmunoTools) 10 ng/ml FGF-2 (Sigma-Aldrich)

Accutase	Enzyme Cell Detachment Medium (Thermo Fisher Scientific)
Induction medium	Culture medium basic stock with 5 ng/ml FGF-2 1% N2 supplement 2% B27
Differentiation medium	1:1 mixture of culture medium basic stock and Neurobasal A with: 0.25 % N2 supplement 2% B27

2. 10. 5. REAGENTS AND BUFFERS USED FOR SDS-PAGE AND WB ANALYSES.

Protease inhibitor solution	stock (in ddH ₂ O) and working solution (in RIPA buffer) prepared according to the manufacturer's protocol (cOmplete EDTA-free Protease Inhibitor Cocktail, Roche)
Laemmli buffer (5x)	0.35 M Tris-HCl 10% SDS 50% glycerol 0.13% bromophenol blue (BIOMOL) 0.5% DTT (BIOMOL) pH 6.8
SDS 10 %	10 g SDS in 100 ml ddH ₂ O
SDS Running buffer	250 mM Tris-HCl 192 mM glycine 1% SDS

SDS running gel 10 %	<p>1.7 ml ddH₂O</p> <p>2.0 ml 30% acrylamide-bisacrylamide (29:1) (SERVA Electrophoresis)</p> <p>2.3 ml 1 M Tris-HCl, pH 8.8</p> <p>60 µl 10% SDS</p> <p>15 µl 10% APS</p> <p>6 µl TEMED</p>
Stacking gel for 5%-gel	<p>1.05 ml ddH₂O</p> <p>0.25 ml 30% acrylamide -bisacrylamide</p> <p>0.2 ml 1M Tris-HCl pH 6.8</p> <p>20 µl 10% SDS</p> <p>10 µl 10% APS</p> <p>4 µl TEMED</p>
Protein Ladder	<p>PageRuler™ Plus Prestained (Thermo Fisher Scientific)</p>
Coomassie staining solution	<p>20% (v/v) methanol</p> <p>80% (v/v) Roti-Blue (Carl Roth)</p>
Coomassie washing solution	<p>25% (v/v) MeOH in ddH₂O</p>
RIPA buffer	<p>20 mM Tris-HCl</p> <p>150 mM NaCl</p> <p>1 mM EGTA</p> <p>1% NP-40</p> <p>1% sodium deoxycholate</p> <p>2.5 mM sodium pyrophosphate</p> <p>1mM β-glycerophosphate</p> <p>25 Units/ml benzonase (Sigma-Aldrich)</p> <p>1x protease inhibitor solution cOmplete EDTA-free Protease Inhibitor Cocktail</p> <p>pH 7.5</p>
TBS	<p>10 mM Tris</p> <p>0.15 M NaCl</p> <p>adjust to pH 7.5 with HCl</p>

TBS-T	50 µl/l Tween 20 in TBS
WB blocking buffer	5% (w/v) skim milk powder (Carl Roth) or 5% (w/v) BSA with fatty acids (PAA Laboratories) in TBS-T
Stripping solution	0.5 M NaCl 0.5 M acetic acid
Neutralization solution	1 M Tris adjust to pH 8.0 with HCl

**2. 10. 6. REAGENTS AND BUFFERS USED FOR EXTRACTION OF
NUCLEAR PROTEINS.**

Homogenization buffer	0.32 M sucrose 20 mM Tris-HCl 2 mM MgCl ₂ 2 mM CaCl ₂ 1 mM PMSF pH 7.4
Gradient buffer	20 mM Tris-HCl 2 mM MgCl ₂ 2 mM CaCl ₂ 1 mM PMSF (Merck Chemicals) pH 7
Sucrose gradient	0.8 M sucrose 1.0 M sucrose 1.2 M sucrose in gradient buffer

Lysis buffer homogenization buffer containing 0.1% NP40

Roeder C buffer
20 mM Tris-HCl
420 mM NaCl
2 mM MgCl₂
2 mM CaCl₂
0.5 mM DTE
1 mM PMSF
5% glycerol
pH 7.5

2. 10. 7. SOLUTIONS AND REAGENTS USED FOR IMMUNOSTAININGS.

Homemade PBS
13.7 mM NaCl
0.27 mM KCl
0.8 mM Na₂HPO₄
0.15 mM KH₂PO₄
pH 7.4

8% formaldehyde fixing solution
8% (w/v) paraformaldehyde
in homemade PBS
adjust to pH 7.5 with NaOH

4% formaldehyde fixing solution
4% (w/v) paraformaldehyde
in homemade PBS

50% Methanol solution
50% methanol in ddH₂O

Blocking serum
0.2% (v/v) TritonX-100
0.02% (w/v) sodium azide
5% (v/v) normal donkey serum (Dianova) or
normal goat serum (Dianova)
in homemade PBS

Blocking solution	2% bovine albumin serum 1% (v/v) TritonX-100 in homemade PBS
Dehydrating solution	15% (w/v) sucrose (in homemade PBS)
Mounting medium	Roti®-Mount FluorCare DAPI (Carl Roth) or Shandon Immu-Mount (Thermo Fisher Scientific) adding DAPI stain at 1 µg/ml

2. 10. 8. *BUFFERS, SOLUTIONS AND CHEMICALS USED FOR ELISA.*

ELISA blocking solution	1% (w/v) BSA fatty acids-free (PAA Laboratories) in PBS with Ca ²⁺ and Mg ²⁺ (PAN Biotech)
ELISA washing buffer (PBS-T)	0.005% (v/v) Tween 20 in PBS with Ca ²⁺ and Mg ²⁺ (PAN Biotech)
OPD solution	0.5 mg/ml OPD (Thermo Fisher Scientific) Stable peroxidase buffer 10x (Thermo Fisher Scientific)
Stopping solution	2.4 M H ₂ SO ₄

**2. 10. 9. *BUFFERS, SOLUTIONS AND CHEMICALS USED DURING AAV
INJECTION OF MICE.***

PBS sterile	PBS Ca ²⁺ and Mg ²⁺ (PAN Biotech)
0.05% Trypan blue dilution	0.4% Trypan blue solution (Sigma-Aldrich) diluted in sterile ddH ₂ O
Ketchum Green Tattoo Paste	(FST)
Betaisodona	Povidone-iodine (Mundipharma)
Isoflurane liquid for inhalation	4% isoflurane in O ₂
Bupivacain 0.25%/ Lidocain 1%	Bupivacain 0.5%/ Lidocain 1% 1:1 in 0.9% NaCl solution (Apotheke UKE, Hamburg)

2. 11. MOLECULAR BIOLOGY METHODS AND CLONING STRATEGIES

2. 11. 1. REVERSE TRANSCRIPTION

Reverse transcription was performed in order to generate the bacterial vectors containing cDNA MeCP2- α . MeCP2 mRNA was extracted from cerebellar granule cells, followed by reverse transcription.

For the reverse transcription, Oligo(dT)₂₃ primers and reverse transcriptase were used. Oligo(dT)₂₃ primers were used in order to prime mRNA with a poly(A) tail for cDNA synthesis. The primers had 23 thymidine residues and one G, C or A residue (the anchor) at the 3' end. The anchor ensured that the Oligo(dT) primers could bind at the start of the message, in order to avoid long regions of useless sequence.

For the synthesis of 1 sample: first strand cDNA, 1 μ l Oligo(dT)₂₃ Primers (70 μ M), 1 μ l 10 mM dNTP mix, 3 μ g of extracted RNA, and nuclease free water till a volume of 10 μ l were placed inside a thin-walled 200 μ l PCR tube on ice, which was gently mixed, and briefly spun down. The tube was heated up to 70 °C for 10 min using the SimpliAmp Thermal Cycler (Life Technologies). The tube was briefly spun down and placed on ice, and 2 μ l of 10x M-MLV Reverse Transcriptase Buffer, 7 μ l of nuclease-free water and 1 μ l of M-MLV Reverse Transcriptase were added and mixed by pipetting. The tube was incubated at room temperature for 10 min, in order for the Oligo(dT)₂₃ primers to be extended by the reverse transcriptase before the higher reverse transcriptase temperature. Finally, the tube was incubated at 37 °C, and the cDNA strand was produced. The reaction was terminated by heating up the reaction tube at 90 °C for 10 min, in order to denature the reverse transcriptase. The samples were stored at -20 °C. All the reagents of this section were purchased from Sigma Aldrich.

2. 11. 2. POLYMERASE CHAIN REACTION (PCR)

For the amplification of DNA fragments via PCR, the SimpliAmp Thermal Cycler (Life Technologies) was used.

In order to amplify MeCP2- α cDNA, the MECP2 cDNA ORF Clone in Cloning Vector pUC19 (SinoBiological) was used as template; while for the amplification of MeCP2- β cDNA, reverse transcribed RNA from cerebellar granule cells was used. For every PCR, approximately 80 ng of cDNA template, 12.5 μ l of CloneAmp HiFi PCR™ premix (Clontech), and 10 μ M of the primers, either *pSP64 MeCP2- α for* and *pSP64 MeCP2- α rev*, or *pSP64 MeCP2- β for* and

pSP64 MeCP2- β rev, were used. The final volume was adjusted to 25 µl by addition of nuclease free water. The reactions were performed in 0.2 ml thin-walled tubes (Biozym). The parameters of the PCR cycles are listed in Table 2.5.

Table 2. 5. General PCR cycling protocol.

Step	Temperature	Time	Cycles
Denaturation	98 °C	10 s	35
Annealing	62 °C	10 s	
Extension	72 °C	8 s	

2. 11. 3. PCR PRODUCT CLEAN-UP

In order to purify DNA products after a PCR reaction, from a tube, or from an agarose gel, NucleoSpin® Gel columns and PCR Clean-up Kit (Macherey-Nagel) was used according to the manufacturer's instructions.

2. 11. 4. AGAROSE GEL ELECTROPHORESIS

After PCR, the negatively charged DNA products were applied to an agarose gel in a horizontal electrophoresis chamber (BioRad) and separated by the application of constant voltage (100 - 150 V). For the preparation of the agarose gels, the agarose powder was dissolved in 1x TAE buffer by heating up the solution. For optimal resolution, the concentration of the agarose was decided depending on the size of the DNA product, as detailed in Table 2.6. For the visualization of the DNA, Roti-Safe GelStain (Carl Roth) was applied to the agarose solution (5 µl Roti-Safe/ 100 ml of solution). The solution was poured into a gel tray, and a 20 well comb was placed in order to create space for the samples. Afterwards, the solidified gel was transferred to an electrophoresis chamber, and immersed in 1x TAE buffer. For evaluating the size of the DNA products, a DNA ladder was applied to one of the wells. The DNA sample was mixed with Loading Dye (Thermo Fisher Scientific) and loaded into the wells. The gel was run for 25 - 40 min or until the dye reached the end of the gel. A picture of the gel was taken using the E.A.S.Y. UV-light documentation system (Herolab, Wiesloch, Germany).

Table 2. 6. Optimal agarose gel concentrations for resolving DNA fragments. *Modified from (Makovets, 2013).*

DNA fragment size	% agarose
4 – 12 kb	0.4 – 0.5 %
500 bp –10 kb	1 %
100 – 500 bp	2 %
40 – 100 bp	3 – 4 %

2. 11. 5. IN-FUSION CLONING METHOD AND PRIMER DESIGN

This cloning method is based on the ability of the In-Fusion enzyme to merge the PCR-generated insert with any linearized vector, by recognizing 15 homologous bp (base pairs) at its ends. The In-Fusion HD Cloning KIT (Clontech) was used in accordance to the manufacturer's instructions. Special primers were designed to include a 15 bp overhang on its 5' end which is homologous to 15 bp at one end of the linearized vector, followed by the 18-25 bp specific to the target PCR insert sequence. The primer melting temperature (T_m) was calculated as the T_m of the annealed part of the primer, not including the length of the whole primer. The T_m difference between forward and reverse primers were not more than 4 °C.

In order to generate the pSP64 Poly(A) vectors carrying MeCP2- α or MeCP2- β , the primers used (detail in section '2. 8') were: *pSP64 MeCP2- α for*, *pSP64 MeCP2- α rev*, *pSP64 MeCP2- β for*, *pSP64 MeCP2- β rev*.

For the vector carrying MeCP2- α , a sample of DNA obtained from reverse transcription of mRNA from cultured wild-type mouse cerebellar granule cells was used as template, and the primers *pSP64 MeCP2- α for* and *pSP64 MeCP2- α rev* were used. For generating the vector carrying MeCP2- β , the amplicon was obtained from the commercial vector MECP2 cDNA ORF clone in cloning vector pUC19 vector (SinoBiological).

After purification of the linearized vector and the insert, the In-Fusion cloning reaction was performed: a 0.2 ml thin-walled tube was prepared, containing 100 ng of linearized vector, 50 ng of insert, together with 4 μ l of 5x In-Fusion HD Enzyme Premix (Clontech), and nuclease free water till a total volume of 20 μ l. The reaction was incubated for 15 min at 50 °C, and placed on ice. 5 μ l of the reaction were used to transform *E. coli* One Shot™ TOP10 (Thermo Fisher Scientific).

2. 11. 6. LIC CLONING AND BASIS OF PRIMER DESIGN

The Ligation Independent Cloning (LIC) technology uses the 3' → 5' exonuclease activity, and the 5' → 3' polymerase activity of the T4 DNA polymerase to create specific 10-15 bp overhangs in the expression vector. The exonuclease activity removes nucleotides from the 3' ends of the DNA while the polymerase activity restores the chain using dNTPs and the complementary DNA strand as a template, as illustrated in Figure 2.1.

In the LIC protocol, only dGTP is included in the reaction, causing the 3'→5' exonuclease and 5'→3' polymerase activities to equilibrate at the first occurrence of cytosine in the complementary strand. The annealing of the insert and the vector occurs in the absence of ligase.

In order to produce a bacterial vector for the expression of recombinant MeCP2 protein in *E. coli*, the aLICator LIC Cloning and Expression System (Thermo Fisher Scientific) was used.

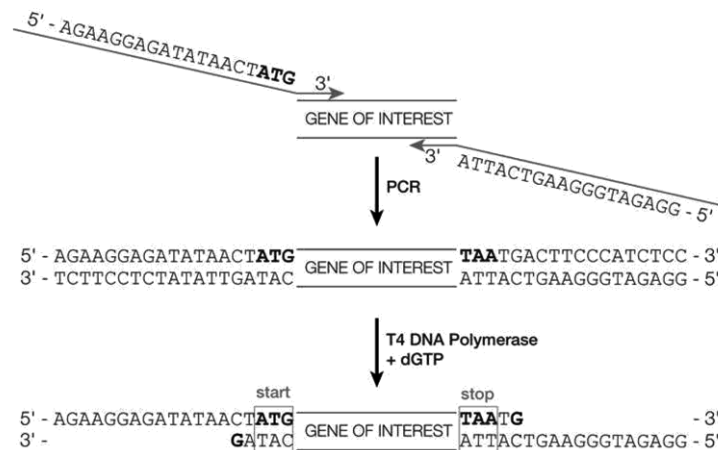


Figure 2. 1. Generation of sticky ends on the gene of interest with T4 DNA polymerase and dGTP.

For the design of the primers, it was ensured that the 5' end of the primer included vector-specific sequences and sufficient 3' overlap with the gene of interest. The melting temperature of the region of primer complementary to the gene of interest was 60 °C or higher. The primers used: *MeCP2v2ALI_for* and *MeCP2v2ALI_rev* are shown in section '2. 8'.

To linearize the pSP64 Poly(A) vector, the *HincII* restriction enzyme and NEB buffer were used (New England BioLabs-NEB). A 0.2 ml thin-walled tube was prepared, containing 500 µg (0.5 µl of insert DNA, 2.5 µl of NEB buffer, 0.5 µl (5 u) of *HincII*, and nuclease free water till a total volume of 25 µl. The tube was incubated for 30 minutes at 37 °C. The linearized vector was subjected to agarose gel electrophoresis, and purified as described in section '2. 11. 3'.

On the other hand, the pLATE52 vector was pre-linearized, so restriction digestion was not necessary. Once the insert was purified, the optimal amount of insert for the LIC reaction was estimated according to the manufacturer's protocol, for a length of 1488 bp, 96.72 ng of insert were used.

In order to generate the 5' and 3' overhangs, a 0.2 ml thin-walled tube was prepared, containing 2 μ l of 5x LIC buffer, 96.72 ng of insert, 1 μ l (1 U) of T4 DNA polymerase, and nuclease free water till a total volume of 10 μ l. The mixture was briefly vortexed, quickly spun down, and incubated at room temperature for 5 min. The reaction was stopped by the addition of 0.6 μ l of 0.5 M EDTA.

For the annealing reaction, 1 μ l of pLATE52 pre-linearized vector (60 ng) was added to the previous tube, briefly vortexed, quickly spun down, and incubated at room temperature for 5 min, and placed on ice. Finally, 5 μ l of the reaction were used to transform *E. coli* One Shot™ TOP10.

2. 11. 7. TRANSFORMATION OF *E. COLI* AND PLASMID ISOLATION

E. coli One Shot™ TOP10 were transformed after the In-Fusion, and LIC reactions for generating the vectors. 5 μ l of vector were pipetted into the tube containing 50 μ l of bacteria, which were gently mixed, and placed on ice for 30 min. The bacteria were heat-shocked at 42 °C for 45 s using a water bath, and immediately chilled down on ice for 2 min. 450 μ l of S.O.C. medium (Thermo Fisher Scientific) was added to the tube, which was incubated for 1 h at 37 °C with gentle shaking using a Thermomixer 5436 (Eppendorf). After incubation, 100 μ l of transformed bacteria were applied in a T-streak into LB (lysogeny broth) agar plates containing ampicillin, and grown at 37 °C for 24 h. The agar plate was then examined, and single colonies were picked and used to inoculate separated bacterial culture tubes containing 10 ml of LB containing ampicillin, which were grown at 37 °C under agitation (~180 rpm) overnight. From each culture, 9 ml were separated for small scale plasmid isolation, and 1 ml was kept for a short period at 4 °C in order to keep a sample of successful vector producing bacteria in case the DNA sequencing of individually isolated plasmids proved correct.

A bacterial culture tube containing 10 ml of LB containing the antibiotic of selection (100 μ g/ml ampicillin, 25 μ g/ml kanamycin, or both) was inoculated with a single bacterial colony and grown overnight at 37 °C under agitation (~180 rpm).

In order to perform small scale bacterial plasmid isolation ('Miniprep'), the NucleoSpin Plasmid kit (Macherey-Nagel) was used. The culture was centrifuged at 11,000 x g for 30 s in order to pellet the cells, and lysed as recommended by the NucleoSpin Plasmid kit (Macherey-Nagel)

protocol. Plasmid DNA was released from the bacteria by SDS/alkaline lysis, and bound to NucleoSpin columns. The plasmid DNA was eluted with elution buffer (5 mM Tris/HCl, pH 8.5).

For the isolation of large amounts of bacterial plasmid ('Maxiprep'), the NucleoBond Xtra kit (Macherey-Nagel) was used. The bacteria of the 10 ml tube (1st paragraph of this section) were transferred to a 1 l Erlenmeyer flask containing 300 ml of LB containing the selection antibiotic. The cells were pelleted at 6,000 x g for 15 min at 4 °C, and lysed as described in the manufacturer's protocol. The bacterial lysate was loaded into the filter columns and cleared by gravity flow. Plasmid DNA was eluted from the columns using the provided elution buffer, precipitated using isopropanol and dissolved in nuclease-free water.

The plasmid DNA concentration was measured using the NanoDrop 1000 spectrophotometer (Thermo Fisher Scientific). After aliquoting, the DNA was stored at -20 °C.

2. 11. 8. DETERMINATION OF DNA CONCENTRATION AND PURITY

The DNA concentration was determined using the NanoDrop 1000 spectrophotometer (Thermo Fisher Scientific) utilizing a small 1.5 µl sample of DNA, and 1.5 µl of the diluent used in the sample were used for taking the blank measurement of absorbance. The device uses the absorbance at 260 nm to estimate the amount of DNA, and the ratios of absorbance 260/280 nm, or 260/230 nm to assess purity (Wilfinger et al., 1997). The accepted 260/280 and 260/230 ratios for the DNA were approximately 1.8 and 2.0, respectively.

2. 11. 9. DNA SEQUENCING

To prepare DNA samples for sequencing, 500 ng DNA, and 10 pmol of primer and nuclease free water till a final volume of 8 µl were added to a 1.5 ml Eppendorf tube. The samples were sent to the ZMNH Core Facility Bioanalytics, where they were sequenced using the ABI PRISM Genetic Analyzer (Thermo Fisher Scientific). The electronic data were analysed by using '*Benchling: Cloud-Based Informatics Platform for Life Sciences*', and performing a sequence alignment with the reference DNA sequences.

2. 11. 10. EXPRESSION AND PURIFICATION OF RECOMBINANT PROTEINS

In order to synthesize CHL1-ICD and L1-ICD (Richter, 2002; Wolters, 2009), competent *E. coli* M15 pREP4 were transfected with pQE-30 vector carrying CHL1-ICD or L1-ICD, whereas for the production of MeCP2, competent *E. coli* One Shot™ BL21 Star™ (DE3) were transfected with the pLATE52 MeCP2- β vector.

For transformation, a 1.5 ml microcentrifuge tube containing 40 μ l of competent *E. coli* was thawed on ice, and 1-5 μ l of ligation reaction were pipetted directly into the vial, which was mixed by tapping gently. The vial was incubated on ice for 30 min, and heat shocked at 42 °C for 45 s in a water bath. The vial was then placed on ice for 2 min, and 250 μ l of S.O.C. medium were added to the tube. The tube was kept shaking for 1 h at 225 rpm using a Thermomixer 5436 (Eppendorf). 100 μ l of the transformation vial were streaked on an LB agar plate containing the antibiotic for selection, and incubated for 24 h at 37 °C.

Afterwards, a single colony of each transformant was inoculated to an Erlenmeyer flask containing 100 ml of LB supplemented with the selection antibiotic and grown overnight in 180 rpm agitation. The culture was transferred then to a larger Erlenmeyer containing 2 l of LB supplemented the antibiotic of selection, and incubated at 37 °C in agitation.

The OD₆₀₀ was measured every hour using a μ Quant™ Microplate Spectrophotometer (Bio-Tek Instruments, Bad Friedrichshall, Germany), once the OD₆₀₀ had reached a value between 0.6 and 0.8, IPTG (Isopropyl β -d-1-thiogalactopyranoside) was added to the culture at a final concentration of 1 mM. The culture was further incubated, and 500 μ l of culture were sampled periodically (before and after IPTG induction) as controls.

After 4-5 h, the culture was placed on ice for 10 min, and then centrifuged at 5,000 x g for 10 min at 4 °C. The supernatant was discarded, and the cell pellet was stored at – 20 °C.

The cell pellet was weighed, and for every gram of wet weight, 2-5 ml of lysis buffer for native purification were added in order to resuspend the pellet. Lysozyme to a concentration of 1 mg/ml was added to the lysate, and incubated on ice for 30 min. The lysate was sonicated at 6 intervals of 10 s on ice, and afterwards 10 μ g/ml RNase A, and 5 μ g/ml DNase I were added, and incubated for 15 min on ice. The lysate was then centrifuged at 10,000 x g for 30 min at 4 °C. The pellet (insoluble protein) was discarded, and the supernatant (soluble protein) was incubated together with Ni-NTA agarose beads (Qiagen) in a proportion of 1:5, and incubated overnight at 4 °C using an overhead shaker.

The agarose beads were pelleted by centrifugation at 1,000 x g at 4 °C for 4 min. The beads were then washed with 10 ml of the washing buffers 1, then 2, and 3 for 30 min, and pelleted by centrifugation at 1,000 x g at 4 °C for 4 min. The beads were finally incubated with 1 ml of elution buffer for 30 min, and pelleted again by centrifugation at 1,000 x g at 4 °C for 4 min.

The eluate was then dialyzed and concentrated in PBS using Vivaspin 20 columns (GE Healthcare) for 30 min at 5,000 x g. Samples of the bacterial culture and of the different washes and eluates were subjected to SDS-PAGE and the gel was stained with Coomassie blue to evaluate the success of the protein production.

2. 11. 11. IN VITRO CELL-FREE PROTEIN SYNTHESIS

The kits TnT® Coupled Wheat Germ Extract System and TnT® Coupled Reticulocyte lysate System were used (Promega). These systems offer coupled transcription/translation in a single tube.

Wheat germ was used for the production of MeCP2- α and MeCP2- β (using the pSP64 Poly(A) MeCP2- α and pSP64 Poly(A) MeCP2- β vectors), and reticulocyte lysate for the production of L1-70 and L1-30 (using pSP64 Poly(A) Vector carrying L1-30 or L1-70).

A 200 μ l PCR tube was prepared, containing 25 μ l of either TnT® wheat germ extract or TnT® reticulocyte lysate, 2 μ l of TnT® reaction buffer, 1 μ l of TnT® RNA polymerase SP6, 1 μ g of DNA for the specific protein (vectors mentioned above), 2 μ l of 1mM amino acid mixture, and nuclease free water to adjust a final volume of 50 μ l. The tube was incubated at 30 °C for 90 min.

2 μ l of the extract were analysed by WB in order to validate the production of the proteins of interest.

2. 11. 12. GENOTYPING OF MICE

For the genotyping, MyTaq Extract-PCR Kit (BIOLINE) was used.

To extract DNA, tailcuts from neonatal mice were sampled in 200 μ l PCR tubes, and in each tube, 20 μ l of Buffer A, 10 μ l of buffer B, and 70 μ l of nuclease free water were added. The tubes were briefly vortexed and incubated at 75 °C for 7 min, then 95 °C for 7 min.

After extracting the DNA, a master mix was prepared for the number of samples +1. The amounts for one sample consisted of 12.5 μ l of 2xRed Mix buffer, and then the primers:

For genotyping **L1-deficient mice**: the primers used 25 nM of L1arm2, 20 tTA-up3 nM, and 10 nM of L1 -5UP2 (sequence in section '2. 8'); water was added till a total volume of 23 μ l. 2 μ l of extracted DNA were added to the tube, which was vortexed. The tubes were incubated in the SimpliAmp Thermal Cycler (Life Technologies) as detailed in Table 2.7.

Table 2. 7. PCR cycling scheme for genotyping of L1 mice.

Step	Temperature	Time	Cycles
Initial denaturation	98 °C	3 min	1
Denaturation	98 °C	10 s	
Annealing	65 °C	1 min	35
Extension	72 °C	20 s	
Final extension	72 °C	1 min	1
Cooling	4 °C	∞	1

The PCR product was analysed by running a 2.5% agarose gel as described in section '2. 11. 4', The DNA marker was 1 kb Plus DNA Ladder (Thermo Fisher Scientific), and the running was performed at 150 V for 30 min. When imaging the gel, the genotypes were distinguishable as shown in Figure 2.2.

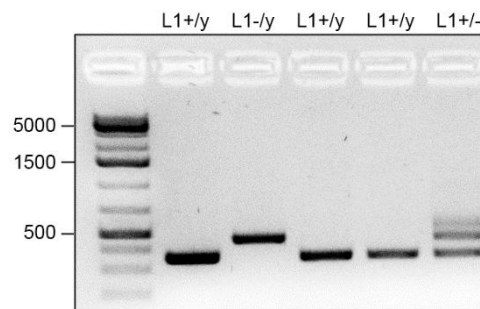


Figure 2. 2. PCR products after genotyping L1 mice. Showing wild-type mice ($L1^{+/y}$), $L1$ -deficient mouse ($L1^{-/y}$) and heterozygous female mouse ($L1^{+/-}$). A representative image of an agarose gel after DNA staining is shown.

For genotyping of **L1RA mice** the primers 25 nM of L1-RA fw, and 25 nM of L1-RA rev were used (sequence in section '2. 8'). The tubes were incubated in the SimpliAmp Thermal Cycler (Life Technologies) as shown in Table 2.8.

Table 2. 8. PCR cycling scheme for genotyping of $L1^{RA}$ mice.

Step	Temperature	Time	Cycles
Initial denaturation	98 °C	3 min	1
Denaturation	98 °C	10 s	
Annealing	60 °C	1 min	35
Extension	72 °C	20 s	
Final extension	72 °C	1 min	1
Cooling	4 °C	∞	1

Following PCR, restriction digestion of the PCR product was performed, preparing a restriction master mix for all samples+1. For one sample the mix contained: 3 μ l of Cutsmart Buffer (NEB), 1.8 μ l of nuclease free water, and 0.2 μ l (2 units) of *Acil* (NEB). 5 μ l of the restriction master mix were added to 25 μ l of PCR product, mixed, and incubated at 37 °C for 1 h.

Finally, the digestion product was loaded into an agarose gel, in the same way as in the genotyping of L1 mice (previous section). When imaging the gel, the genotypes were distinguished as shown in Figure 2.3.

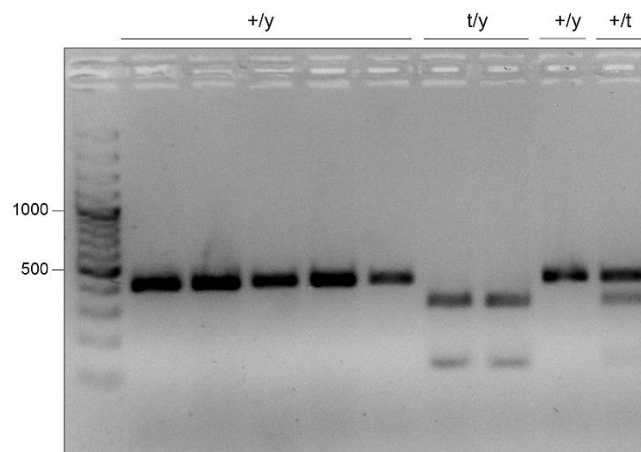


Figure 2. 3. DNA fragments after genotyping $L1^{RA}$ mutant mice, showing wild-type mice (+/y), mutant mice (t/y) and heterozygous female (+/t). A representative image of an agarose gel after DNA staining is shown.

2. 11. 13. DESIGN OF SHRNAS

Short hairpin RNAs (shRNAs) are artificial RNA molecules with a tight hairpin turn, which are used to silence target gene expression via RNA interference (RNAi). This is important for my thesis in the context of investigating the impact of the MeCP2 knockdown on L1-functions.

I selected a target sequence to be encoded in adeno associated viruses (AAVs) in order to knockdown MeCP2- α and MeCP2- β in neurons.

For choosing the target, different considerations were taken into account and implemented: the sequence was present in all targeted isoforms, had a length of 19 bp (as most effective shRNA targets), started with a G (because this shRNA is expressed from a U6 promoter), and the target did not overlap with potential SNP regions (Taxman et al., 2010).

A *BLAST* search was performed in order to eliminate potential target sequences with a matching 16 nucleotides or more to off-target mouse genes.

The sequence was selected considering all the above, from the outputs shown in Figure 2.4, generated by the online tool *BLOCK-iT™ RNAi Designer* (Thermo Fisher Scientific).

A scrambled control (non-targeting shRNA including the same nucleotides in scrambled order) which also controlled for potential side effects of the viral transduction, was also generated. Exact sequences shown in Figure 2.5.

Oligo Type	Oligo Sequence
Top Strand	5' - CACCGCCGATCTGCTGGAAAGTATGCGAACATACTTTCCAGCAGATCGGC -3'
Bottom Strand	5' - AAAAGCCGATCTGCTGGAAAGTATGTTTCGCATACTTTCCAGCAGATCGGC -3'
ds Oligo	5' - CACCGCCGATCTGCTGGAAAGTATGCGAACATACTTTCCAGCAGATCGGC -3' 3' - CGGCTAGACGACCTTTCATACGCTTGTATGAAAGGTCGTCTAGCCGAAAA -5'

Figure 2. 4. Output from the online tool BLOCK-iTTM RNAi Designer. (Thermo Fisher Scientific).

Cloning of the viral vector was performed by Dr. Ingke Braren, at the Vector Facility (Universitätsklinikum Hamburg-Eppendorf, Germany). The final MeCP2 shRNA sequence was assembled as shown in Figure 2.5.

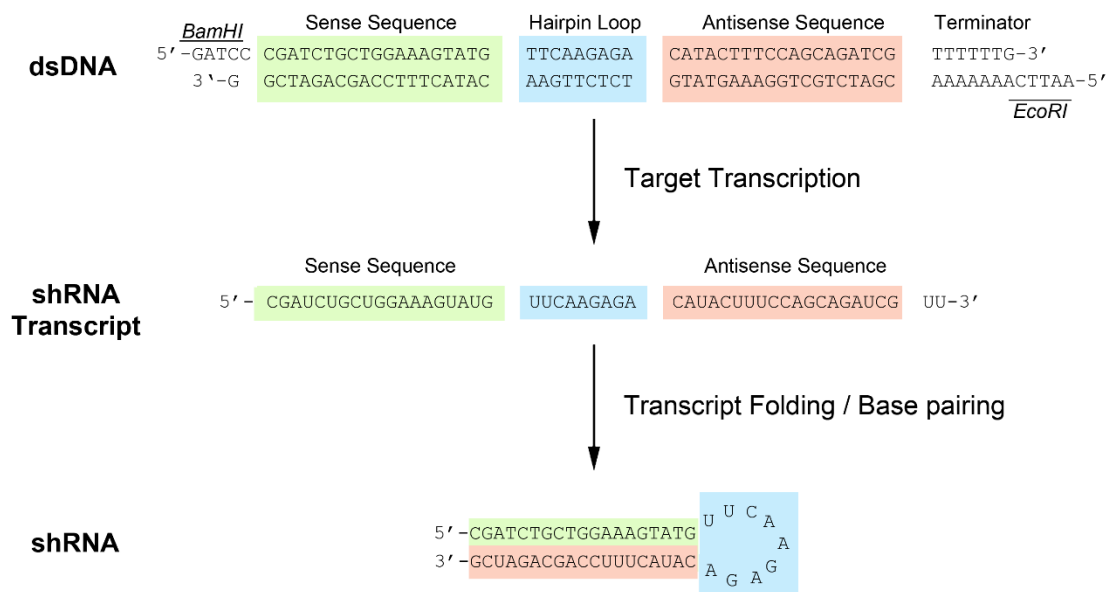


Figure 2. 5. Final sequence and structure used for MeCP2 knockdown.

dsDNA used for shRNA scrambled sequence control:

	Sense Sequence	Linker	Antisense Sequence
5'-	GGTCGCTAATGACGTATGA	TTCAAGAGA	TCATACGTCATTAGCGACC -'3
3'-	CCAGCGATTACTGCATACT	AAGTTCTCT	AGTATGCAGTAATCGCTGG -'5

2. 12. BIOCHEMICAL METHODS

2. 12. 1. PREPARATION OF BRAIN AND CEREBELLAR EXTRACTS AND CELL LYSATES

Brains or cerebella were homogenized in ice-cold RIPA buffer (0.5 – 1 ml/cerebella or brain) containing protease inhibitor cocktail (Roche). An Elvehjem Potter was used to disrupt the tissue. The homogenates were pelleted at 17,000 x g for 15 min and 4 °C, and the liquid phase was recovered as brain/ cerebellar extract.

For the recovery of cell lysates, the cell cultures were placed on ice and the culture medium was removed. The cells were lysed using 80 µl of RIPA buffer containing protease inhibitor cocktail for every 1.6 cm². The plate was kept on ice for 15 min with gentle shaking. Finally, the cell lysates were collected and pelleted at 17,000 x g for 15 min and 4 °C.

2. 12. 2. DETERMINATION OF PROTEIN CONCENTRATION

In order to determine the protein concentration, the Bicinchoninic acid (BCA) Protein Assay Reagent Kit (Thermo Fisher Scientific) was used. A small fraction of the sample whose concentration had to be determined, was diluted several times (more or less diluted depending on the suspected approximate initial concentration), and 10 µl from each dilution were placed in a microtiter 96-well plate. As standard, different dilutions of bovine serum albumin (BSA) at concentrations of 62.5, 125, 250, 500, 1000, 2000 µg/ml were prepared and placed in the 96-well plate. The plate was incubated for 30 min at 37°C, and the absorbance was measured at 562 nm using the µQuant™ spectrophotometer (Bio-Tek Instruments). The calibration of the absorbance curve of the BSA standards provided the information for determining the protein concentration of the samples.

2. 12. 3. SDS – PAGE GEL ELECTROPHORESIS

Proteins were separated by SDS-PAGE using the Mini-Protean II system (Bio-Rad). The protein samples were diluted in 1x Laemmli buffer for a final concentration of 3.3 mg/ml. The proteins of the samples were denatured by heating up the sample at 95 °C for 5 min, and loaded in a 10%Tris-glycine SDS polyacrylamide gel (40 µg of protein/well). The gels were run using a Power Pac 200 (Bio-Rad) at an initial voltage of 75 V for 15 min and at 140 V until the bromphenol blue of the Laemmli buffer ran out of the gel. As a molecular weight standard, the PageRuler™ Plus Prestained Protein Ladder (Thermo Fisher Scientific) was used. The gel was either used for Western Blot, or for Coomassie Blue staining.

2. 12. 4. COOMASSIE STAINING OF POLYACRYLAMIDE GELS

Coomassie staining allows us to visualize the proteins separated by the SDS-Page electrophoresis. The gels were stained using the RotiBlue kit (Carl Roth). The gels were placed in a plastic container containing the Roti-Blue staining solution overnight with gentle shaking. The next day the gel was washed several times using Coomassie washing solution till the background was reduced. The gel was visualized using a light table, and scanned using a documents scanner for obtaining a digital image.

2. 12. 5. WESTERN BLOT ANALYSIS

Western Blot analysis was used in order to identify and examine relative quantity of proteins. The Mini Trans-Blot[®] blotting system (Bio-Rad) was used to transfer proteins to nitrocellulose or PVDF membranes. For proteins larger than 20 kDa 0.45 µm nitrocellulose Amersham[™]Protran[™] (GE Healthcare) was used and for proteins smaller than 20 kDa, 0.20 µm PVDF membrane (Macherey-Nagel) pre-incubated in methanol for 5 min was used. Membranes were incubated, for 1 min in blotting buffer and then used for assembly of the blotting sandwich according to the manufacturer's instructions. The blotting sandwich was transferred to the blotting chamber, which was filled with ice-cold blotting buffer and placed on ice. The proteins were transferred at a constant voltage of 120 V for 1 h.

Following electrophoretic transfer, the membranes were placed in a glass container and blocked with 4% skim milk powder in TBS-T for 1 h at room temperature. The membranes were then incubated overnight with primary antibodies diluted in 4% skim milk powder in TBS-T or 4% BSA in TBS-T at the manufacturer's recommended concentration. Afterwards the membranes were washed 4 times for 5 min with TBS-T, and incubated with HRP-coupled secondary antibodies for 1 h at room temperature. The membranes were washed 4 times for 5 min with TBS-T, and visualized using ECL select or ECL prime reagents (Amersham, GE Healthcare) and the LAS4000 Mini f (GE Healthcare, Freiburg, Germany).

2. 12. 6. QUANTIFICATION OF RELATIVE PROTEIN CONCENTRATIONS

In all the quantified Western Blots, a reference protein was used (GAPDH or α Tubulin). The quantification of relative protein concentrations was performed using the software *Image Studio Lite* from LI-COR Biosciences. Briefly, in the picture visualizing the bands of the membrane, each band was selected using the 'Draw rectangle' tool. On the 'profiles tab' the profile plots were shown, and their intensity values were displayed in the table on the 'shapes' section (bottom). The values appearing under 'signal' were used for analysis, by copying them

to *Excel*, and calculating the ratio between the signal value of the protein of interest, and the one of the protein of reference (GAPDH or α Tubulin).

2. 12. 7. ELISA

The ELISA was performed as follows: 25 μ l of 5 μ g/ml MeCP2 (NP_004983.1, amino acids 1-486; Abnova; Taipei, Taiwan) full-length recombinant protein with GST-tag were substrate-coated in a 384-well microtiter plates with high binding surface (Corning, Tewksbury, MA, USA) at 4 °C overnight. After washing with DPBS with Ca^{2+} and Mg^{2+} pH 7.4, blocking with 1% w/v bovine serum albumin in PBS at room temperature for 1 h, and washing with PBS-T (PBS with 0.005% Tween 20), increasing concentrations of recombinant L1 intracellular domain (L1-ICD) with His-tag or CHL1 intracellular domain (CHL1-ICD) with His-tag (control) were added as ligand and incubated at room temperature for 1 h under gentle agitation. After washing several times with PBS-T, primary mouse monoclonal anti-L1-ICD antibody (CD171 (L1CAM) #838101 (BioLegend); 1:200) or primary goat polyclonal anti-CHL1-ICD antibody (CHL1 (C-18) #sc-34986 (Santa Cruz Biotechnology) 1:200) were applied and incubated for 1 h, and after several washes with PBST (Phosphate buffered saline 0.005 % tween20) followed by application of secondary antibodies and incubation for 1 h, either anti-mouse HRP-coupled secondary antibody (Dianova Hamburg, Germany; 1:2,000) or an anti-goat HRP-coupled secondary antibody (Dianova; 1:2,000). Wells were washed again with PBS-T, and ortho-phenylenediamine dihydrochloride (ThermoFisher Scientific) was used for detection of bound L1 and CHL1 intracellular domains. The reaction was terminated by addition of 25 μ l 2.5 M sulphuric acid. Absorbance was measured at 492 nm with an ELISA reader (μ Quant; BioTek).

2. 12. 8. LABEL-FREE BINDING ASSAY (BIND)

To confirm the interaction between L1-ICD and MeCP2 complementing the ELISA, photonic crystal optical biosensors were used as alternative method. Optical biosensors based on photonic crystals can be used to measure the electric adsorption of biomolecular materials thanks to their greater dielectric permittivity at optical wavelengths compared to water (Cooper, 2002). The biosensor used (SRU Biosystems) includes a narrowband guided-mode resonance filter, in which the reflected colour is modulated by the attachment/detachment of biochemical material to the surface (Cunningham et al., 2004). One of the main advantages of this method is the possibility of detecting protein-protein interactions without the necessity of labelling the proteins or to use antibodies, reducing the consequences of unspecific binding. 384 well plates with titan oxide surface (SRU Biosystems, Woburn, TX, USA) were washed three times with PBS containing Ca^{2+} and Mg^{2+} (PAA Laboratories) (PBS+), and coated

overnight at 4 °C with 125 ng of MeCP2 (NP_004983.1, amino acids 1 - 486; Abnova) full-length recombinant protein with GST-tag.

Wells were washed three times with PBS+ and the peak wavelength shift (PWV) was measured (BIND PROFILER; SRU Biosystems). To control for sufficient coating, wells were then blocked with 2% BSA in PBS+ for 3 h at room temperature. After three washes with PBS+, peak wavelength shift was determined, and different amounts of ligands (L1-ICD or CHL1-ICD) in PBS+ were added to the wells. Binding of ligands to substrate-coat protein was measured every 30 s during 60 min. The values obtained from wells without ligands were considered background, and subtracted from the values obtained from the wells with ligand solution. All the interaction tests were performed in triplicates.

2. 12. 9. CO-IMMUNOPRECIPITATION USING NUCLEAR PROTEIN EXTRACTS FROM MOUSE BRAINS

200-500 µg of nuclear protein were incubated together with 5 µg of primary antibody directed against an epitope in the intracellular domain of L1 (NCAM-L1 (C-2): #sc-514360 (Santa Cruz Biotechnology)) or MeCP2 (MeCP2 D4F3 XP Rabbit mAb #3456 (Cell Signaling Technology)), or IgG control of the same species (Dianova). DPBS with Ca²⁺ and Mg²⁺ was added to the mixture until a total volume of 250 µl was reached, and the solution was incubated overnight at 4°C with gentle rotation. To isolate the antibodies with their attached proteins, magnetic beads coupled with protein G (20 µl, corresponding to 0.62 mg protein G) were added to the mixture, and the samples were then incubated for 2 h at room temperature with gentle rotation. Subsequently, the beads were washed 4 times with DPBS and separated with a magnet for removing the liquid phase containing non-bound proteins. The magnetic beads were suspended in 15 µl of 1x Laemmli sample buffer and boiled for 5 min at 95°C. Finally, the beads were separated using a magnet, and the liquid phase was applied to a 10% SDS-PAGE gel for detection of proteins by Western Blot.

2. 12. 10. CO-IMMUNOPRECIPITATION USING IN VITRO EXPRESSED PROTEINS

The L1 fragments L1-30 and L1-70 were produced using the cell free in-vitro protein expression system TNT® SP6 Reticulocyte Lysate Systems (Promega), and MeCP2- α and MeCP2- β were produced using the TNT® SP6 High-Yield Wheat Germ (Promega), following the manufacturer's guide, and described in section '2. 11. 11'.

For preclearing of the sample, 10 µl of magnetic beads coupled with protein G, corresponding to 0.31 mg of protein G, were incubated together with 25 µl of reticulocyte lysate expressed L1-30 or L1-70, and 25 µl of wheat germ expressed MeCP2- α or MeCP2- β for 30 min at 4 °C. The beads were then separated from the sample using a magnet and discarded, the precleared solution was used for further analysis. For co-immunoprecipitation, 1 µg of primary antibody directed against L1-ICD (Santa Cruz Biotechnology) was added to the precleared solution, and PBS was added to the sample until a total volume of 200 µl was reached. Samples were incubated for 1 h at 4 °C with gentle rotation. To isolate the antibodies with their attached proteins, 10 µl of protein G-coupled magnetic beads were added to the sample, and incubated overnight at 4 °C with gentle rotation. The beads were then washed 4 times with PBS and separated with a magnet for removing the liquid phase containing non-bound proteins. The magnetic beads were suspended in 15 µl of 1x Laemmli sample buffer and boiled for 5 min at 95 °C. Finally, the beads were separated using a magnet, and the liquid phase was applied to a 10% SDS- PAGE gel for detection of proteins by Western Blot.

2. 12. 11. RNA ISOLATION FROM CELL LYSATES

For the RNA extraction from cells, the RNeasy Plus Mini Kit (Quiagen) was used, considering the recommendations of the manufacturers. Briefly: cultured cerebellar granule cells of p7 (postnatal day 7) wild-type mice ($3 \cdot 10^6$ cells) were disrupted by the addition of 350 µl of Buffer RLT Plus supplemented with 10% mercaptoethanol. The lysate was pipetted into a QUIAshredder spin column placed into a 2 ml collection tube, and centrifuged for 2 min at maximum speed. The homogenized lysate was transferred into a gDNA eliminator spin column placed in a 2 ml collection tube and centrifuged at 8,000 x g for 30 seconds. The column was discarded and 350 µl of 70% ethanol were added to the flow-through and mixed by pipetting. The sample was transferred into a RNeasy spin column placed in a 2 ml collection tube, and centrifuged at 8,000 x g for 15 s. The flow-through was discarded, and 700 µl of Buffer RW1 were added to the column, which was centrifuged at 8,000 x g for 15 s. Flow-through was discarded, and 500 µl of Buffer RPE were added to the column, which was centrifuged at 8,000 x g for 15 s; this cleaning step was repeated twice, followed by centrifugation at 10,000 x g for 2 min. In order to elute RNA from the column, the column was transferred to a new 1.5 ml collection tube, and 30 µl of RNase-free water was added directly into the column and the column was centrifuged at 8,000 x g for 1 min to elute the RNA.

RNA concentration and purity of the eluate was determined using the NanoDrop 1000 spectrophotometer (Thermo Fisher Scientific). The concentration was evaluated by examining the absorbance at 260 nm, and its purity by using the absorbance ratios 260 nm/280 nm, and

260 nm/230 nm. A 260/280 ratio of ~2 is considered pure for RNA. A high 260/230 ratio may indicate the presence of co-purified contaminants. The 'pure' RNA accepted value ranged from 2.0-2.2. Extracted RNA was frozen at -80 °C for further use.

2. 13. CELL CULTURE METHODS AND ASSAYS

2. 13. 1. PREPARATION OF COVERSLEIPS

For performing immunocytochemistry of cultured cerebellar primary granule cells and primary cortical neurons, the glass coverslips needed to be coated with PLL, as follows:

Glass coverslips were placed inside an Erlenmeyer flask, and immersed in 3 M hydrochloric acid solution, at room temperature and for 30 min in gentle shaking. The coverslips were then washed twice with ddH₂O, immersed in acetone for 3 h at room temperature in gentle shaking, and washed 5 times with ddH₂O. The coverslips were then washed twice for 10 min with absolute ethanol. The Erlenmeyer flask containing the coverslips was then heated up to 160 °C for 2 h. From this point the steps were performed under sterile conditions, the coverslips were cooled down at room temperature, and coated with sterile 0.01 % PLL in ddH₂O overnight at 4 °C in gentle shaking. The coverslips were washed twice with autoclaved ddH₂O and dried under the hood at room temperature. Finally, they were stored in a sterile 50 ml Falcon tube until used.

2. 13. 2. CULTURE OF MOUSE PRIMARY CEREBELLAR GRANULE CELLS

In order to culture cerebellar granule cells, 6 to 8-day-old wild-type, L1-deficient, or L1^{RA} mutant mice were used. The mice were sacrificed by decapitation, and using clean and sterilized dissection material (scissors, forceps and tweezers), the cerebella were extracted and placed inside of a petri dish containing ice-cold HBSS. Under the stereomicroscope, the cerebella were cleaned from blood vessels and placed into a new petri dish containing ice-cold HBSS. Each cerebellum was cut in 3 pieces, and placed inside of a 15 ml Falcon tube and washed using 5 ml of ice-cold HBSS/ 3 cerebella. The HBSS was discarded and 1 ml/ 3 cerebella of trypsin/DNase solution was added to the tube, which was incubated for 15 min at room temperature. The trypsin/DNase solution was discarded, the cerebella were washed 3 times using 5 ml/ 3 cerebella of ice-cold HBSS, and 1 ml/ 3 cerebella of DNase solution was added to the tube. The cerebella were then disrupted using 3 glass Pasteur pipettes with rounded tip, from wider to thinner diameter, till obtaining a single cell suspension. The cells were then centrifuged for 15 min at 1000 x g at 4°C. The cell pellet was then suspended in medium X-1 without serum if cultured for 1-2 days, or with serum if cultured for a longer time.

10 μ l of the cell suspension were mixed 1:1 with 0.4% trypan blue solution to determine the cell number under the microscope using a glass Neubauer chamber. The cells were then diluted to a density of $1-2 \times 10^5$ cells/ml for neurite outgrowth experiments, or $1-2 \times 10^6$ cells/ml for everything else, seeded on PLL-coated 6-well-plates or glass coverslips, and cultured for at least 24 h at 37°C, in 5% CO₂ and in 90% relative humidity.

2. 13. 3. CULTURE OF MOUSE PRIMARY CORTICAL NEURONS

For the culture of cortical neurons, embryos were collected on the embryonic day 16-18.

Using sterilized tools, after sacrificing the female using CO₂, the abdomen was sprayed with 70% ethanol, and using sterilized surgical tools, the uterus was exposed, and cut in order to extract the embryos, which were transferred to a clean petri dish containing ice-cold HBSS. The heads of the embryos were separated, and fixed to a Sylgard dish, where the skin and skull were opened, and both cortical lobes dissected. Each cortex was cut into 1.5 mm³ pieces, which were collected and mixed with 2 ml of ice-cold HBSS and placed in a 15 ml Falcon tube. 100 μ l of Trypsin solution were added, and the tube was incubated for 30 min at 37 °C. After the incubation, the tissue pieces were spun down by centrifuging at 1,500 x g for 3 min at 4 °C, the supernatant was discarded, and after addition of 5 ml of ice-cold HBSS the tube was centrifuged again. The supernatant was discarded, 2 ml of pre-warmed (37 °C) culture medium were added, and the tissue was disrupted using 3 glass Pasteur pipettes with rounded tip, from wider to thinner diameter, till attaining a single cell suspension. 10 μ l of the cell suspension were mixed with 1:1 with 0.4% trypan blue solution to determine the cell number under the microscope using a glass Neubauer chamber. The cells were then diluted to a density of $1-2 \times 10^6$ cells/ml, and seeded on PLL-coated 6-well-plates or glass coverslips, and cultured for at least 24 h at 37°C, in 5% CO₂ and in 90% relative humidity.

2. 13. 4. CULTURE AND DIFFERENTIATION OF MOUSE NEURAL STEM CELLS

Undifferentiated neural stem cells (NSCs) were seeded in ECM gel coated glass coverslips and initially grown in culture medium for maintenance. In order to achieve differentiation, they were grown for 3 days in induction medium (5 ng/ml FGF-2, 1% N2, and 2% B27), followed by 4 days in differentiation medium (1:1 mixture of culture medium for maintenance and Neurobasal, supplemented with 0.25% N2 and 2% B27).

2. 13. 5. STIMULATION OF L1-SIGNALLING

The L1 antibody 557 recognizes a sequence within the 3rd FNIII repeat of L1 (aas 818- 832), and promotes neurite outgrowth to the same extent as the substrate-bound L1 molecule itself (Holm et al., 1995).

Stimulation of L1-signalling was thus performed by addition of antibody 557 (final concentration of 25 µg/ml) to cerebellar granule cells in culture, 1 h after seeding. The antibody remained in the medium for 24 hours, until fixing with 4% formaldehyde in PBS.

2. 13. 6. CELL TRANSDUCTION USING AAVs

Different AAVs (section '2.9') were used for transduction, for knockdown, expression or overexpression of proteins. For transducing cells, the virus was simply applied directly to the cells in culture, for 48 h (AAVs for L1 expression), or 7 days for AAVshRNA for MeCP2 knockdown.

For achieving L1 expression using AAVs carrying L1, a MOI of 1,000 was used (Kraus, Kleene, Henis, et al., 2018). In order to achieve MeCP2 knockdown, the AAV1-s0cCMV-GFP U6-MecP2 or its scrambled control were used at a MOI of 3000, in cerebellar granule cell cultures, or cortical neuron cultures.

The effectiveness of the shRNA for MeCP2 was tested in cerebellar granule cell cultures at different timepoints using immunostainings and Western Blot (after 24, 48, 72, 94, 124, 146 and 158 hours), and using different MOIs (300, 1000, 3000, 5000). The half half-life of MeCP2-β is as long as 100 h (Ausió et al., 2014), and this isoform is the most abundant in the cerebellar granule cells (Olson et al., 2014), therefore effective knockdown of MeCP2 occurred 7 days after addition of the virus of the cells, as shown in the results from the Western Blot from transduced cell lysates in Figure 2.6.

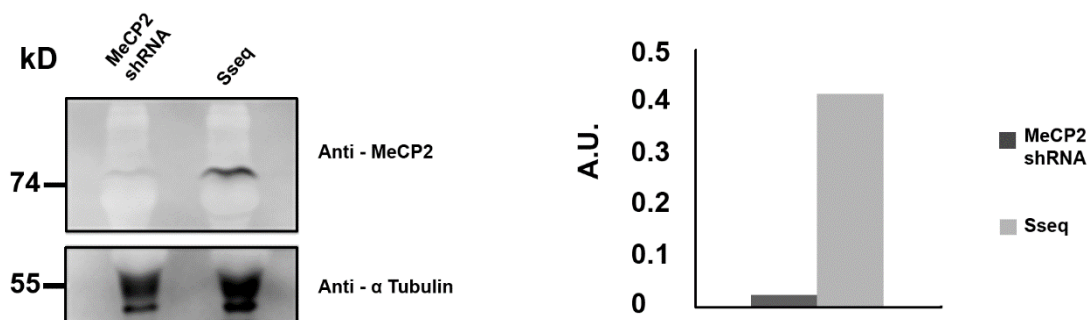


Figure. 2. 6. Effectiveness of MeCP2 knockdown using shRNA in cerebellar granule cell cultures. WB from cerebellar granule cell lysates 7 days after MeCP2 knockdown using AAVs containing MeCP2 shRNA (MeCP2 shRNA) or Scrambled sequence (Sseq) MOI 3000.

2. 13. 7. NEURITE OUTGROWTH ASSAY

Cerebellar granule cells were seeded on PLL-coated glass coverslips and maintained in serum-free medium. After 24 hours, the cells were fixed in 4% formaldehyde for 15 minutes at room temperature. The coverslips were then stained as described in section '2. 14. 1', using primary antibodies against GFP and β III-tubulin. After mounting, pictures were taken using the microscope ZEISS Apotome.2, and the neurites of at least 100 neurons per condition were measured (longest neurite of the neuron, at least longer than twice the size of the cell body) using the plugin *NeuronJ* from *ImageJ2* software.

2. 14. IMMUNOSTAININGS AND HISTOLOGY

2. 14. 1. IMMUNOCYTOCHEMISTRY

The cells (cerebellar granule cells, cortical neurons, or neural stem cells) in glass coverslips, were fixed for 15 min at room temperature using 4% formaldehyde in homemade PBS. The cells were washed twice with PBS, and incubated in 50% methanol solution for 30 min at room temperature. After 2 washes with PBS, the cells were blocked using blocking solution (containing 2% Bovine albumin serum 1% (v/v) TritonX-100 in PBS). After blocking, corresponding primary antibodies dissolved in PBS were added at the appropriate concentrations and incubated overnight at 4 °C. The cells were washed 5 times with PBS, and appropriate secondary antibodies against the species of the primary, were dissolved in PBS (1:200) added to the cells, and incubated for 2 h at room temperature. The coverslips were then washed 5 times with PBS, and the coverslips were mounted using Roti®-Mount FluorCare DAPI (Carl Roth) or Shandon Immu-Mount (Thermo Fisher Scientific) adding DAPI stain at 1 μ g/ml.

2. 14. 2. PERFUSION OF THE MOUSE BRAIN

The adult mice (L1^{-y} and L1^{+y}) were anesthetized by intraperitoneal injection of ketamine/xylazine mixture (up to 80 mg/kg body weight ketamine and 10 mg/kg body weight xylazine). The depth of the anaesthetic plane was determined by using the pinch-response method, and once there was no response, the mouse was fixed to a plastic surface using adhesive tape. A 5 cm lateral incision just beneath the rib cage, through the integument and abdominal wall, was cut. The liver was carefully separated from the diaphragm, which was cut from its connection to the thoracic pleura. The ribs were cut carefully from both sides up to the collarbone, and a haemostat was clamped to the sternum and placed over the head of the mouse in order to expose the heart. A small incision was performed on the posterior end of

the left ventricle, and an olive-tipped perfusion needle was passed through the cut ventricle into the ascending aorta, and fixed there using a little bulldog forceps. Finally, a small incision was performed on the right atrium of the animal, for the perfusion to begin.

A plastic outlet was attached to the needle, and 10 ml were pumped to a pressure of around 80-130 mm Hg, followed by 50 ml of the fixative 4% formaldehyde solution.

After the fixation was done, the brain was collected and stored in fixative for 24 h at 4°C. Afterwards the brain was immersed in 30% sucrose in PBS for cryoprotection, and incubated for 2 days at 4°C, then frozen for 2 minutes in 2-methyl-butane precooled to -80 °C and stored at -80 °C until use.

2. 14. 3. IMMUNOHISTOCHEMISTRY

Twelve-day-old L1^{-y} and L1^{+y} mouse littermates were sacrificed by decapitation. The brains were dissected and fixed in 4% paraformaldehyde (in 0.2 M phosphate buffer) for 14 days, immersed in 30% sucrose (in 0.2 M phosphate buffer) for cryoprotection and incubated for 2 days at 4 °C. The brains were then frozen for 2 minutes in 2-methyl-butane precooled to -80 °C and stored at -80 °C until use.

For the adult mouse brains, the animals were perfused with formaldehyde as described in section '2. 14. 2'; cryoprotection and freezing of the brains was performed as explained in the previous paragraph.

The brains were cut in serial sagittal or coronal sections of a thickness of 25 µm in a cryostat (Leica CM3050, Leica Instruments). The sections were then stored in PBS containing 0.02% sodium azide at 4 °C in a 48-well plate.

Free floating sections were treated with 50% methanol in ddH₂O at room temperature for 15 minutes, washed with PBS (3 x 5 min), and blocked using 4% normal goat serum with 1% Triton X-100 for 1 h at room temperature. The sections were incubated with primary antibodies diluted in PBS for L1-ICD (1:100 NCAM-L1 (C-2)) and MeCP2 (1:200 MECP2 (D4F3)) diluted in PBS at 4 °C overnight. After washing with PBS (3 x 5 min), the sections were incubated with fluorescently labelled secondary antibodies (1:200 in PBS; Cy3 goat anti-mouse, and Cy5 goat anti-rabbit, Dianova) for 2 hours at room temperature in the dark. Afterwards the sections were washed with PBS (3 x 5 min), shortly dried, and mounted on SuperFrost Plus glass slides (Carl Roth) with mounting solution containing the nuclear marker DAPI (Roti-Mount FluorCare DAPI, Carl Roth).

2. 14. 4. PROXIMITY LIGATION ASSAY

Proximity ligation assay allows the in-situ detection of protein interactions with high specificity and sensitivity. Two primary antibodies from different species are used to detect the two protein targets of the sample (cells or tissue), and a pair of oligonucleotide-labelled secondary PLA probes bind to the primary antibodies. Hybridizing connector oligos are then added to the sample, and they bind to the PLA probes only if the complementary probes are in close proximity (<40 nm), and ligase forms a closed circle DNA template which is used for rolling-circle amplification. The PLA probe acts as a primer for a DNA polymerase, which generates concatemeric sequences during rolling-circle amplification. Labelled oligonucleotides hybridize to the complementary sequences in the amplicon, and are then visualized as discrete spots (PLA signals) by microscopy image analysis.

The proximity ligation assay was performed using Duolink PLA products according to the manufacturer's protocol (Sigma-Aldrich; Duolink PLA technology). Cerebellar granule cells from L1^{y/-} and L1^{y/+} mice were used. Cells were blocked using Duolink blocking solution supplemented with 0.5% Triton X-100 and incubated for 24 h at 4 °C with mouse monoclonal L1 antibody C-2 and with either rabbit polyclonal PSPC1, NonO or SFPQ antibody diluted 1:10 in Duolink antibody diluent. Cells were washed 2 times using Duolink Wash Buffer A and incubated with a mixture of secondary antibodies conjugated with oligonucleotides (Duolink anti-mouse PLA probe MINUS and Duolink anti-rabbit PLA probe PLUS. Then the proximity ligation reaction was performed according to the manufacturer's protocol using the Duolink detection reagents RED. The coverslips were mounted using Roti-Mount FluorCare DAPI (Carl Roth) and 10 images per condition were taken using an Olympus F1000 confocal microscope. The images were analysed using the *ImageJ2* software.

2. 14. 5. CONFOCAL MICROSCOPY

Before performing experiments involving fluorescence microscopy, the spectral characteristics of the dyes used were carefully examined, by using the *BD Biosciences Spectrum viewer online tool*, narrowing the detection window for the channels and using the sequential mode of acquisition minimized cross talk between channels.

For sampling appropriately, the online *Nyquist calculator* from *Scientific Volume Imaging* was used, providing information for acquiring images with a good optical resolution to pixel size relationship.

Finally, the sensitivity of the detectors and the intensity of the lasers were carefully set, in order to avoid saturated pixels, and therefore information loss or background noise.

2. 14. 6. ANALYSIS OF PLA SIGNAL

In order to distinguish which PLA signals were inside of the nucleus, the colour of the image was modified for the red pixels (signal of Texas red without mixing with the blue of the nuclear DAPI staining) switching the hue to yellow, while the magenta pixels (signal of Texas red mixed with the blue of DAPI) were left unchanged.

To quantify the number of PLA signals per cell, first the number of cells per image had to be measured. The RGB channels were split, and the area of DAPI signal was measured (total area occupied by cell nucleus), this value was divided by the average area of one cell, to calculate the number of cells per image. I programmed a macro in order to perform this process automatically with *ImageJ2* software:

```
setTool("line");
makeLine(916, 998, 1016, 1000);
run("Set Scale...", "distance=100.0200 known=10 pixel=1 unit=µm");
run("32-bit");
setAutoThreshold("Huang dark");
run("Threshold...");
setThreshold(14, 85);
run("Create Selection");
run("Measure");
String.copyResults();
```

For quantification of the number of red dots (signal of the proteins being in close proximity), the red channel was analysed using the threshold function and the particle analysis counter. The number of red dots per image was divided by the number of cells per image. I programmed a macro in order to perform this process automatically with *ImageJ* software:

```
run("32-bit");
setAutoThreshold("Default dark");
run("Threshold...");
setThreshold(29.67, 85);
setOption("BlackBackground", false);
run("Convert to Mask");
run("Analyze Particles...", "size=15-400 pixel add");
```

The average values of the number of red dots per cell were determined in all 10 images per condition and to assess the effect of stimulation using antibody 557 on the cells, the average values for the stimulated cells were normalized to the values for the non-stimulated cells (set to 100%).

2. 14. 7. ANALYSIS OF CO-LOCALIZATION

Fluorescence microscopy images were taken in order to compare subcellular distributions of MeCP2 and L1, and the degree of co-localization between L1 and MeCP2 was quantified by calculating the Pearson's Correlation Coefficient (PCC) and Manders' Colocalization Coefficients (MCCs) with the co-localization toolbox *Coloc2*, included in the *ImageJ2* software.

In order to adjust the parameters of *Coloc2*, the point spread function (PSF) was calculated using the *Nyquist calculator* from the *Scientific Volume Imaging* website. The background noise was reduced by using the *HiLo* function (*ImageJ2*) in order to remove the dimmest pixels around cells. After preparing the images by selecting the region of interest, *Coloc2* calculated the pixel grey values of each image from the red channel and these were plotted against the pixel grey values of each image from the green channel, and the Costes automatic threshold function was used. A 2D Histogram (the brighter the colour, the more pixels with those two intensity values for their two-colour channels) was created. Correlation can be observed by the presence of a cloud of information in the middle of the 2D histogram, which is then fitted to a linear regression.

Coloc2 was used to calculate the PCC, and MCCs. The PCC measures the pixel-by-pixel covariance in the signal levels of two images, as it subtracts the mean intensity from each pixel's intensity value, PCC is independent of signal levels and signal offset (background), and the value of the coefficient ranges between 1 for perfect correlation, 0 for no correlation, and -1 for perfect anti-correlation. Alternatively the MCCs accounts for the total amount (or abundance) of fluorophores that overlap with each other, and this results in two coefficients (one for each fluorophore's overlap), providing an important distinction over the simpler area overlap calculation of PCC (Aaron et al., 2018). Unlike PCC, MCCs strictly measures co-occurrence independent of signal proportionality. The value of MCCs ranges from 0 to 1, expressing the fraction of intensity in a channel located on the same pixel where there is above zero (or threshold) intensity in the other colour channel.

2. 15. TRANSDUCTION IN VIVO USING AAVS

To elucidate the functional consequences from the interaction between L1 and MeCP2, the possibility of knocking down or overexpress MeCP2 *in vivo* and observing its effects on L1-related events of postnatal development, was a promising idea. This could be achieved by the injection of AAVs carrying MeCP2 shRNA or MeCP2 overexpression sequences, into the neonatal mouse brain.

2. 15. 1. INTRACEREBROVENTRICULAR INJECTION OF PERINATAL MICE

Injection of AAVs viruses into the lateral ventricles of the neonatal mouse (first 24-48 h) brain, allows widespread viral transduction throughout the brain (Passini & Wolfe, 2001), and the patterns of expression are maintained at least 1 year after injection.

With the aim of studying the effects of MeCP2 knockdown on L1- related events of postnatal development, L1^{y/+} mouse, and L1^{RA} mice were injected with AAVs encoding for shRNA MeCP2, or scrambled control sequence.

Each mouse pup used was collected 12 h or less after birth, and placed on a heating mat to preserve appropriate body temperature. A drop of lidocaine was applied on the skin of the mouse head, and the mouse was anesthetized with a mixture of isoflurane and oxygen inside an anaesthesia box. When the mouse was in deep anaesthetic plane, the injection sites were identified at 2/5 of the distance from the lambda suture to each eye, and the skin over the place of injection was sterilized using iodine. Using a Hamilton syringe with a sharp needle, 1 µl of virus were very slowly inoculated in each ventricle. Finally, the skin was cleaned again with iodine, the mouse was kept on the heating mat till awake, and returned to its mother.

The mice were sacrificed 7-14 days after injection, and the effectiveness of the injection and viral transduction were assessed by evaluating the presence of the GFP reporter protein in the different brain regions.

2. 15. 2. DIRECT CEREBELLAR CORTICAL INJECTION OF PERINATAL MICE

Direct cerebellar cortical injection of AAVs allows transduction of the cerebellum (Huda et al., 2014). For studying the effects of MeCP2 knockdown on L1-induced neurite outgrowth of cerebellar neurons, L1^{y/+} mouse, and L1^{RA} mice were injected in the cerebellum with AAVs encoding for shRNA MeCP2, scrambled control sequence, or MeCP2 overexpression sequence.

Each mouse pup used was collected 12 h or less after birth and placed on a heating mat to preserve appropriate body temperature. A drop of lidocaine was applied on the skin of the mouse head over the cerebellum region, and the mouse was anesthetized with a mixture of isoflurane and oxygen inside an anaesthesia box. When the mouse was in deep anaesthetic plane, the injection site was identified, centred on the middle line, 1 mm caudal to the bregma suture, and the skin over the place of injection was sterilized using iodine. Using a Hamilton syringe with a sharp needle, 1 μ l of virus was very slowly inoculated in the cerebellar cortex. Finally, the skin was cleaned again with iodine, the mouse was kept on the heating mat till awake and returned to its mother.

The mice were sacrificed 7 days after injection, and the effectiveness of the injection and viral transduction were assessed by evaluating the presence of the GFP reporter protein in the cerebellum.

2. 16. STATISTICAL ANALYSIS

All the statistical tests were performed using the software *IBM Statistics SPSS 26 for Windows*. The normality of the data distributions was tested using the Shapiro-Wilk test.

For normal data, Student's T-Test was performed when comparing two groups, and for comparison of more than two groups ANOVA followed by Bonferroni test for multiple comparison. Equality of variances was assessed using the Levene test. When possible, the magnitude of the difference between groups was estimated by the mean difference and its 95% confidence interval.

In order to compare small samples or not normal data, Mann-Whitney U-Test was performed for comparing two groups, and if samples were paired, Wilcoxon Signed Ranks Test was used. Kruskal–Wallis test by ranks was used when there were more than two groups.

For the analysis of ELISA data, the curves were compared using a multiple linear regression after exponential transformation of the absorbance data.

The p-value for accepting a significant difference between groups was always <0.05 , and it is depicted by one star in the graph (*), lower p-values are indicated as well with <0.01 (**), $p<0.001$ (***), and $p<0.0005$ (****) respectively.

All graphs representing data were made using *IBM Statistics SPSS*, *Sigma Plot*, or *Excel*.

3. RESULTS

The results of this thesis examine the interaction between L1, the DBHS and MeCP2, and explore the functional consequences of these interactions.

3. 1. INTERACTION BETWEEN L1 AND THE DBHS PROTEINS NONO, SFPQ AND PSCP1

3. 1. 1. L1-ICD DIRECTLY BINDS TO NONO AND SFPQ, BUT NOT TO PSCP1

Direct binding between L1-ICD, NonO and SFPQ was confirmed by ELISA, (performed by Jelena Brasanac). Recombinant NonO, SFPQ or PSCP1 proteins were immobilized, and increasing concentrations of recombinantly produced L1-ICD or CHL1-ICD were used as ligand (CHL1-ICD was used as negative control).

The results showed concentration-dependent binding of L1-ICD, but not of CHL1-ICD, to immobilized NonO and SFPQ, suggesting that L1-ICD binds directly to NonO and SFPQ. For PSCP1 there was no concentration-dependent binding of L1-ICD or CHL1-ICD (Fig. 3.1).

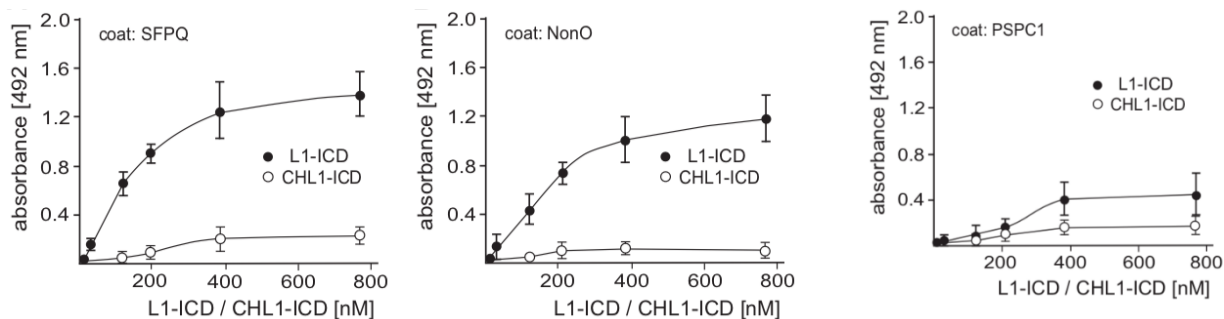


Figure 3. 1. ELISA: L1 intracellular domain binds directly to SFPQ and NonO, but not to PSCP1. Recombinant SFPQ, NonO, and PSCP1 were substrate-coated and incubated with increasing concentrations of L1-ICD or CHL1-ICD. Binding was determined by ELISA using mouse L1 antibody 172R, goat CHL1 antibody and horseradish peroxidase-conjugated secondary antibodies. Mean values \pm SEM from three independent experiments carried out in triplicates are shown. (Experiments were performed by Jelena Brasanac).

In order to confirm the previous result, soluble nuclear and cytoplasmic protein fractions from wild-type early postnatal mouse brains were used for co-immunoprecipitation, using

antibodies targeting SFPQ, NonO or PSPC1, and L1-ICD. This experiment was performed by Prof. David Lutz.

Using nuclear protein fraction, SFPQ and NonO, but not PSPC1 were detected in the L1 immunoprecipitate (Fig. 3. 2), while neither NonO, SFPQ nor PSPC1 were detected in the IgG control. Using a cytoplasmic fraction for immunoprecipitation, a ~70 kDa L1 fragment was found in the SFPQ and NonO immunoprecipitates, but not in the PSPC1 and control immunoprecipitates. These results indicate that L1 associates with SFPQ and NonO, but not PSPC1, via its intracellular domain.

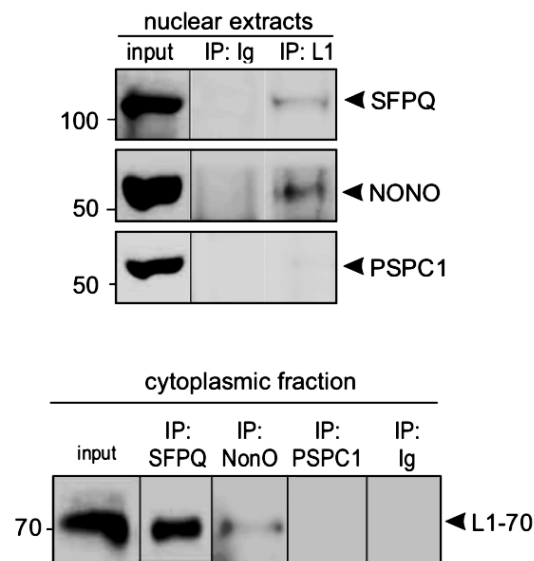


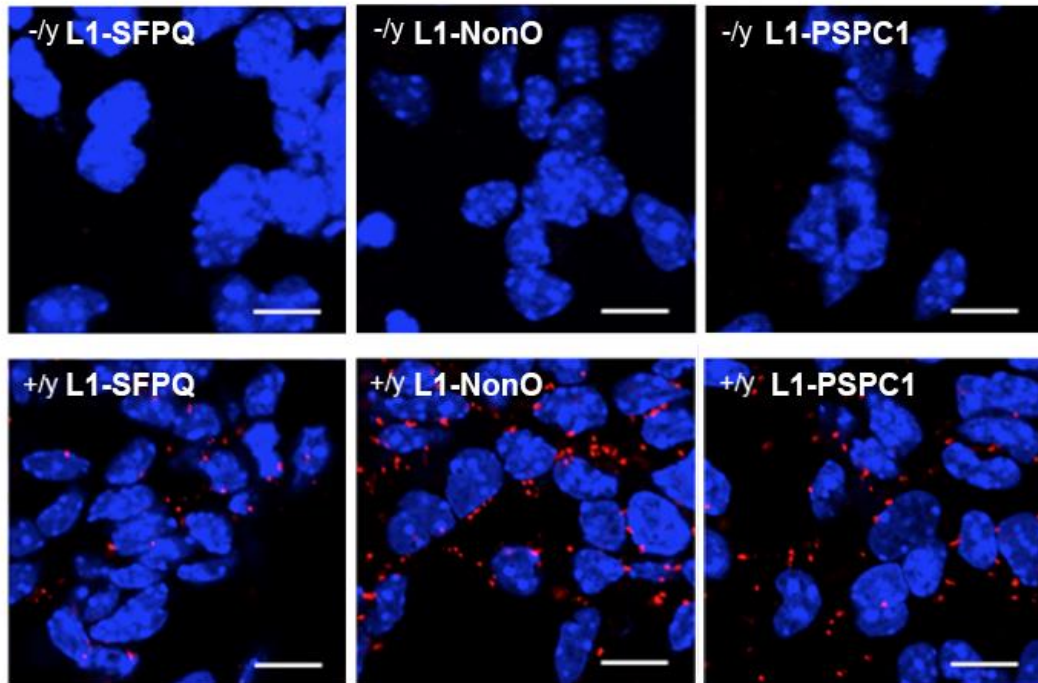
Figure. 3. 2. Co-immunoprecipitations using nuclear extracts or cytoplasmic fraction from mouse brains. IP: immunoprecipitate, Ig: non-immune IgG. (Experiments were performed by Prof. David Lutz).

3. 1. 2. L1 AND THE DBHS PROTEINS ARE FOUND IN CLOSE PROXIMITY IN CEREBELLAR GRANULE CELLS

To examine if SFPQ, NonO and PSPC1 interact with L1 in a cellular context, cerebellar granule cell cultures from 6-day-old wild-type or L1-deficient mice were used for proximity ligation assay (PLA) using antibodies against SFPQ, NonO, or PSPC1, and L1-ICD. This method allows detecting close protein interactions by generation and amplification of fluorescent signal from a pair of oligonucleotide-labelled secondary antibodies, when the antigens reacting with the primary antibodies are in close proximity of 40 nm or less. Using the mouse antibody C-2 against the L1 intracellular domain, and rabbit antibodies against SFPQ, NonO or PSPC1, positive fluorescent signals were observed as red spots on wild-type, but not L1-deficient cerebellar neurons (Fig. 3.3A). These results indicate that L1 is in very

close proximity to SFPQ, NonO, and PSPC1, both inside and outside the nucleus (Fig. 3.3.B). The fact that the DBHS proteins produce heterodimers could allow the presence of positive PLA signals for PSPC1-L1 without direct interaction.

A



B

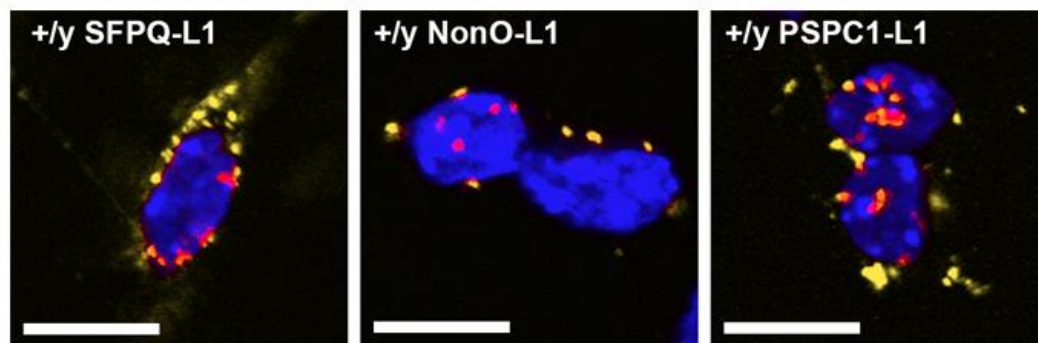


Figure 3.3. Proximity ligation assay in cultured cerebellar granule cells from $L1^{-/-}$ and $L1^{+/+}$ mice. Testing close proximity between SFPQ-L1, NonO-L1 and PSPC1-L1. (A) $-/-$: L1-deficient granule cells in top row, $+/+$: L1 wild-type granule cells in bottom row. Nuclei are stained with DAPI (blue); red spots indicate close proximity between SFPQ-L1, NonO-L1 and PSPC1-L1 (less than 40 nm). (B) PLA images from $+/+$ mice with modified colours to visualize cellular distribution of the PLA signals: signals in the nucleus (red), signals outside of nucleus (yellow). Scale bars: 10 μ m.

3. 1. 3. **SFPQ AND NONO INTERACT WITH L1 IN THE CELLULAR CONTEXT, AND THESE INTERACTIONS ARE ENHANCED BY STIMULATION OF L1 SIGNALLING**

The results obtained by ELISA and co-immunoprecipitation experiments indicate that SFPQ and NonO interact with L1 via its intracellular domain. Previous work (Lutz et al., 2012, 2016; Lutz, Loers, et al., 2014) showed that treatment of neurons with the function-triggering L1 antibody 557 enhances the generation of the L1 fragments L1-70 and L1-30, as well as their import into the nucleus. Therefore, I analysed the effect of this antibody-treatment on the interaction of L1 with SFPQ, NonO and PSPC1 by PLA.

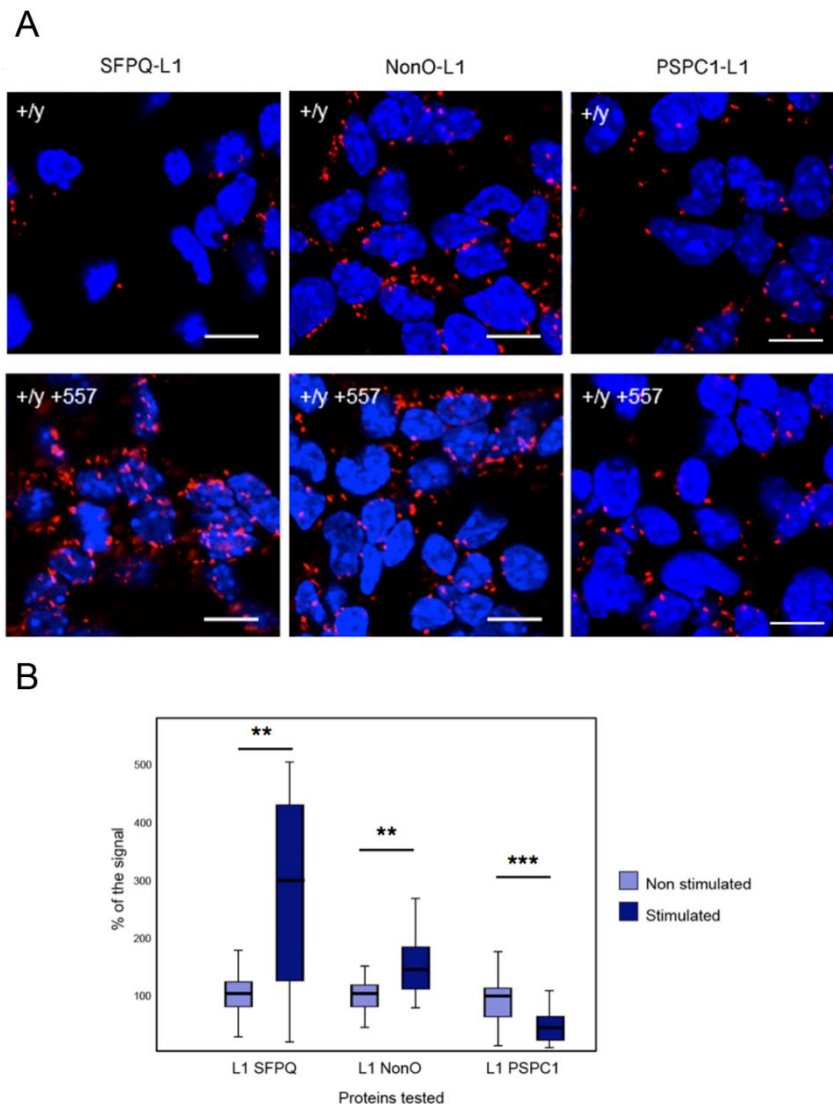


Figure 3. 4. PLA in cultured cerebellar neurons shows L1 in close proximity to DBHs with and without treatment with L1-function triggering antibody 557. Interaction of L1 with NonO and SFPQ, but not with PSPC is enhanced by treatment with function-triggering L1 antibody 557. (A) Representative images of cultured cerebellar neurons from wild-type mice treated without (+/y) or with (+/y 557) function-triggering L1 antibody 557, and then

subjected to proximity ligation assay (PLA) with mouse L1 antibody C-2 and rabbit antibodies against SFPQ, NonO or PSPC1. Nuclei were stained with DAPI (blue); red spots indicate close proximity between L1 and NonO, SFPQ and PSPC (less than 40 nm). Scale bars: 10 μ m. **(B)** Box plot graph depicting quantification of PLA signals for the interactions between L1 and SFPQ, NonO and PSPC1 in cerebellar neurons, with (Stimulated) or without stimulation (Non stimulated) with antibody 557. Box plots are shown for the average numbers of red spots per cell from 3 independent experiments normalized to non stimulated (set as 100%), stars show level of significance ** $p < 0.01$, *** $p < 0.001$; Mann-Whitney U test was used.

Quantification of the red spots on non-stimulated and stimulated cerebellar neurons showed that the average number of SFPQ/L1- and NonO/L1-positive spots per cell was approximately 3- and 1.5-times higher in neurons with antibody 557 treatment than without treatment, while the numbers of PSPC1-positive spots were decreased in 557 antibody-treated neurons (Fig. 3.4). This result indicates that SFPQ and NonO are in close proximity with L1 in a cellular context which would allow the proteins to interact, and that L1 signalling and/or generation of the L1 fragments enhance this interaction. In contrast, 557 antibody-treatment led to reduced PLA signals for L1 and PSPC1, suggesting that PSPC1 is reduced in DBHS-L1 complexes after stimulation of L1-signalling.

In order to examine the distribution of L1 and DBHS in tissue, immunostainings were performed. The stainings were performed only for NonO-L1 interaction, since our available antibodies for SFPQ did not show a high-quality staining, and PSPC1 did not show interaction indications in the previous experiments. Brain slices from twelve-day-old male L1 wild-type ($L1^{+/y}$) and L1 knockout ($L1^{-/y}$) littermate mice were immunostained with L1 and NonO antibodies. As the antibody targeting L1 (L1-C2) targets an epitope in the intracellular domain of L1, the L1 fragments L-30 and L1-70 can be visualized as well as full-length L1. The results showed that L1 and NonO are localized in similar compartments, e.g. in areas like border between the molecular layer and the pia matter of the cerebellum (Figs. 3.5 and 3.6 top), and the boundary between the dentate gyrus and the CA3 region of the hippocampus from wild-type but not L1-deficient brains (Figs. 3.5 and 3.6 bottom).

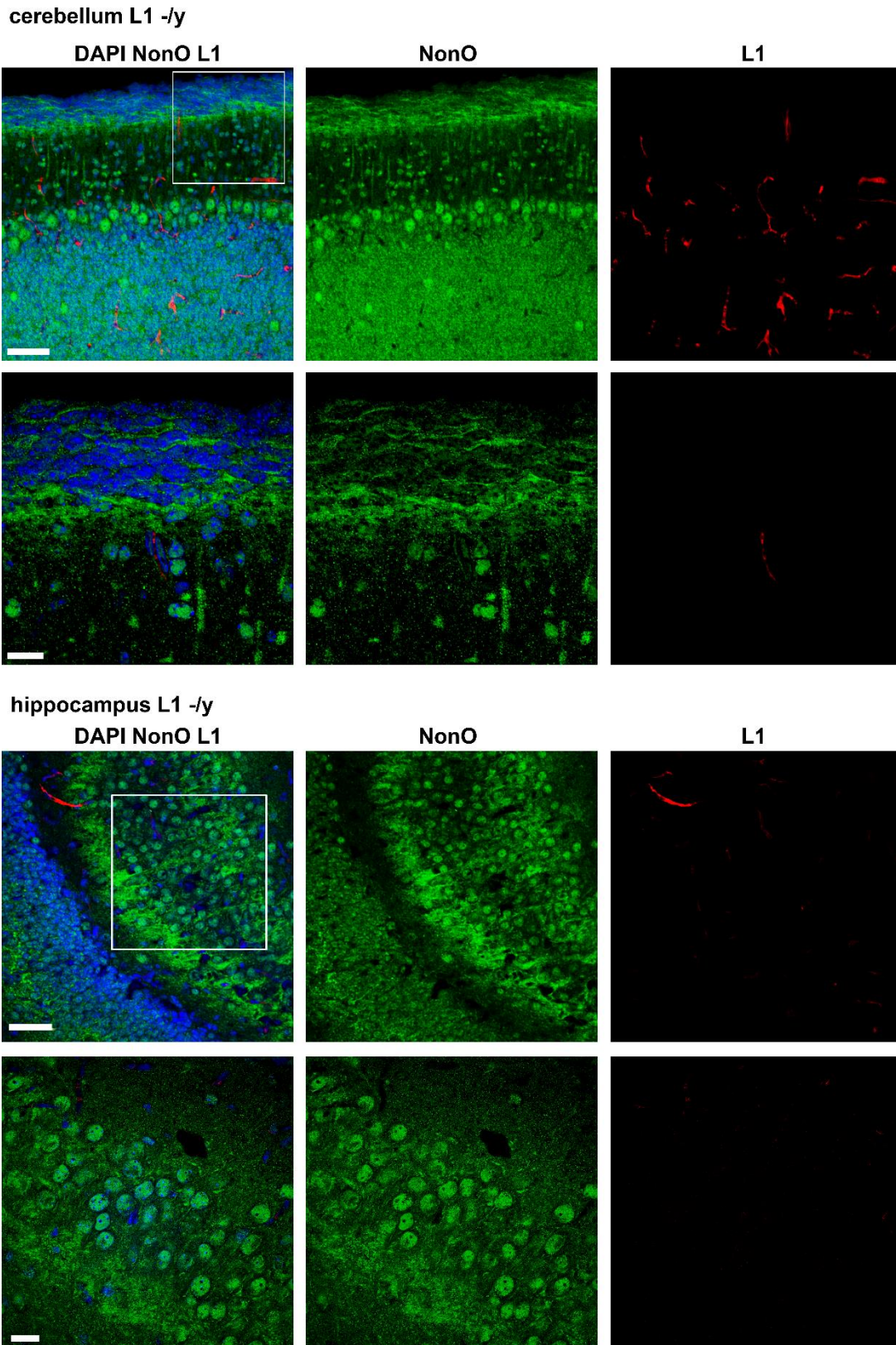


Figure. 3. 5. Immunostaining for L1 and NonO in 12-day-old L1- γ mouse brain. NonO stained in green, L1 stained in red, nuclei stained with DAPI in blue. Scale bars: 20 μ m in top row images from hippocampus and cerebellum, and 50 μ m in bottom images. The boxes in the upper images indicate the areas from which the higher magnification images shown below are derived.

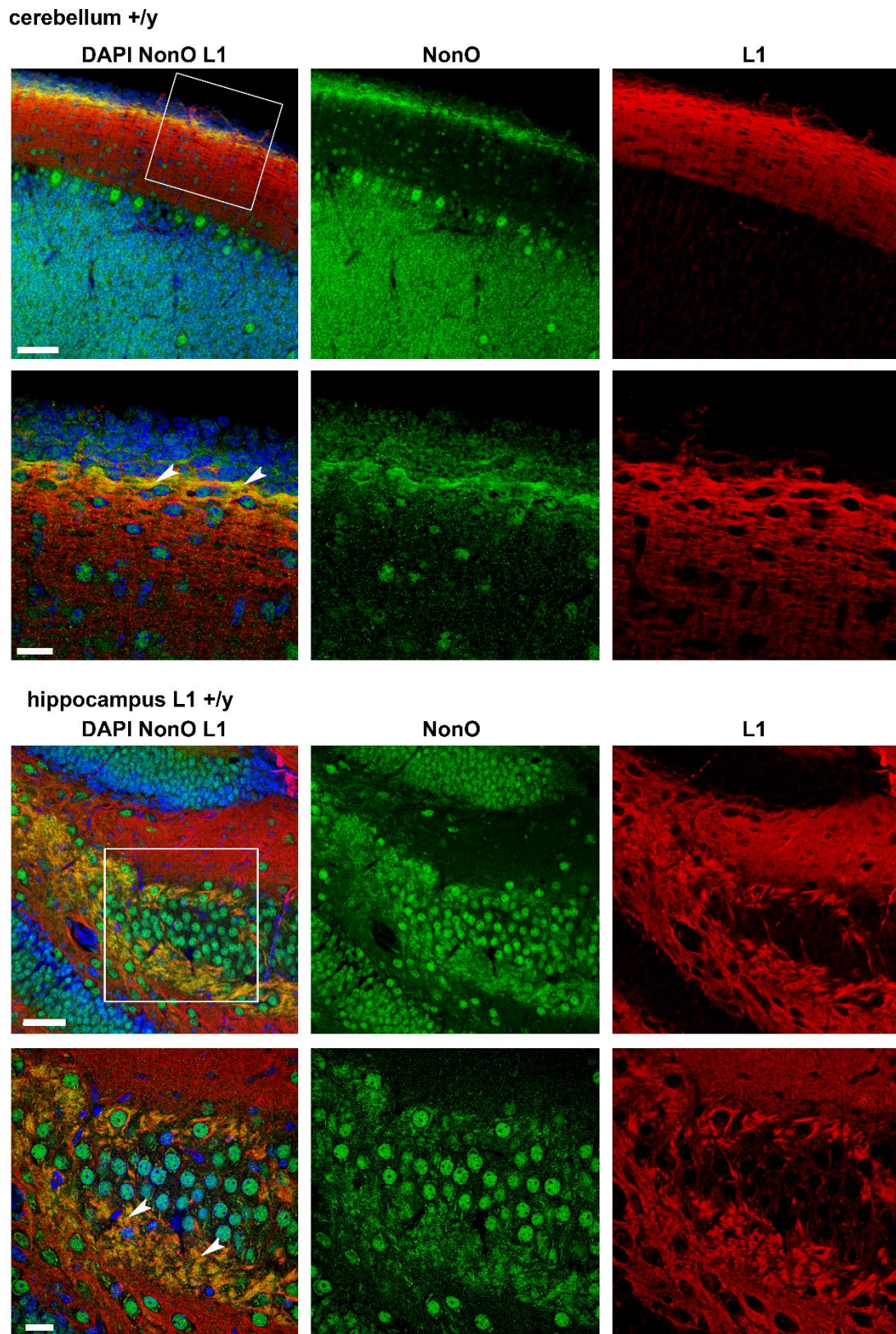


Figure. 3. 6. Immunostaining for L1 and NonO in 12-day-old L1+/y mouse brain. NonO stained in green, L1 stained in red, nuclei stained with DAPI (blue). Scale bars: 20 μ m in top row images from hippocampus and cerebellum, and 50 μ m in bottom images. The boxes in the upper images indicate the areas from which the higher magnification images shown below are derived. Arrows indicate similar distributions of NonO and L1.

3. 2. INTERACTION BETWEEN L1 AND MECP2

3. 2. 1. MECP2 DIRECTLY BINDS TO L1 INTRACELLULAR DOMAIN

To investigate whether MeCP2 directly binds to L1-ICD, ELISA was performed using recombinant MeCP2 protein as coating and increasing concentrations of recombinant L1-ICD were used as ligand, while equivalent increasing concentrations of CHL1-ICD were used as negative control.

Concentration dependent and saturable binding of L1-ICD to MeCP2 was observed, while CHL1-ICD did not bind to MeCP2 (Fig. 3.7A). This result indicates that MeCP2 binds directly to the intracellular domain of L1.

In order to complement the ELISA, label free assay was performed using the BIND system. MeCP2 was immobilized on the titan oxide surface, and increasing concentrations of L1-ICD as ligand were added to the wells. CHL1-ICD at equivalent concentrations was used as a negative control (Fig. 3.7B). The result obtained shows that L1-ICD, but not CHL1-ICD, binds to MeCP2 in a concentration dependent manner.

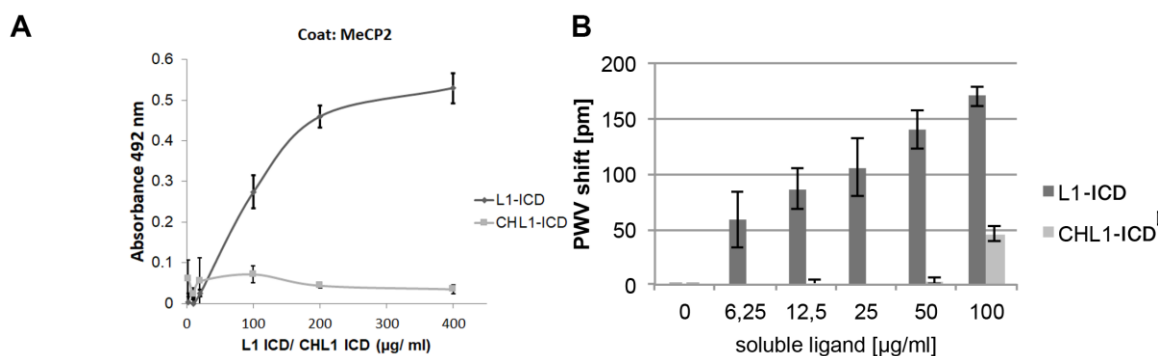


Figure 3. 7. ELISA and BIND assay: L1-ICD but not CHL1-binds to MeCP2. (A) Binding was determined by ELISA using mouse L1 antibody 172R, goat CHL1 antibody and horseradish peroxidase-conjugated secondary antibodies. The experiment was repeated three times obtaining similar results. Mean values \pm SEM from one representative performed in triplicates result are shown. (B) Label-free technology BIND was used for analysing if L1-ICD binds to MeCP2, using substrate-coated MeCP2 protein and increasing amounts of soluble L1-ICD or CHL1-ICD. Mean values \pm SD (triplicates) are shown.

In order to study the relationship between absorbance and concentration of ligand in the results from the ELISA, an exponential transformation of the data was applied for the variable absorbance (*Absorbance*), in order to obtain a linear model. *Absorbance* was used as a dependent variable, while the ligand (*Ligand*) and the concentration (*Concentration*) were

included as predictive or independent variables. The interaction between *Ligand* and *Concentration* was also included in the model (*Interaction*).

The model was significant ($F=53.9$, $p<0.0001$), and explained 83.7% of the observed variability. In Table 3.1, the parameters obtained in the model and their significance are shown.

The equation of the model was:

$$e^{Abs}=1.066 - 0.035 \cdot Ligand + 8.864 \cdot 10^{-7} \cdot Concentration + 0.002 \cdot Ligand \cdot Concentration$$

Where *Ligand* = 0 (CHL1-ICD), or 1 (L1-ICD)

The model can be better understood as two different regression lines (Fig. 3.8), one for CHL1-ICD (*ligand* = 0) (Fig. 3.8A), equation:

$$e^{Abs}=1.066 + 8.864 \cdot 10^{-7} \cdot Concentration$$

and one regression line for L1-ICD (*Ligand* = 1) (Fig. 3.8B), equation:

$$e^{Abs}=1.031 + 0.002 \cdot Concentration$$

We can see that for the whole model, the interaction between ligand and concentration is significant. When the ligand is CHL1-ICD (*Ligand* = 0), there is no relationship between concentration and absorbance. However, when the ligand is L1-ICD (*Ligand* = 1), there is a significant dependence between concentration and absorbance.

Table 3.1. Relationship between absorbance and concentration for the ligands CHL1-ICD and L1-ICD in ELISA. Coefficients obtained after multiple linear regression.

	B	95% CI of B	t	Significance (p)
Constant	1.066	1.010 to 1.122	39.047	<0.0001
Ligand	-0.035	-0.116 to 0.046	-0.882	0.385
Concentration	$8.864 \cdot 10^{-7}$	-0.0003 to 0.0003	0.005	0.996
Interaction	0.002	0.001 to 0.002	8.228	<0.0001

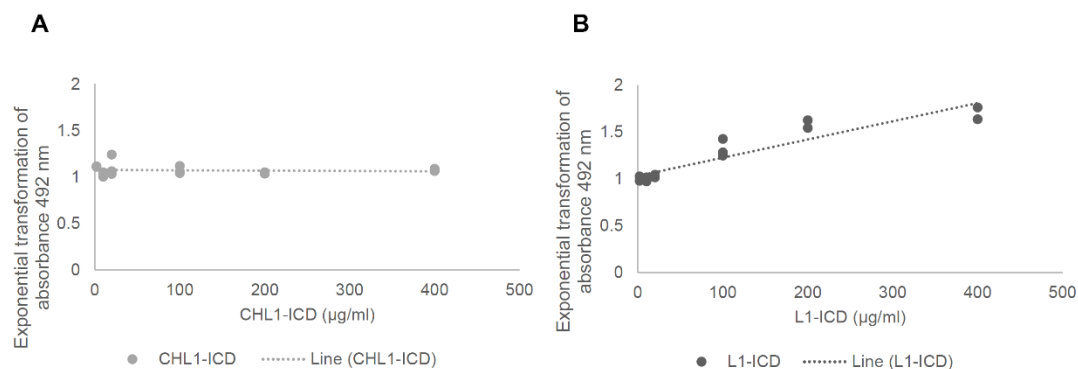


Figure 3. 8. ELISA with exponential transformation of absorbance for MeCP2 and CHL1-ICD and L1-ICD.

To verify the interaction between L1 and MeCP2 in the mouse brain, co-immunoprecipitation experiments were performed using nuclear extracts from early postnatal mouse brains. When the L1 antibody against the intracellular domain was used for immunoprecipitation (Fig. 3.9A), MeCP2 was detected in the immunoprecipitate, but it was not detected in the immunoprecipitate obtained with non-immune antibody control. In addition, when MeCP2 antibody was used for immunoprecipitation (Fig. 3.9B), an L1 fragment containing the intracellular domain was detected in the MeCP2 immunoprecipitate, but not in the non-immune antibody control. These results suggest that MeCP2 and an L1 fragment containing the intracellular domain are present in a complex enabling/allowing them to interact.

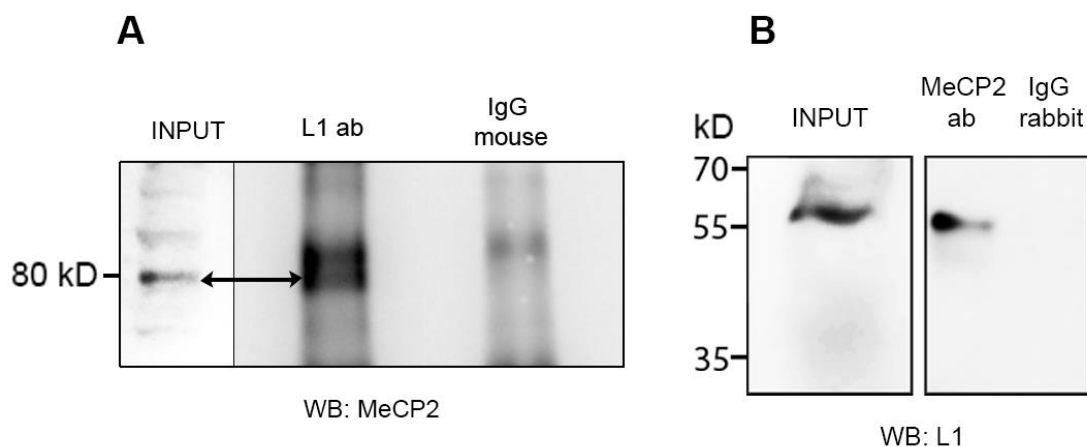


Figure 3. 9. Co-immunoprecipitation using soluble mouse brain nuclear extracts shows that an L1 nuclear fragment can be precipitated with MeCP2. (A) MeCP2 is detected in L1 immunoprecipitate. Arrow shows specific MeCP2 bind in line with INPUT, non-immune IgG shows slight unspecific binding. (B) An L1 fragment is detected in MeCP2 immunoprecipitate using L1 antibody C2 targeting an epitope in L1 intracellular domain.

After having shown in biochemical experiments that the intracellular domain of L1 binds to MeCP2, I wanted to narrow down the binding site within the L1-ICD using ELISA, by coating the peptides comprising fragments of the L1-ICD, and using MeCP2 as ligand. In order to do so, I produced MeCP2 using *E. coli*. After producing and purifying MeCP2 (Fig. 3.10A), I tested its ability to binding to L1 in ELISA, and the result showed that my produced protein was not able to bind to L1 (Fig. 3.10B). According to the literature, MeCP2 produced in *E. coli* is able to bind to DNA (Nan et al., 1997), but in *E. coli* possibly the protein folding is not appropriate to allow its interaction with L1. As the commercial MeCP2 used in the experiments above had been produced in wheat germ, it is likely that the tertiary structure of MeCP2 is crucial for L1-MeCP2 interaction.

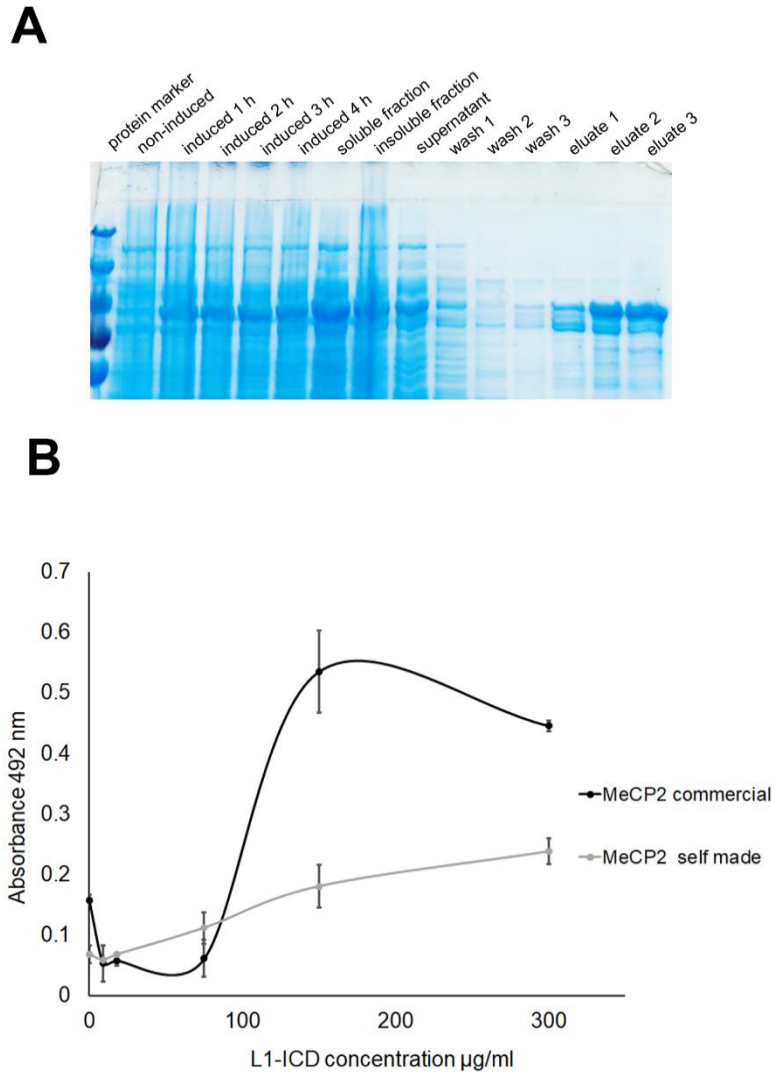


Figure 3. 10. Production of recombinant MeCP2 and test of its L1-ICD binding ability. (A) Coomassie staining of SDS-Page gel showing different protein bands during the production of MeCP2 in *E. coli*. (B) ELISA evaluating binding between home-made MeCP2 (produced in *E. coli*) and L1-ICD, compared to commercial MeCP2 (produced in wheat germ). Mean values from triplicates \pm SEM Error bars.

3. 2. 2. MECP2 BINDS TO THE L1 FRAGMENTS L1-70 AND L1-30

In order to distinguish which fragment of L1 is interacting with MeCP2, co-immunoprecipitation experiments were performed using MeCP2 (isoforms α , β), L1-70, and L1-30 expressed *in vitro*, antibodies against the intracellular domain of L1 for immunoprecipitation, and MeCP2 antibody for detection.

The experiments revealed the presence of MeCP2 (α or/and β) in L1-70 and L1-30 immunoprecipitates (Fig. 3.11A). When testing for MeCP2 α , it was detected clearly in L1-30

and L1-70 immunoprecipitates, although only the non-immune IgG control was clearly negative for L1-70, while the non-immune IgG control showed strong unspecific binding for L1-30 (Fig. 3.11B). When examining MeCP2 β (Fig. 3.11C), it was detectable in both L1-30 and L1-70 immunoprecipitates, and the non-immune IgG controls did not show such strong unspecific binding. The slight molecular weight shift between inputs and tests could be explained by the different buffer conditions used during the co-immunoprecipitation procedure, which were different than the used in the input.

Since MeCP2 interacts with the L1-ICD in ELISA, and the L1-ICD is present in both fragments, it is conceivable that both L1-30 and L1-70 could interact with MECP2, but it is also possible that only L1-70 binds to MeCP2 and that although the interaction is mediated by the intracellular domain present in both L1 fragments parts of the transmembrane domain or the extracellular domain of L1 influence the interaction with MeCP2.

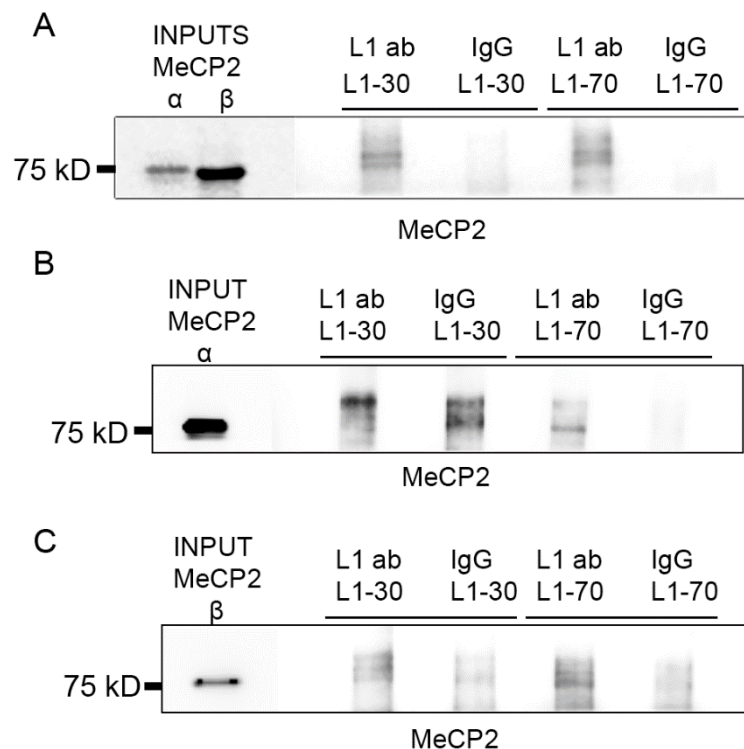


Fig. 3. 11. Co-immunoprecipitation using in vitro expressed L1-30, L1-70 and MeCP2. (A) Inputs: MeCP2 α and β . L1 fragments were pulled down using L1-C2 antibody targeting the intracellular domain. MeCP2 was detected in L1-70 and L1-30 immunoprecipitates, non-immune IgG controls appear clean. (B) Input: MeCP2 α . L1 fragments were pulled down using L1-C2 antibody targeting the intracellular domain. MeCP2 was detected in L1-70 and L1-30 immunoprecipitates, non-immune IgG control for L1-70 appears clean, while non-immune IgG control for

L1-30 shows unspecific binding. (C) Input: MeCP2 β . L1 fragments were pulled down using L1-C2 antibody targeting the intracellular domain.

To examine the interaction of the L1 fragments in the cellular context, cerebellar granule cells from L1-deficient mice were transduced with AAVs containing the sequences of wild-type L1, or the L1 mutated sequence the L1^{RA}, which is mutated in the MBP cleavage site, and L1 would not be cleaved to generate L1-70 and probably also not L1-30.

The results of this experiment showed positive PLA signals in the L1-deficient cerebellar granule cells after transduction with AAV carrying the L1 wild-type sequence, but not in the L1-deficient cerebellar granule cells after transduction with AAV carrying the mutated L1 sequence (Fig. 3.12). These results indicate that MeCP2 interacts with the L1 fragment L1-70 and/or L1-30 in the cellular context.

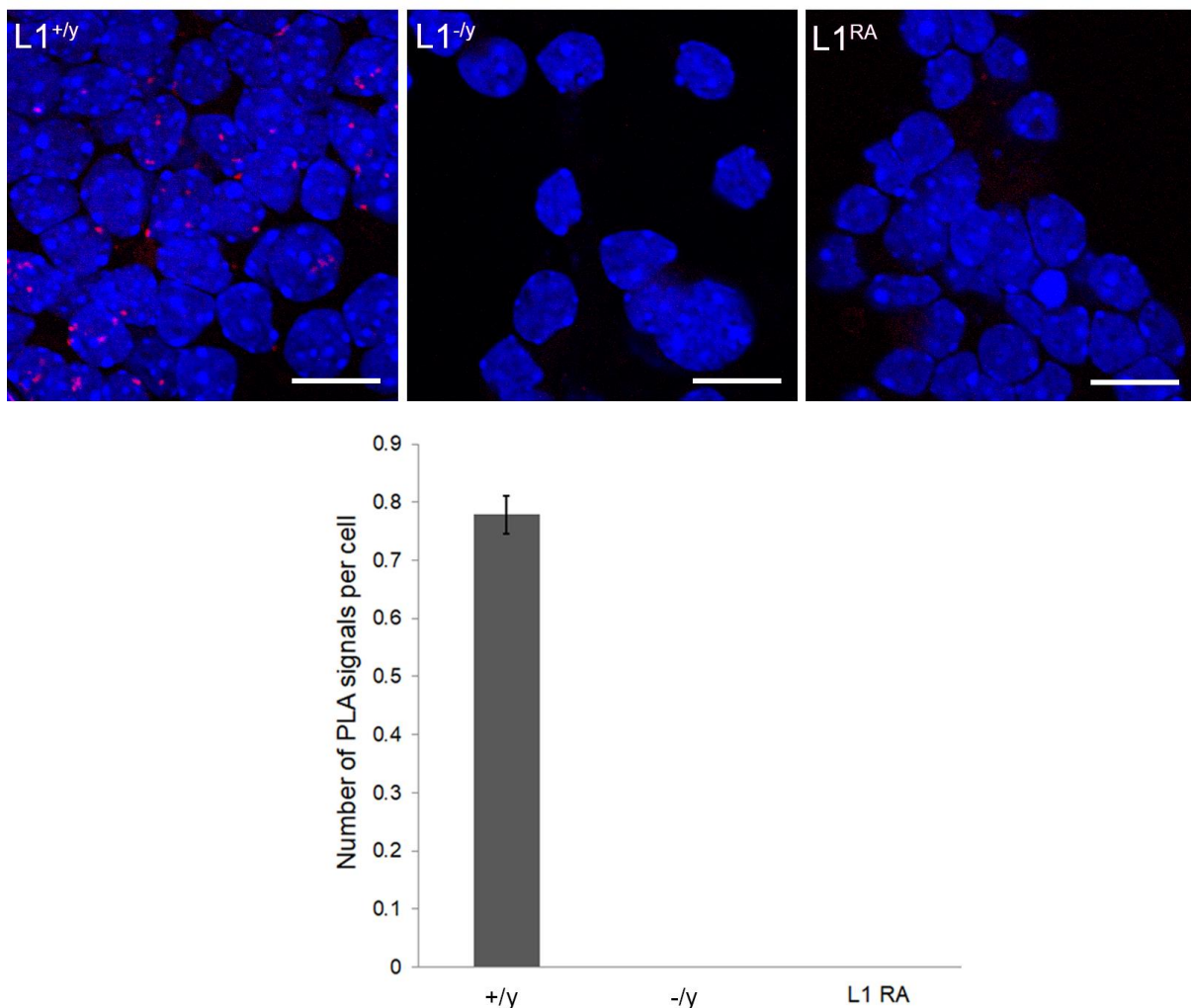


Figure. 3. 12. PLA in cultured cerebellar granule cells from L1-deficient mice after transduction with AAVs. Representative images from PLA using antibodies targeting MeCP2, and L1 intracellular domain in L1-deficient cerebellar granule neurons, untransduced

($L1^{-/y}$), or transduced with AAVs containing L1 wild-type sequence ($L1^{+/y}$) or $L1^{RA}$ mutant sequence ($L1^{RA}$). PLA signals in red, nuclei stained with DAPI (blue). Scale bars: 10 μ m. Graph on bottom showing quantification of PLA signals across genotypes.

3. 2. 3. **L1 AND MECP2 ARE IN CLOSE PROXIMITY IN NEURAL CELLS AND TISSUE**

In order to verify the interaction between MeCP2 and L1 in the cellular context, cerebellar granule cell cultures from 6-day-old wild-type or L1-deficient mice were used for proximity ligation assay (PLA) using the mouse antibody C-2 against an epitope located in the intracellular domain of L1, and rabbit MeCP2 antibody.

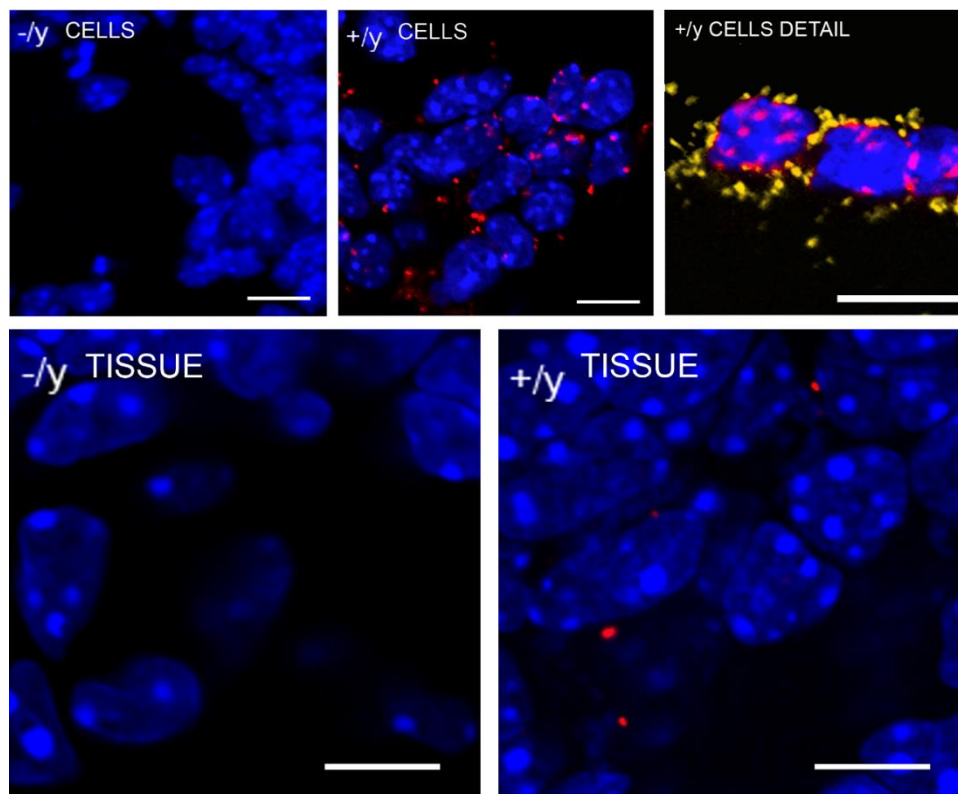


Figure. 3. 13. PLA shows L1 binding to MECP2 in cerebellar neurons and slices. Representative images from PLA using antibodies targeting MeCP2, and L1 in cerebellar granule cells, and cerebellar tissue slices. Red spots indicate close proximity between L1 and MeCP2 (less than 40 nm). Nucleus stained in blue (DAPI). (**-/y CELLS**) and (**+/y CELLS**): L1-deficient and L1 wild-type cerebellar granule cells. (**-/y TISSUE**) and (**+/y TISSUE**): L1-deficient and L1-wild-type cerebellar slices. (**-/y CELLS DETAIL**): L1 wild-type cerebellar granule cells showing PLA signals in modified colours to visualize the cellular distribution of

the PLA signals: signals in the nucleus (pink), signals outside of nucleus (yellow). Scale bar equal 10 μ m.

The result showed positive fluorescent signals observed as red spots on wild-type, but not L1-deficient cerebellar neurons, indicating that full-length L1 and/or L1 fragments containing the intracellular domain of L1 are in very close proximity to MeCP2, both inside and outside the nucleus (Fig. 3.13) which allows the two proteins to interact. The results from this PLA were further confirmed by performing PLA in cerebellar tissue slices from 12-day-old L1 wild-type and L1-deficient mice. PLA positive signals were visible in the slices from L1-wild-type mice, but not in L1-deficient mice. These results indicate that L1 and MeCP2 are also in very close proximity in tissue (Fig. 3.13; bottom).

3. 2. 4. L1 - MECP2 INTERACTION IS ENHANCED AFTER STIMULATION OF L1 SIGNALLING

Considering the fact that stimulation of the cells with the function-triggering L1 antibody 557 induces L1 signalling and enhances the generation of the L1 fragments L1-70 and L1-30 (Loers et al., 2005; Lutz et al., 2012, 2016; Lutz, Wolters-Eisfeld, et al., 2014), I analysed the effect of the antibody 557 treatment on the interaction between L1 and MeCP2 by performing PLA in wild-type cerebellar granule cells, with and without stimulation with L1 antibody 557 (Fig. 3.14).

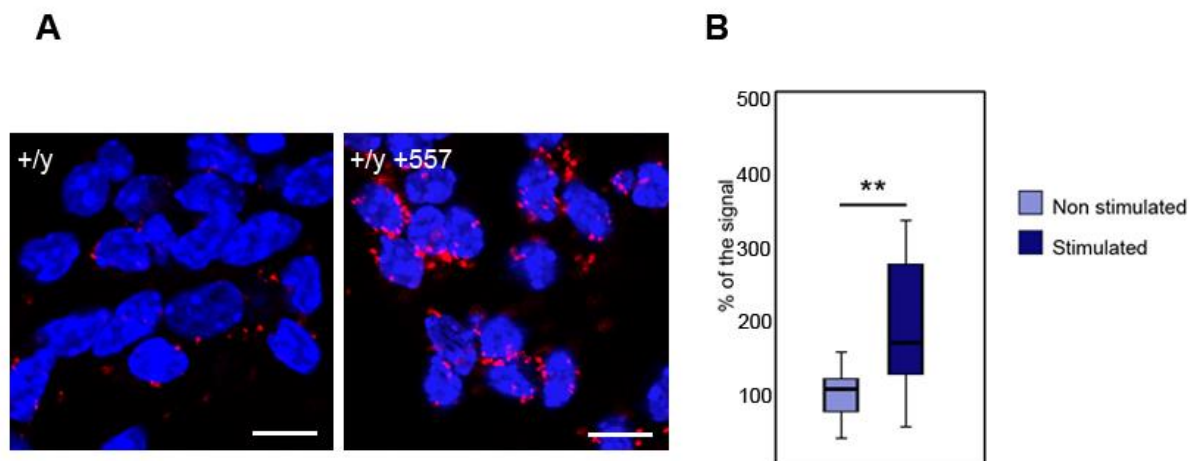


Figure. 3. 14. PLA in cultured cerebellar granule cells studying consequences of L1-function triggering antibody treatment on L1-MeCP2 interaction. (A) Representative images from PLA using antibodies targeting MeCP2, and L1 intracellular domain in cerebellar granule neurons, with (+/y +557) and without (+/y) function-triggering L1 antibody (antibody 557). Nuclei are stained with DAPI (blue); red spots indicate close proximity between L1 and MeCP2 (less than 40 nm). Scale bars: 10 μ m. (B) Box plot graph depicting quantification of PLA signals in cerebellar neurons with antibody 557 (Stimulated) or without (Non stimulated).

Box plots are shown for the average numbers of red spots per cell from 3 independent experiments, normalized to signals on non-stimulated cells (set a 100%), stars show level of significance, ** $p < 0.01$; Wilcoxon-Mann-Whitney U test was used.

Quantification of the PLA signals on non-stimulated and stimulated cerebellar neurons showed that the average number of MeCP2/L1 positive signals per cell was two times higher in neurons with antibody treatment than without treatment (Fig. 3.14B). This result indicates that MeCP2 interacts with full-length L1 and/or L1 fragments in a cellular context, and that L1 signalling and/or enhanced generation of L1 fragments increase this interaction.

3. 2. 5. L1 AND MECP2 CO-LOCALIZE IN THE MOUSE HIPPOCAMPUS

In the previous results I showed that L1 binds to MeCP2 in biochemical assays, and *in vitro* using early postnatal cerebellar granule cells and cerebellar slices. In order to further confirm the previous results, I studied the distribution of L1 and MeCP2 in the early postnatal mouse brain using immunostainings (Fig. 3.15), and determined co-localization of L1 and MeCP2.

Brain slices from twelve-day-old male wild-type ($L1^{+/y}$) and L1 knockout ($L1^{-/y}$) littermate mice were immunostained with L1 and MeCP2 antibodies. As the antibody targeting L1 (L1-C2) targets an epitope in the intracellular domain of L1, full-length L1, and the L1 fragments L1-30 and L1-70 can be visualized. Co-localization of L1 and MeCP2 was found in the $L1^{+/y}$ mice (Fig. 3. 15B, left) inside the nucleus of cells in the area of transition between the pyramidal layer of CA3 region and the polymorph layer of the dentate gyrus. Of note, no nuclear fluorescent signal for L1 was detected in the $L1^{-/y}$ brain (Fig. 3.15B, right).

For analysing co-localization, the Pearson Correlation Coefficient (PCC), and Manders' Co-localization Coefficients for MeCP2 (tM1) and for L1 (tM2) were calculated (Fig. 3.15C) for 25 Z-stacks comprising 3 whole cell nuclei.

It is important to note that in images where the signal levels of two probes are not linearly related, the PCC can represent a poor measure of colocalization (Dunn et al., 2011). When interested in probe co-occurrence alone, the tM1 and tM2 are better measures of co-localization because they are independent of signal proportionality but sensitive to co-occurrence (Dunn et al., 2011). The tM1 and tM2 show strong co-occurrence of the signals of MeCP2 and L1, with co-occurrence of pixels occupied for MeCP2 on L1 (tM1), and for L1 on MeCP2 (tM2).

These results show co-localization between L1 and MeCP2 in the hippocampal region of early postnatal mouse brain.

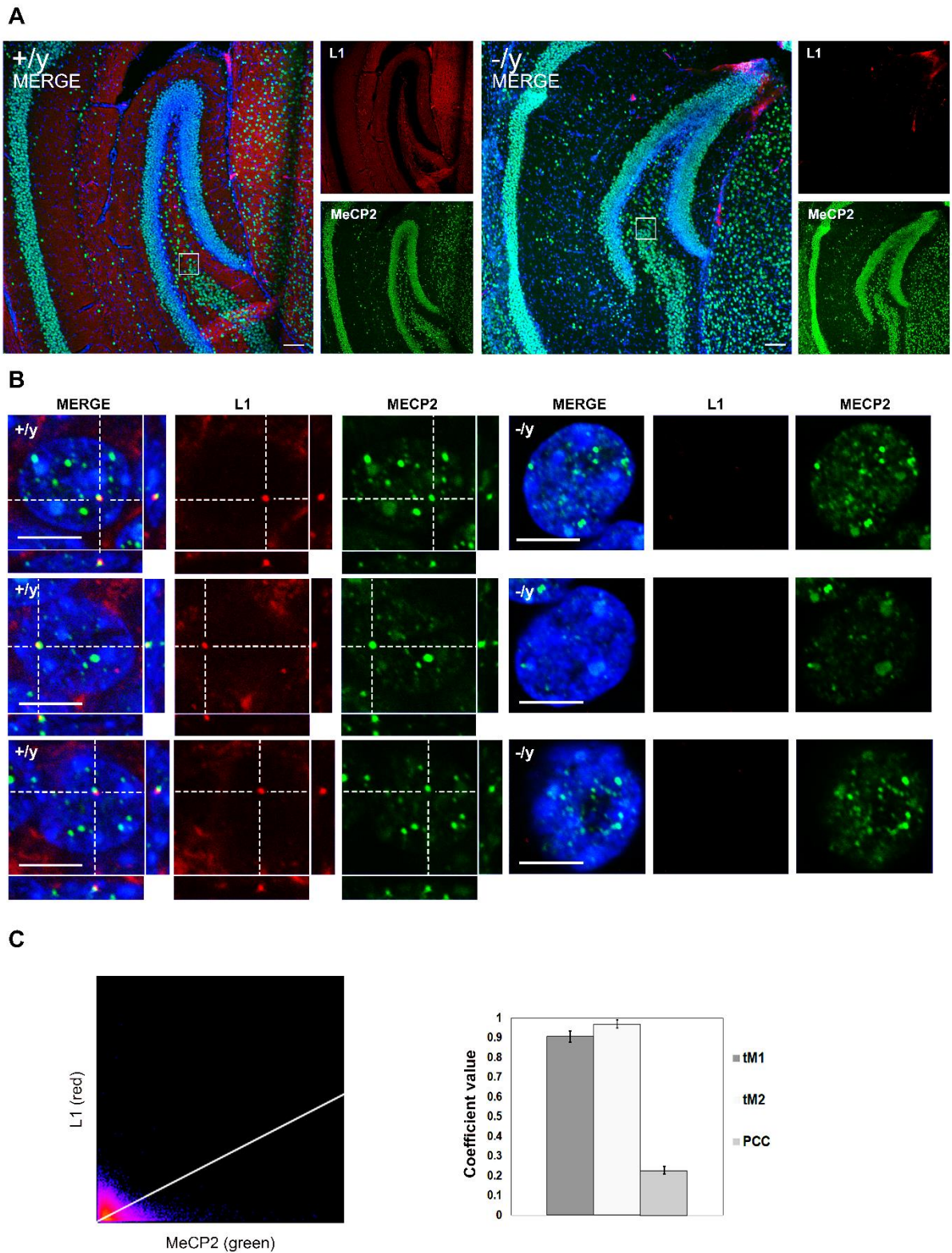


Figure 3. 15. L1 co-localizes with MeCP2 in the hippocampus of twelve-day-old mice. (A) Representative images of L1+/y (+/y, left) and L1-/y (-/y, right) mouse brains stained for L1 (red), MeCP2 (green), and nuclear staining DAPI (blue), white square marks CA3 region.

Scale bars: 200 μm . **(B)** Higher magnification images showing nuclei of cells in the area of transition between pyramidal layer of CA3 region, and polymorph layer of the dentate gyrus from L1+/y (left) and L1-/y (right) mouse brains; intersection of discontinuous lines signals co-localization and slicing of Z-axis. Scale bars: 5 μm . **(C)** Quantification of colocalization; the left 2D histogram shows intensity values for each pixel from the red channel plotted against each other, (L1, Y-axis) against the green channel (MeCP2, X-axis), white line shows regression curve fit; the right bar graph indicates the values of Pearson Correlation Coefficient (PCC), and Manders' Co-localization Coefficients of MeCP2 (tM1) and L1 (tM2).

3. 2. 6. L1 AND MECP2 CO-LOCALIZE IN THE CYTOPLASM OF MOUSE NEURAL STEM CELLS

Since MeCP2 and L1 play important roles in neuronal maturation and differentiation (Dihn e et al., 2003; Kishi & Macklis, 2004), I wanted to examine the distribution and expression levels of L1 and MeCP2 in mouse neural stem cells, and their changes after differentiation into neurons. I cultured neural stem cells (NSCs) and stained them using L1 antibody C2, and MeCP2 antibody before and after differentiation.

For analysing co-localization, the Pearson Correlation Coefficient (PCC), and Manders' Co-localization Coefficients for MeCP2 (tM1) and for L1 (tM2) were calculated (Fig. 3.16C) using 6 pictures.

During neuronal development MeCP2 is located in the cytoplasm, but later in postnatal development it is abundant in the nucleus of postmitotic neurons (Miyake & Nagai, 2007). In stainings of neural stem cells before and during differentiation, I could detect MeCP2 in the nucleus and cytosol (Fig. 3.16). Full-length L1 is abundant in the mouse brain early after birth, so is L1-70, being most abundant during the first five days after birth (Lutz, 2013). In NSCs I could detect L1 in the cytoplasm (Fig. 3.16A), and the amount increased during differentiation, co-localizing with cytoplasmic MeCP2 increasingly with differentiation (Fig. 3.16B and C).

Moreover, these results show that L1 and MeCP2 are located in the cytoplasmic compartment during neural differentiation, suggesting their interaction might play a role in neuronal differentiation.

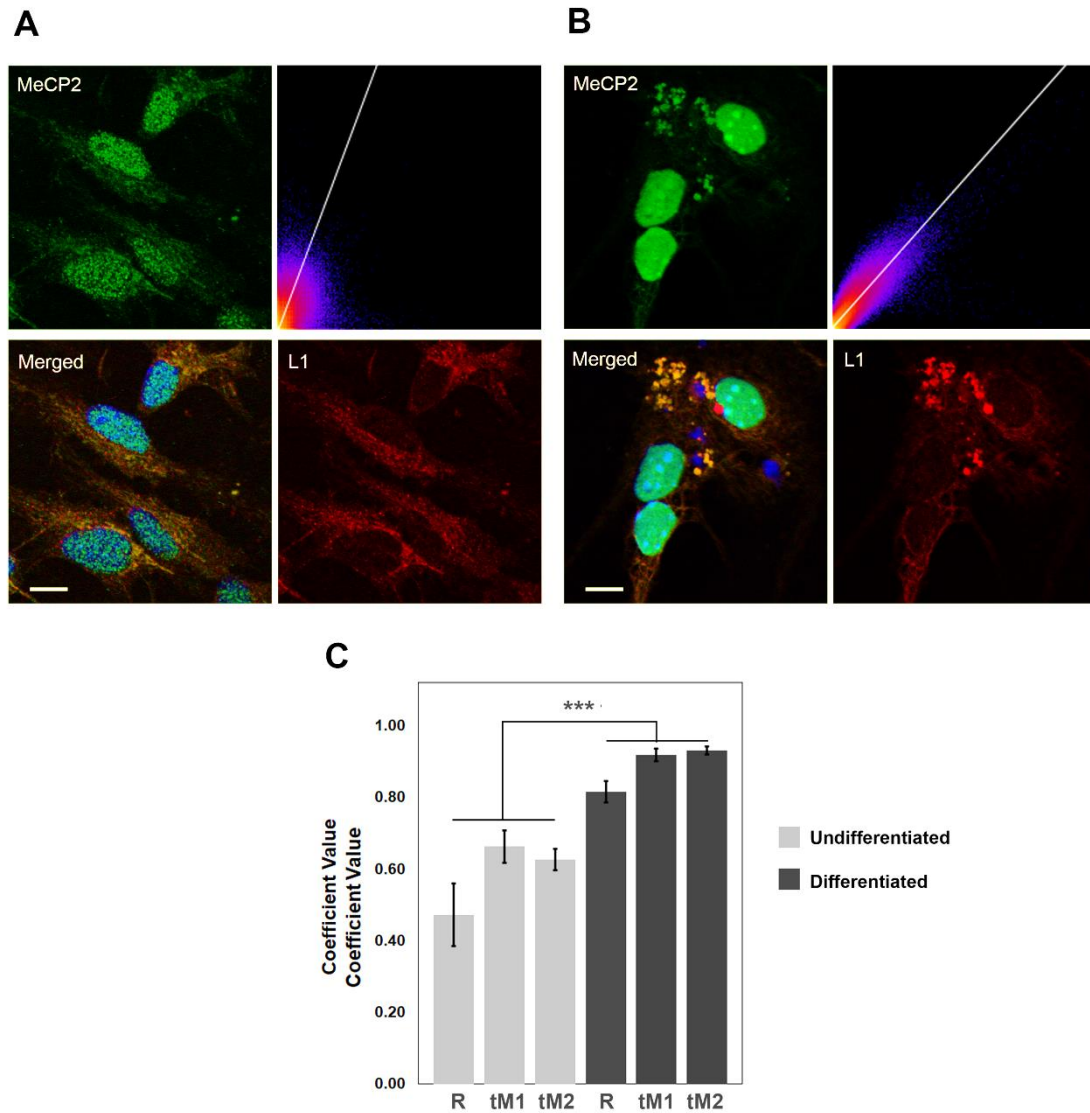


Figure. 3. 16. L1 co-localizes with MeCP2 in the cytoplasm of neural stem cells. Representative image of mouse neural stem cells before (**A**) and after differentiation (**B**), stained for L1 (red), MeCP2 (green), and nuclear staining DAPI (blue). Scale bars: 5 μm . On the right top of A and B, 2D histogram showing intensity values for each pixel from the red channel (L1, Y axis) plotted against, the green channel (MeCP2, X axis), white line shows regression curve fit. Co-localization of MeCP2 and L1 is present in the cytoplasm, and it increases after differentiation. (**C**) Quantification of co-localization; the bar graph indicates the values of Pearson Correlation Coefficient (R), and Manders' Co-localization Coefficients of MeCP2 (tM1) and L1 (tM2), for undifferentiated and differentiated NSCs. Mann-Whitney U test was used, stars show level of significance *** $p < 0.001$. Error bars with $\pm\text{SEM}$.

3. 2. 7. **MECP2 REGULATES THE PRODUCTION OF L1 FRAGMENTS VIA UP-REGULATION OF MYELIN BASIC PROTEIN IN THE MOUSE CORTEX AND CEREBELLUM**

MeCP2 is a transcriptional repressor and activator of multiple genes (Chahrour et al., 2008; Zachariah & Rastegar, 2012), and some of its targets are relevant to L1 function. MeCP2 has been found to regulate myelin related genes (Moore, 2011; Sharma et al., 2015; Vora et al., 2010), and since myelin basic protein (MBP) cleaves full-length L1 to generate L1-70 (Lutz et al., 2016; Lutz, Loers, et al., 2014), I was interested in studying the effect of MeCP2 knockdown on the generation of L1-70.

Since previous studies showed that MeCP2-deficient mice exhibit increased levels of MBP mRNA in the frontal cortex (Vora et al., 2010), I used cortical neuron cultures as a model to study the effects of MeCP2 knockdown on the production of L1-70. The first relevant fact I needed to elucidate was if cultured cortical neurons produce MBP themselves, specifically the MBP isoform that cleaves L1 to generate L1-70. After culturing cortical neurons from embryonic wild-type mice, I used Western Blot to analyse the levels of L1 using an antibody against its intracellular domain and MBP using an antibody targeting the exon II encoded domain of mouse MBP, which is the isoform that cleaves L1. These results show that L1-70 is present in cortical neurons, and so is the specific MBP isoform, which was found to cleave L1 (Fig. 3.17).

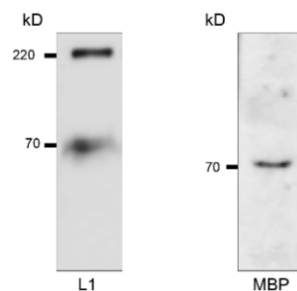


Figure. 3. 17. Western Blot: Cortical neurons produce exon II-containing MBP and L1-70. Results from WB using lysates of cortical neurons from L1+/y mouse brain showing bands for full-length L1, L1-70, and MBP.

Having seen that cultured cortical neurons produce MBP and L1-70, they served as model cells for testing the effects of MeCP2 knockdown on levels of full-length L1 and L1-70. Studies on MeCP2 (Vora et al., 2010) already showed that higher levels of MBP mRNA were been found in the cortex of MeCP2-deficient mice compared with MeCP2 wild-type mice, and it could be expected that the levels of MBP protein could be increased as well.

Embryos from two different litters were used to test effective knockdown of MeCP2 by Western Blot, 7 days after addition of the AAV carrying MeCP2 shRNA in the media. The WB results show effective knockdown (Fig. 3.18A), with a 50% decrease in MeCP2 after using AAV carrying MeCP2 shRNA compared to the control virus (scrambled sequence).

After confirming MeCP2 knockdown in cortical neurons using Western Blot, cortical neurons were used to examine the levels of L1-70 after MeCP2 knockdown. For this aim, four different pools of cells from the pups of 4 different breedings were prepared, and each pool was separated in 3 groups to be transduced using: AAV carrying MeCP2 shRNA, AAV carrying a scrambled sequence, and not transduced. The cells were lysed and subjected to Western Blot, incubated with antibodies against L1, and GAPDH (loading control) (Fig. 3.18B). After quantification, the results show a significant increment in the amount of L1-70 for the AAV MeCP2 shRNA transduced cells, while no significant difference in the amount of L1-70 between untransduced cells and cells transduced with AAV carrying scrambled sequence was found (Fig. 3.18 B, Table 3.2).

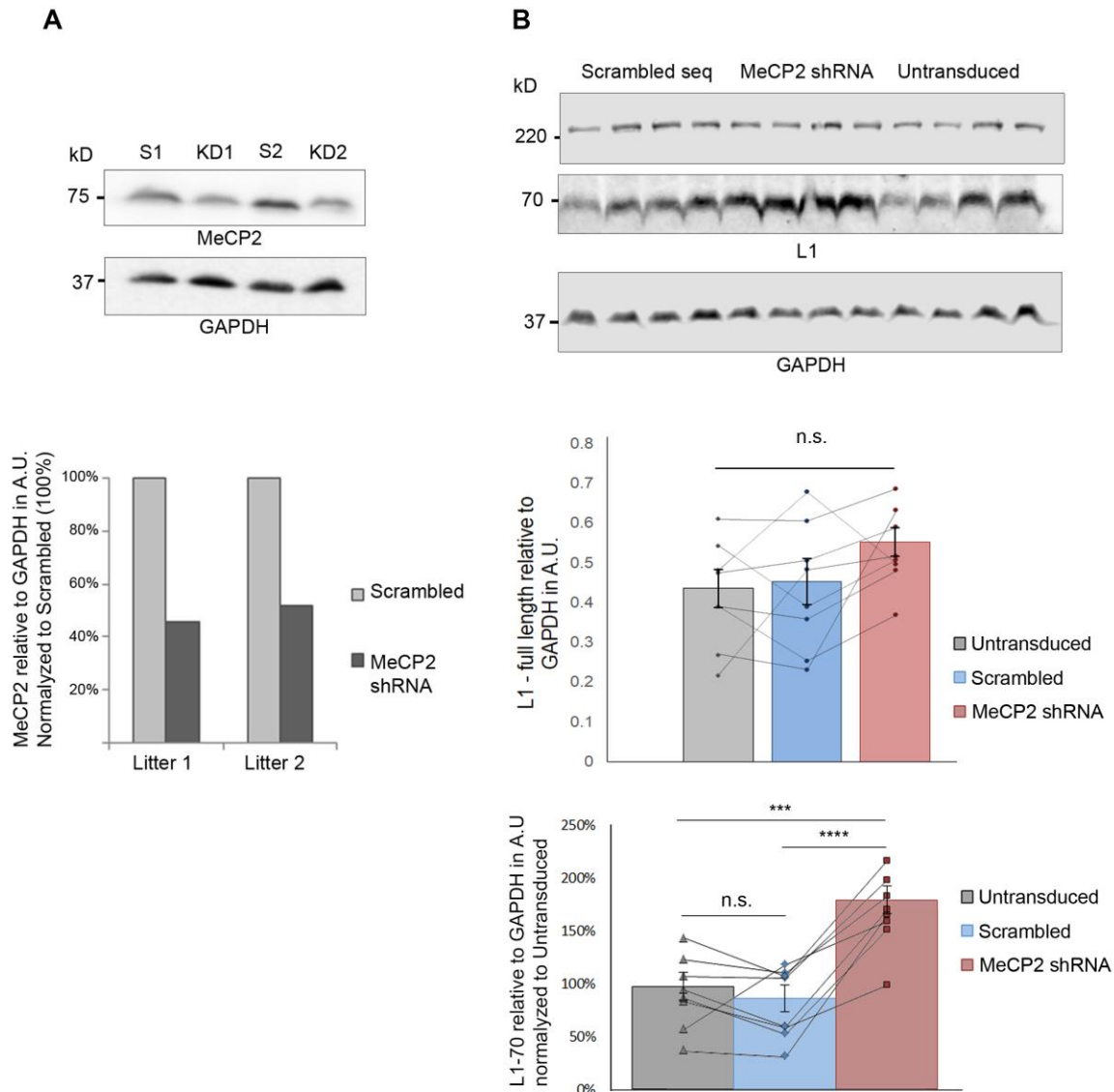


Figure 3. 18. MeCP2 knocked-down leads to a higher amount of L1-70 in cultured cortical neurons. (A) Results from WB analyses using MeCP2 antibody and GAPDH (loading control) of cortical neuron lysates from L1+*y* mice transduced with AAV carrying Scrambled sequence (S1 and S2), or AAV carrying MeCP2 shRNA (KD1 and KD2), and quantification. (B) Representative result from WB of cortical neuron lysates from L1+*y* mice transduced with AAV carrying Scrambled sequence (Scrambled seq), AAV carrying MeCP2 shRNA (MeCP2 shRNA), or untransduced (Untransduced) using L1 antibody targeting the intracellular domain, and GAPDH antibody (loading control), and quantification of two identical experiments (L1-full-length and L1-70 relative to GAPDH) in bar graphs, bars show average per group, markers show exact values, error bars with \pm SEM, stars show level of significance, *** $p < 0.001$, **** $p < 0.0005$; One-Way ANOVA was used, followed by test Bonferroni for multiple comparisons.

Table. 3. 2. Data analysis comparing the levels of L1-70 in cultured cortical neurons after viral transduction. *Neurite length (dependent variable) across AAVs (independent variable). Descriptive statistics are shown, and the result of One-Way ANOVA. Bonferroni test for multiple comparisons was performed, and level of significance across groups is shown in Fig.3.18.*

Protein	Group	n	Mean	SD	F	Significance
L1 full-length	Scrambled	8	0.45	0.16	1.7	p = 0.2
	shRNA MeCP2	8	0.55	0.10		
	Untransduced	8	0.44	0.14		
L1 - 70	Scrambled	8	0.06	0.03	15.66	p < 0.0001
	shRNA MeCP2	8	0.13	0.03		
	Untransduced	8	0.07	0.03		

As the articles published by our group regarding important functions of L1 fragments have often relied on cerebellar granule cell culture as a useful tool to test L1 functions (Lutz, 2013; Lutz et al., 2012, 2017; Lutz, Loers, et al., 2014), and considering that cerebellar granule cells produce L1-70 and MBP (Lutz, Loers, et al., 2014), I wanted to test whether this difference in the amount of L1-70 was also existing in cerebellar granule cells after MeCP2 knockdown. For this aim, I cultured cerebellar granule cells from 3 mice (p7), transduced them using AAV MeCP2 shRNA or AAV Scrambled sequence, and assessed the effectiveness of MeCP2 knockdown by Western Blot. The results show (Fig. 3.19A and D) that MeCP2 knockdown was effective.

These cells were also used for Western Blot using L1 antibody, and the results showed that there is a significantly higher amount of L1-70 in the cerebellar granule cells which were transduced with AAV MeCP2 shRNA compared to the cells transduced with AAV Scrambled sequence (Fig. 3.19B). This experiment was repeated using 6 more animals, showing identical result (Fig. 3.19C), and both experiments were jointly quantified in Figure 3.19E.

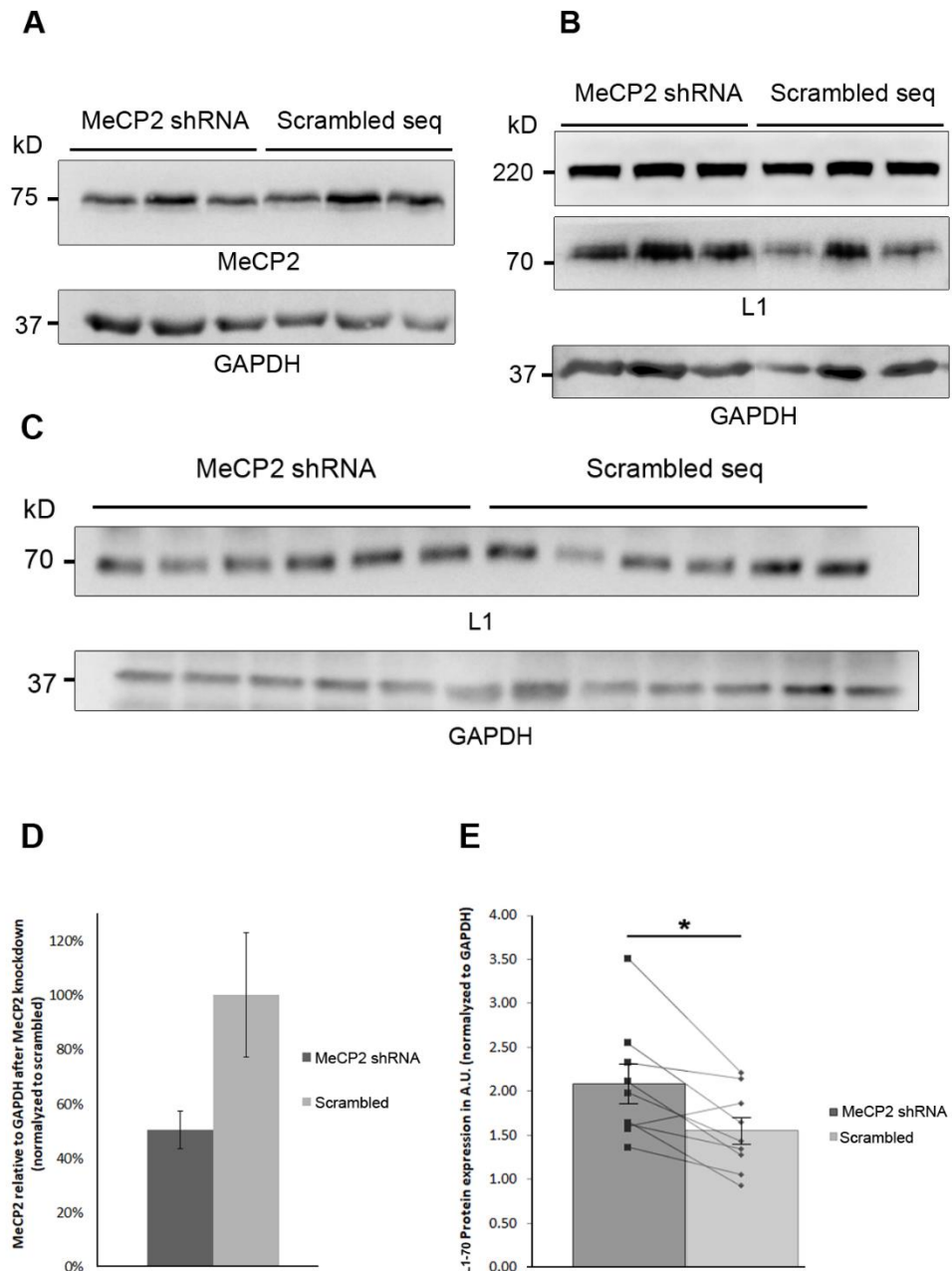


Figure 3. 19. MeCP2 knockdown leads to a higher level of L1-70 in cerebellar granule cells. (A) Results from WB analyses using MeCP2 antibody and GAPDH (loading control) on cerebellar granule cell lysates from L1+/y mice transduced with AAV carrying MeCP2 shRNA or Scrambled sequence, and quantification of the Western Blot in (D). (B) Result from WB analysis of the same samples as (A) using L1 antibody (L1-C2) and GAPDH antibody (loading control). (C) Replication of the experiment shown in (B) using more animals. (E) Quantification of both experiments (L1-70 relative to GAPDH) in bar graph; bars show average per group, markers show exact values, error bars with \pm SEM, and stars show level of significance, * $p < 0.05$ in Wilcoxon Signed Ranks Test.

Triggering of L1 signalling and proteolytic processing of L1 is vital for L1-regulated neurite outgrowth, neuronal migration, and myelination (Lutz, 2013; Lutz et al., 2012; Lutz, Loers, et al., 2014; Lutz, Wolters-Eisfeld, et al., 2014), so studying these functions after MECP2 knockdown would be of help for understanding the effects of MeCP2 in L1 functions, and the potential implications of this relationship for the pathogenesis of Rett syndrome.

Previous studies performed by our group determining L1-regulated neurite outgrowth and neuronal migration, have relied on cerebellar granule cell cultures or cerebellar explants for this matter (Lutz, 2013; Lutz et al., 2012; Lutz, Loers, et al., 2014; Lutz, Wolters-Eisfeld, et al., 2014). As explained in section '2. 13. 6', effective knockdown of MeCP2 using AAV carrying shRNA occurred 7 days after transduction. This supposed an important limitation to my experiments, since neurite outgrowth experiments using cerebellar granule cells have to be performed 24 h after seeding the cells, and unfortunately 24 h of exposure of the cells to the AAV carrying shRNA are not enough for knockdown of MeCP2. In order to overcome this problem, I had to find an alternative method to knockdown MeCP2 for this experiment.

I came across a publication describing how intracerebroventricular injection of AAVs can be used to achieve persistent and widespread neuronal transduction (J.-Y. Kim et al., 2014). This method would allow me to inject the neonatal mice at p0, and wait until p7 to culture cerebellar granule cells/ cerebellar explants to test neurite outgrowth or neuronal migration, once MeCP2 is knocked-down. I therefore performed intracerebroventricular injection in 8 neonatal L1^{+/-} mice, using AAVs carrying MeCP2 shRNA (4 mice) or Scrambled sequence (4 mice), and analysed the efficacy of transduction and knockdown using immunostainings and Western Blot (Fig. 3.20).

Figure 3.20A. depicts a brain from a 14-day-old mouse which had been injected at p0 using AAV. The fluorescence emitted by GFP (reporter protein included in the AAVs) is visible under UV light, showing transduction in the brain. However, not much fluorescence is present in the cerebellum. Western Blot was used to examine the levels of MeCP2 in lysates of brain without cerebellum, or only cerebellum, and the results confirmed effective knockdown of MeCP2 in the "rest" brains (Fig. 3.20C and E), but not in cerebella (Fig. 3.20B, D and F).

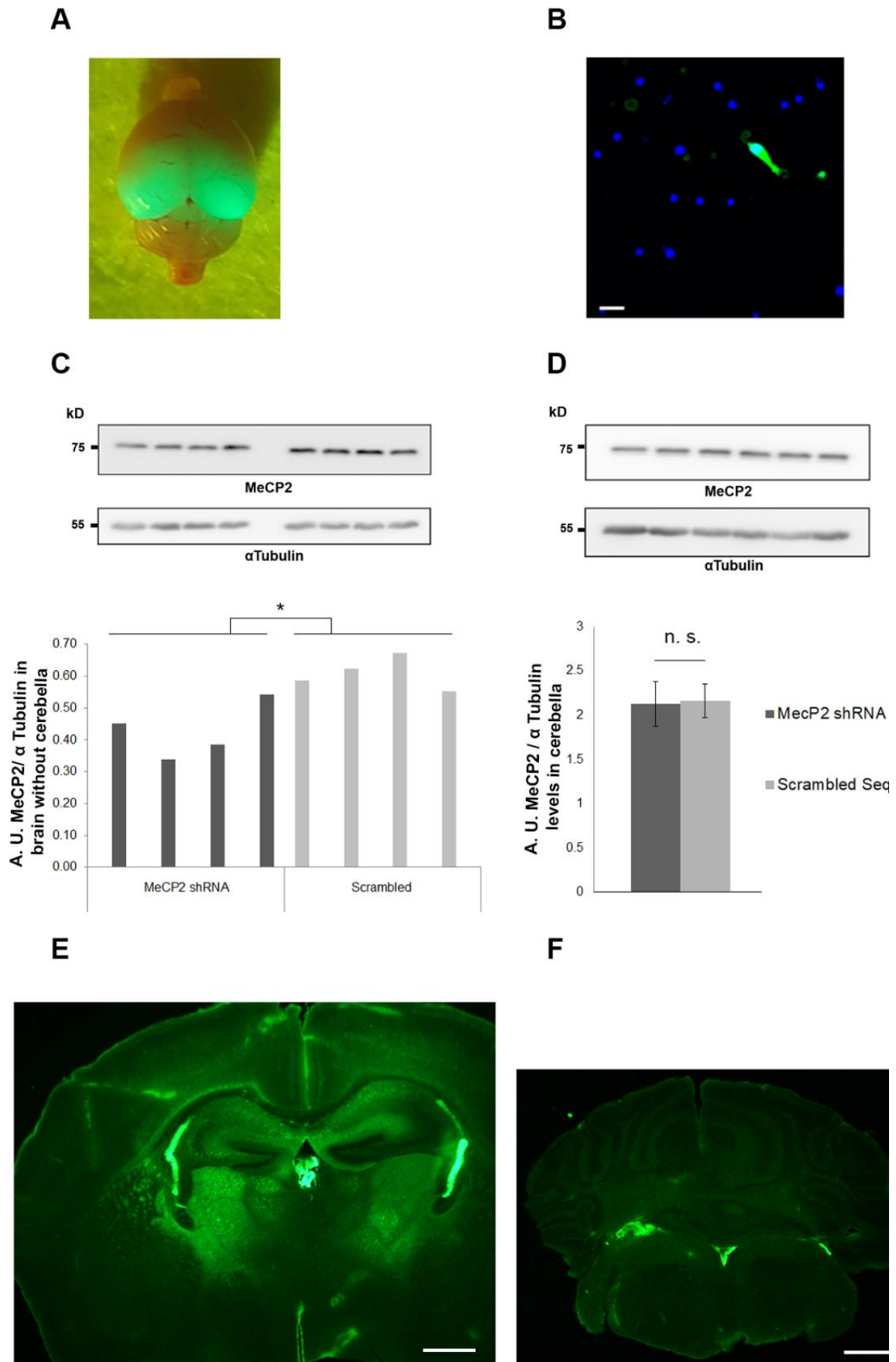


Figure 3. 20. Knockdown of MeCP2 in mouse brain using intracerebroventricular injection. (A) Dissected brain from a L1+/y mouse, 14 days after intracerebroventricular

*injection of AAV carrying MeCP2 shRNA. GFP fluorescence visible under UV light indicates transduction. (B) Confocal image from cultured cerebellar granule cells from a mouse L1+/y mouse 7 days after intracerebroventricular injection of AAV carrying MeCP2 shRNA, GFP fluorescence indicates transduction, nuclei are stained with DAPI (blue). Scale bar: 15 μ m. (C) Western Blot of brain lysates (without cerebella) from mice injected in the ventricles with AAV carrying MeCP2 shRNA or AAV carrying scrambled sequence (7 days after injection), using antibodies against MeCP2 and α -tubulin (loading control), and quantification underneath. Star shows level of significance * $p < 0.05$ in Mann-Whitney U-Test. (D) Western Blot of cerebellar lysates from mice injected in the ventricles with AAV carrying MeCP2 shRNA or AAV carrying scrambled sequence (7 days after injection), using antibodies against MeCP2 and α -tubulin (loading control), and quantification underneath. (E, F) Microscopy images of the brain (E) or cerebellum (F) from a 14-day-old mouse injected in the ventricles with AAV carrying MeCP2 shRNA showing green fluorescence indicating transduction; scale bars: 0.8 mm.*

Considering that after intracerebroventricular injection there was no effective knockdown of MeCP2 in cerebella, possibly because of the AAV type used, which has tropism for the ventricular ependymal lining (C. Wang et al., 2003), I had to find a different approach in order to knockdown MeCP2 in the cerebellum. The literature describes that direct cerebellar cortical injection can be used to transduce the cerebellar tissue (Glascock et al., 2011), so I decided to attempt it.

AAVs carrying MeCP2 shRNA or scrambled sequence were injected directly in the cerebellum of neonatal mice (p0). Seven days after injection, the cerebella were examined under UV light to verify the expression of GFP indicating effective transduction, and the cerebella showed expression of GFP (Fig. 3.21, left). Cerebellar granule cell culture was performed using these cerebella, and the cells were immunostained for β III-tubulin and GFP, and the majority of cells showed expression of GFP (Fig. 3.21, right).

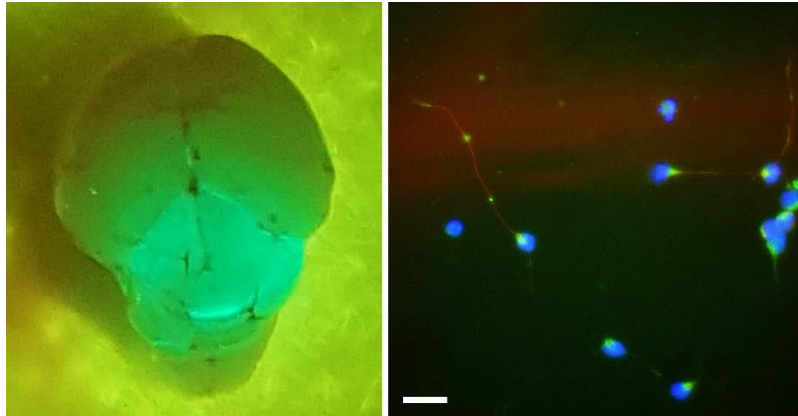


Figure. 3. 21. Knockdown of MeCP2 in the mouse cerebella using direct cerebellar cortical injection. (Left) injected cerebellum from a p7 $L1^{+/y}$ mouse showing GFP fluorescence indicating viral transduction after intracerebroventricular injection of AAV carrying MeCP2 shRNA. (Right) cerebellar granule cells from the here mentioned cerebellum, immunostained using β III-tubulin (red) and GFP (green) antibodies, nuclei were stained with DAPI (blue). Scale bar: 20 μ m.

3. 2. 8. MECP2 KNOCKED-DOWN CEREBELLAR GRANULE CELLS SHOW LONGER NEURITES

Since MBP-mediated generation of L1-70 promotes neurite outgrowth *in vitro* (Lutz, Loers, et al., 2014), and I found a higher amount of L1-70 in neurons after MeCP2 knockdown, I wanted to determine whether MeCP2 knockdown impacts neurite outgrowth in cerebellar granule cells due to the increased generation of L1-70. 4 early postnatal (p0) $L1^{+/y}$ mice, were injected in the cerebellum with AAVs carrying MeCP2 shRNA (2 mice) or scramble sequence (2 mice). After 7 days cerebellar granule cells from each mouse were individually cultured, and immunostained 24 h later with antibodies against β III-tubulin and GFP (reporter of viral transduction). Neurite outgrowth was measured and quantified.

The results showed that MeCP2 knocked-down cerebellar granule cells had longer neurites compared to cerebellar granule cells transduced with the control virus (Fig 3. 22, Table 3.3). This result is consistent with the effect of MeCP2 on MBP. MeCP2 is normally a repressor of MBP expression, but when MeCP2 is knocked-down MBP expression increases (Sharma et al., 2015; Vora et al., 2010), possibly leading to an increment in the cleavage of full-length L1, generation of L1-70, and enhanced neurite outgrowth.

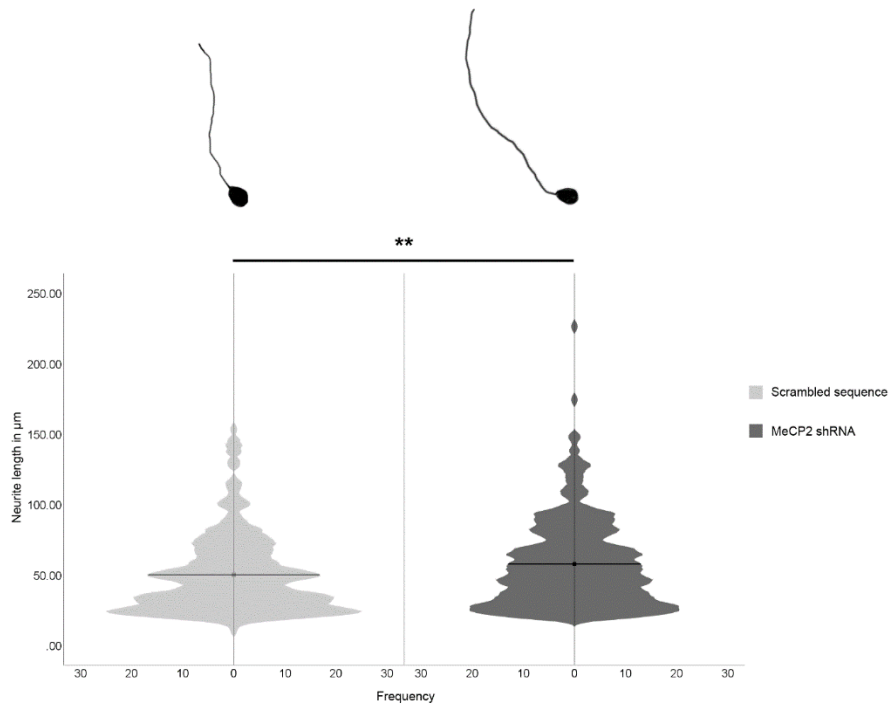


Figure. 3. 22. MECP2 knocked-down cerebellar granule cells show longer neurites. Representative tracings of cerebellar granule cells transduced using AAV containing scrambled sequence (**top left**), or AAV containing MECP2 shRNA (**top right**). On the bottom, violin plot depicting number of cerebellar granule cells (**X axis**) with their measured neurite length (**Y axis**) for cerebellar granule cells transduced with AAV containing scrambled sequence, or MeCP2 shRNA. Bars show mean values of the groups. Stars show level of significance ** $p < 0.01$ in Student t-test.

Table. 3. 3. Data analysis comparing mean neurite length in cerebellar granule cells after viral transduction. Neurite length (dependent variable) across AAVs (independent variable). Descriptive statistics are shown and the result of Student t-test. The effect size is also shown with 95% confidence interval.

Group	n	Mean	Median	SD	Mean difference (CI 95%)	t	Significance
Scrambled sequence	240	50.08	43.96	28.06	-7.76	-2.92	p=0.004
MeCP2 shRNA	269	57.85	50.86	31.52	(-2.54, -13.0)		

3. 2. 9. MECP2 REGULATES NEURITE OUTGROWTH IN CEREBELLAR NEURONS VIA MYELIN BASIC PROTEIN

An experiment was performed in order to confirm the previous result, and to examine if the enhanced neurite outgrowth present in MeCP2 knocked-down cerebellar granule cells (Fig. 3.22) was caused by increased cleavage of L1 and production of L1-70.

Early postnatal (p0) mice from two breedings (13 mice) containing the genotypes L1^{+y}, and L1^{RA} mutation (mutation which prevents MBP to cleave L1 and to generate L1-70), were injected into the cerebellum with AAVs carrying MeCP2 shRNA, a scramble sequence, or the MeCP2 overexpression sequence. The mice were injected without knowing their specific genotype, only one mouse had the L1^{RA} genotype, and this mouse was injected with AAV carrying MeCP2 shRNA. After seven days, cerebellar granule cells from each mouse were cultured individually, and immunostained after 24 h for β III-tubulin and GFP (reporter of viral transduction). Neurite outgrowth was measured and quantified in cells from different cerebella showing intense GFP expression indicative of viral transduction: cells from 2 L1^{+y} cerebella injected with AAVs carrying MeCP2 shRNA, cells from 2 L1^{+y} cerebella injected with AAVs carrying scrambled sequence, cells from 2 cerebella injected with AAVs carrying MeCP2 overexpression sequence, and cells from 1 L1^{RA} cerebellum injected with AAVs carrying MeCP2 shRNA.

The results showed (Fig. 3.23, Table 3.4) that L1^{+y} cells after MeCP2 knockdown, and L1^{+y} cells transduced with MeCP2 overexpression sequence were not significantly different in neurite length, but had significantly longer neurites than L1^{+y} cells transduced with the control virus. However, L1^{RA} mutated cells knocked-down for MeCP2 did not show longer neurites compared to L1^{+y} cells transduced with the control virus, but showed significantly shorter neurites compared to L1^{+y} cells after MeCP2 knockdown, and L1^{+y} cells transduced with MeCP2 overexpression sequence. Cells after MeCP2 overexpression showed longer neurites. However, the phenotype of MeCP2 overexpressing neurons is heterogeneous in the literature, and will be considered in the discussion.

These findings are consistent with MeCP2 knockdown affecting L1-70 production, and therefore enhancing neurite outgrowth, since the neurites of MeCP2 knocked-down L1^{+y} cells are significantly longer than the neurites of L1^{RA} mutated cells knocked-down for MeCP2. L1^{RA} neurons do not show enhanced neurite outgrowth as L1^{+y} neurons, possibly due to the mutation in MBP cleavage site, and impossibility to generate L1-70.

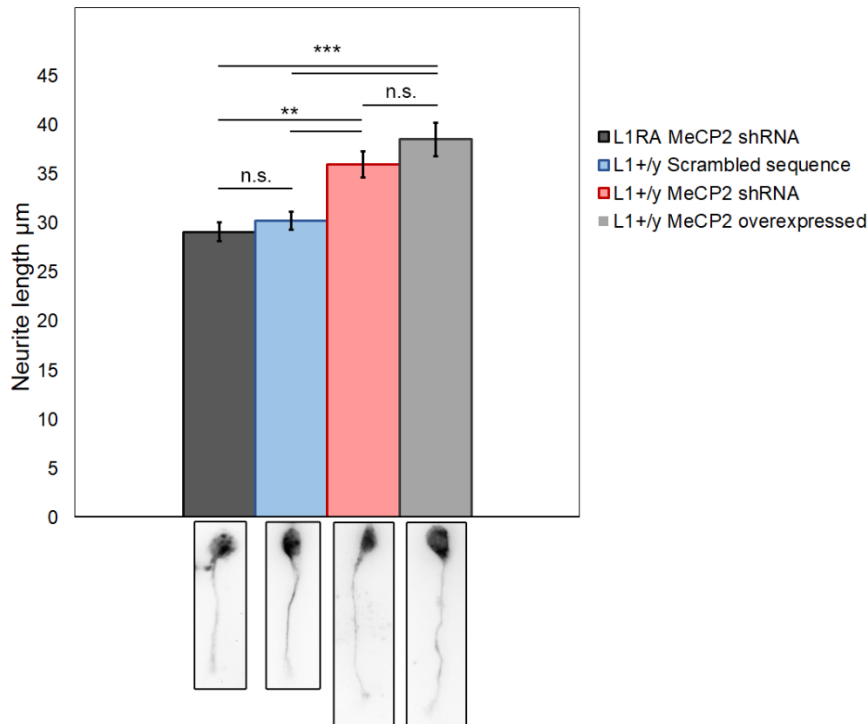


Figure. 3. 23. Effect of MeCP2 expression levels in neurite outgrowth across $L1^{+/y}$ and mutant $L1^{RA}$ genotypes. Neurite measurement in $L1^{+/y}$ cells transduced with AAV carrying MeCP2 shRNA, MeCP2 overexpression, or Scrambled sequences, and in mutant $L1^{RA}$ cerebellar granule cells transduced with AAV carrying MeCP2 shRNA. Bars show mean values of the groups, \pm SEM Error bars. Stars show level of significance ** $p < 0.01$, *** < 0.001 in One-Way ANOVA, followed by Bonferroni test for multiple comparisons.

Table. 3. 4. Data analysis comparing neurite length in cerebellar granule cells after viral transduction. Neurite length (dependent variable) across genotype and AAVs (independent variable). Descriptive statistics are shown, and the result of One-Way ANOVA. Bonferroni test for multiple comparisons was performed, and level of significance across groups is shown in Fig.3.23.

Group	n	Mean	SD	F	Significance
L1 +/y Scrambled sequence	100	30.24	9.10	12.74	p<0.0001
L1 +/y MeCP2 shRNA	102	36.00	13.35		
L1 +/y MeCP2 overexpressed	100	38.51	17.14		
L1 RA MeCP2 shRNA	100	29.09	9.34		

3. 2. 10. MECP2 DOSAGE ALTERS SOMA SIZE OF CEREBELLAR GRANULE CELLS

Since the literature describes differences in the soma size of neurons with MeCP2 loss-of-function mutations (Rangasamy et al., 2016; I.-T. J. Wang et al., 2013) and in particular in MeCP2-deficient cerebellar granule cells (Sampathkumar et al., 2016), I decided also to measure the soma size of cerebellar granule cells after MeCP2 knockdown or overexpression, in the genotypes wild-type L1 and L1^{RA} mutant mice. For this, I could use the pictures from the previous experiment examining neurite outgrowth.

The results (Fig. 3.24, Table 3.5) showed that the soma sizes of L1^{+y} cerebellar granule cells transduced with AAV carrying scramble sequence were significantly larger than the soma sizes of neurons transduced with AAV carrying MeCP2 shRNA, in both L1^{+y} and L1^{RA} genotypes, and also larger compared to L1^{+y} neurons transduced with AAV carrying MeCP2 overexpression sequence.

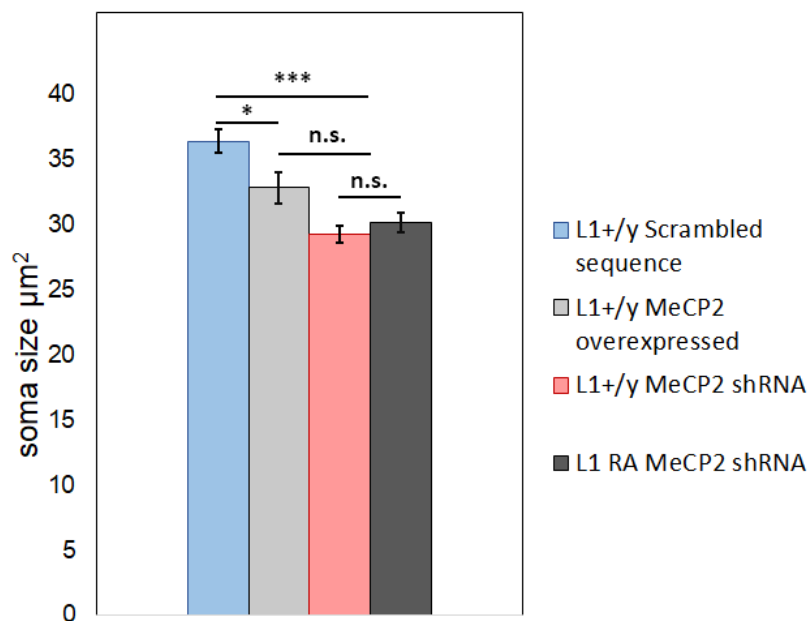


Figure. 3. 24. Effect of MeCP2 expression levels on the soma size of cerebellar granule cells from L1^{+y} and mutant L1^{RA} mice. Soma size was measured in L1^{+y} cells transduced with AAV carrying MeCP2 shRNA, MeCP2 overexpression, or Scrambled sequences, and in mutant L1^{RA} cerebellar granule cells transduced with AAV carrying MeCP2 shRNA. Bars show mean values of the groups, \pm SEM Error bars. Stars show level of significance * $p < 0.05$, *** < 0.001 in One-Way ANOVA, followed by Bonferroni test for multiple comparisons.

Table. 3. 5. Data analysis comparing soma size in cerebellar granule cells after viral transduction. *Soma size (dependent variable) across genotype and AAV (independent variable). Descriptive statistics are shown, and the result of One-Way ANOVA. Bonferroni test for multiple comparisons was performed, and level of significance across groups is shown in Fig.3.24.*

Group	N	Mean	SD	F	Significance
L1 +/y Scrambled sequence	104	36.21	8.78	15.23	p<0.0001
L1 +/y MeCP2 shRNA	131	29.20	7.78		
L1 +/y MeCP2 overexpressed	73	32.78	10.30		
L1 RA MeCP2 shRNA	82	30.07	6.77		

4. DISCUSSION

In previous experiments by our group, L1 fragments containing the intracellular domain were found in the nuclear fraction from mouse brains (Lutz, Loers, et al., 2014; Lutz, Wolters-Eisfeld, et al., 2014), which suggested that these fragments could have nuclear binding partners. In addition, using recombinant L1-ICD and a nuclear extract from early postnatal mouse brain for affinity chromatography, nuclear proteins were identified as potential novel interaction partners of L1-ICD by mass spectrometry. These potential L1 binding partners are SFPQ (also known as polypyrimidine tract binding associated-splicing factor or PSF), NonO (Non-POU domain-containing octamer-binding protein or p54nrb), paraspeckle component 1 (PSPC1), DNA topoisomerase I, importin- β , methyl-CpG-binding protein 2 (MeCP2), WD-repeat protein 5 (WDR5), the heterogeneous nuclear ribonucleoproteins hnRNP-A1, -A2/B1 and -A3, histone H1.4, nucleoporin 93 kDa (Nup93), heat shock cognate protein 71 kDa (Hsc70) and synaptotagmin 1.

In the work presented here I focused on the interaction of L1 with NonO, SFPQ, PSPC1, and MeCP2.

The results of this thesis demonstrate that L1 binds to NonO, SFPQ and MeCP2 via its intracellular domain, and stimulation of L1-signaling which enhances generation of the fragments L1-70 and L1-30 increased the interaction of L1 with these proteins. These interactions could play a role in the functions of L1 and those of the binding partners, and if disturbed could lead to some of the deficits present in humans with mutations in the binding partners, or in L1.

4. 1. L1 BINDS TO THE DBHS PROTEINS NONO AND SFPQ, BUT NOT TO PSPC1

The DNA and RNA binding proteins SFPQ, NonO and PSPC1 interact with one another to form heterodimer complexes, and are involved in the processing and transport of RNA, transcriptional regulation, and DNA repair (J. Huang et al., 2018; Knott et al., 2016).

As a first step, co-immunoprecipitation using nuclear extracts from postnatal mouse brains was performed, and NonO and SFPQ, but not PSPC1 were found interacting with L1. In addition, direct interaction of L1-ICD with NonO and SFPQ, but not with PSPC1 was confirmed using ELISA. In order to examine these interactions in a cellular context, proximity ligation assay was performed using cerebellar granule cells, and close proximity was found between L1 and NonO, SFPQ and PSPC1 both in the nucleus and cytoplasm of neurons.

The treatment of neurons with L1-antibody 557 simulates L1 homophilic interaction, and increases the levels of the L1 fragments L1-70 and L1-30. Proximity ligation assay (PLA) in cerebellar granule cells after L1-antibody 557 treatment increased the amount of PLA signals for NonO and SFPQ, and not for PSPC1. These findings suggest that NonO and SFPQ directly interact with L1, while PSPC1 only indirectly associates with L1 via heterodimer formation with NonO and SFPQ, or that stimulation of L1 signalling leads to displacement of PSPC1 from complexes with nuclear L1-fragments and the other DBHS proteins and that PSPC1 before present in these complexes is then replaced by SFPQ or NonO.

The DBHS proteins rarely function alone, since they are dynamic factors mediating protein-protein and protein-nucleic acid interactions. The availability of interaction partners that can be readily exchanged, regulates dimerization states of these proteins and the composition of dimers regulates distinct cellular functions. SFPQ and NonO dimers are abundant in neurons (Kanai et al., 2004), and are necessary for double stranded DNA repair (Jaafar et al., 2017; S. Li et al., 2014) and neurite outgrowth (Sury et al., 2015; Thomas-Jinu et al., 2017; Won et al., 2017). Since neurons from L1-deficient mice show impaired neurite outgrowth (Fransen, 1998), it is possible that the interaction between L1 and SFPQ/NonO is important for neurite outgrowth. While for DNA repair the absence of NonO can be compensated by SFPQ-mediated recruitment of PSPC1, SFPQ is vital for the DNA repair functions of SFPQ/NonO (Ha et al., 2011; S. Li et al., 2014). Therefore, L1 interaction with SFPQ/NonO might be important for DNA repair, particularly under stress conditions.

While SFPQ/NonO are generally regarded as nuclear proteins, they are present in the cytoplasm during neuronal differentiation, where they regulate RNA transport and neurite outgrowth (Kanai et al., 2004; Sury et al., 2015). Thus, interaction between L1 and SFPQ/NonO in the cytoplasmic compartment could contribute to these functions. SFPQ/NonO in the nucleus are present together with NEAT1 in the paraspeckles (Clemson et al., 2009), and although the function of the paraspeckles has not yet been fully understood, it can be speculated that the interaction of L1 with SFPQ/NonO in the nucleus may influence their activity.

L1-deficient mice have connectivity defects and a small cerebellum, and mice with ablated L1 intracellular domain show deficits in motor function (Nakamura et al., 2010). In addition, L1 has been shown to decrease cholinergic differentiation and accelerate GABAergic differentiation in precursor cell-derived neurons (Z. J. Huang, 2006). SFPQ is required for the regulation of transcripts which drive axon maturation and connectivity, and necessary for normal motor development and cerebellum organization (Thomas-Jinu et al., 2017). On the other hand, humans with mutations in NonO show macrocephaly, distinctive facial features,

shy behaviour, thick corpus callosum and a small cerebellum, symptoms which remain present regardless of upregulation of SFPQ or PSPC1 in response to NonO-dysfunction (Mircsof et al., 2015). The neural abnormalities present in NonO-deficient mice have been attributed to the dysregulation of synaptic transcripts, and particularly down-regulation of GABA, with additional inhibitory synaptic deficits (Mircsof et al., 2015).

I have shown that L1 binds to NonO and SFPQ through its intracellular domain, and in immunostainings; L1 and NonO are located in the same cellular compartments in the cerebellum and hippocampus, in areas like the border between the molecular layer and the pia matter of the cerebellum, and the boundary between the dentate gyrus and the CA3 region of the hippocampus. Since mutations in NonO and L1 are associated with dysregulation of GABA and macrocephaly, it is possible that the disruption of their interaction could be the cause of these deficits. NonO/SFPQ and L1-deficient mice show motor deficits and cerebellar abnormalities; thus, it is conceivable that ablation or disturbance of the interaction between L1 and NonO/SFPQ contributes to these phenotypes.

4. 2. NARROWING DOWN BINDING SITES IN L1 AND NONO/SFPQ THAT MEDIATE THEIR INTERACTIONS

L1 interacts directly with NonO and SFPQ but not with PSPC1, although the DBHS share a high sequence homology. Therefore, NonO and SFPQ might interact with L1 via a common region, which must be different or lacking in PSPC1 for their interaction to not occur.

Only four pathogenic NonO protein variants causing mental disability have been found in humans, but none of these mutations are located in regions identical in NonO and SFPQ but not in PSPC1: p. Asn52Serfs*6 induces a frameshift with premature stop codon with loss of most of the protein, p. Arg365 is located in the coiled coil region, p. Ala 377 is located in the low complexity proline/glutamine rich region, and p. Asn466Lysfs*13 affects the nuclear localization signal (Carlston et al., 2019; Mircsof et al., 2015; Reinstein et al., 2016).

A sequence alignment using the software *Jalview 2.11.0*, shed light on the possible positions where the interaction between L1 and NonO/SFPQ could take place. Future research could aim at mutating distinct protein regions non similar between PSPC1 and NonO/SFPQ, but homologous in NonO and SFPQ (Fig. 4.1, Table 4.1).

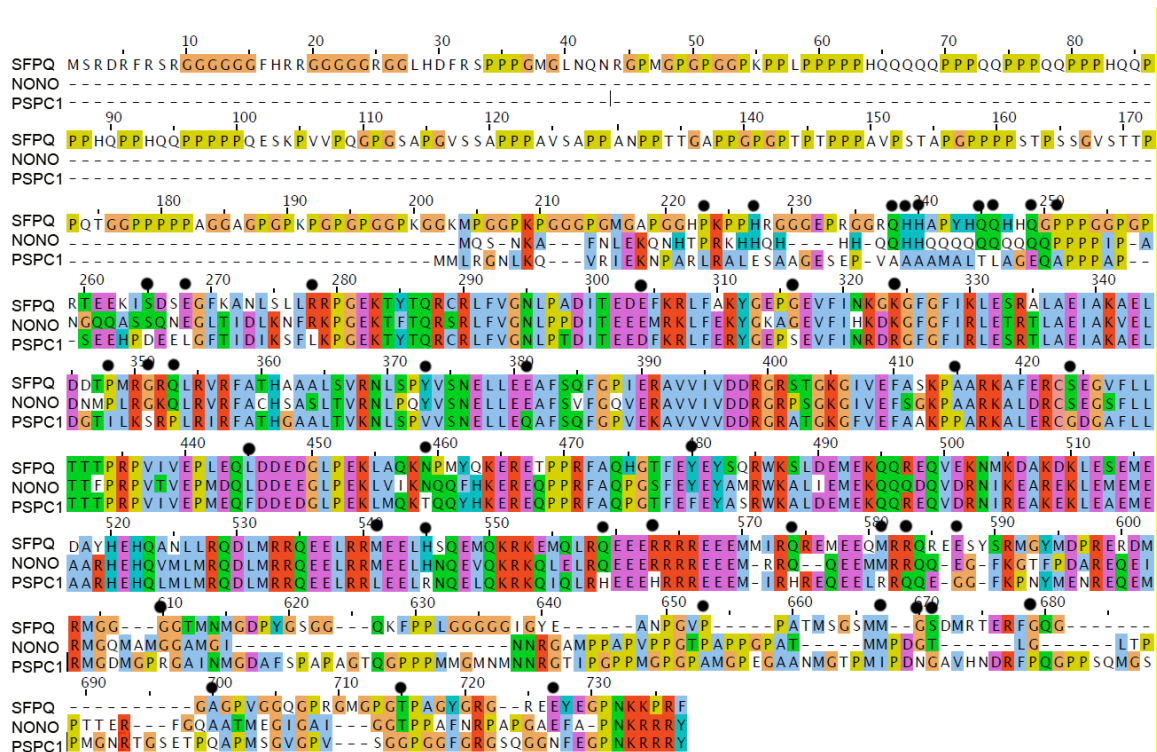


Figure 4. 1. Sequence alignment of the mouse DBHS proteins. Black dots indicate regions with sequence homology between NonO and SFPQ and which are not common to PSPC1. Aminoacid coloring in default colourscheme for alignments in Clustal X, where the colour of a symbol depends on residue type and on the frequency of its occurrence in the column, as detailed in Table 4.1.

Table 4. 1. Colouring scheme of ClustalX.

Residue at position	Residue type	Conservation threshold	Applied colour
A, C, F, H, I, L, M, V, W, Y	Hydrophobic	>60%	BLUE
D, E	Negative charge	>50%	MAGENTA
K, R	Positive charge	>60%	RED
S, T, Q, N	Polar	>50%	GREEN
C	Cysteines	>85%	PINK
G	Glycines	>85%	ORANGE
P	Prolines	>85%	YELLOW
F, Y, W	Aromatic	>50%	CYAN

4. 3. L1 BINDS TO MECP2 VIA ITS INTRACELLULAR DOMAIN

Using ELISA and BIND assay I could show that L1 and MeCP2 directly interact via the L1 intracellular domain. The functional consequences of this interaction can be expected to manifest in mice with ablated L1 intracellular domain, which show a mild phenotype compared with L1-deficient mice and patients with mutations in the extracellular domain of L1 (Nakamura et al., 2010), but remarkably present decreased global L1 expression in adulthood, motor alterations, reduced neurite length, number of neurites and branching.

Since the results from ELISA and BIND assay showed that the intracellular domain of L1 and MeCP2 interact, and this domain is present in the L1 fragments L1-70 and L1-30, which are transported into the nucleus (Lutz et al., 2012; Lutz, Loers, et al., 2014; Lutz, Wolters-Eisfeld, et al., 2014), their interaction with MeCP2 could affect their roles in neurite outgrowth, cell survival, neural migration, and synaptic plasticity (Kraus et al., 2018; Lutz et al., 2016; Lutz, Loers, et al., 2014; Lutz, Wolters-Eisfeld, et al., 2014).

4. 4. MECP2 BINDS TO THE L1 FRAGMENTS L1-70 AND L1-30

Since MeCP2 binds to the intracellular domain of L1, all the L1 fragments carrying the intracellular domain could potentially interact with MeCP2. In order to examine if L1-70 and/or L1-30 interact with MeCP2, co-immunoprecipitation experiments using nuclear extracts from mouse brains or *in vitro* expressed L1 fragments and MeCP2 (MeCP2 α and MeCP2- β isoforms), were performed. MeCP2- α is 10 times more abundant in brain (Mnatzakanian et al., 2004) but less abundant than MeCP2- β in the cerebellar granule cell layer (Olson et al., 2014), and these isoforms have different functions and distributions. Particularly in the cerebellum, in cerebellar granule neurons, MeCP2- β promotes neuronal cell death under the control of FoxG1 (Dastidar et al., 2012). The results showed that L1-70 and L1-30 bind to MeCP2: MeCP2- β was found to interact with both L1-30 and L1-70, while MeCP2- α was found to interact with L1-70, but unspecific signal in the non-immune IgG control for L1-30 made hard to confirm whether MeCP2- α interacts with L1-30.

It is possible that both L1 fragments interact with MeCP2 since both fragments contain the L1 intracellular domain, which has been shown to interact with MeCP2 in ELISA and BIND assay. Moreover, the amino acid sequence of MECP2- β is fully present in the long form MeCP2- α . However, it is important to note that regardless of their sequence similarity, the N-terminus of MECP2- α confers the protein with a lower structural stability and a higher susceptibility to degradation, indicating that the N-terminus contributes to the capacity of MeCP2 to interact with DNA or proteins (Martínez de Paz et al., 2019).

4. 5. L1 BINDING TO MECP2 IS ENHANCED AFTER STIMULATION OF L1-SIGNALLING

In order to examine if MeCP2 and L1 are in close proximity in the cellular context, proximity ligation assay experiments in cerebellar granule cells and cerebellar tissue slices were performed. The results showed that they are present in close proximity in cerebellar granule cells and cerebellar slices. Since the generation of L1-70 and L1-30 is increased after stimulation of the cells with L1 antibody 557, proximity ligation assay experiments in cerebellar granule cells after stimulation with antibody 557, were performed. Increment in the positive signal of the proximity ligation assay in the cells stimulated with 557 antibody indicates that the interaction between MeCP2 and L1 increased upon stimulation, supporting the previous results which showed that MeCP2 interacts with L1-70 and L1-30. These fragments are important for neurite outgrowth, cell survival, neural migration, and synaptic plasticity (Kraus, Kleene, Henis, et al., 2018; Lutz, Wolters-Eisfeld, et al., 2014; Lutz, Loers, et al., 2014; Lutz et al., 2016), and these functions are of particular importance during early postnatal development, suggesting that the interaction between MeCP2 and L1 may influence L1/MeCP2-related functions during postnatal development.

The interaction between MeCP2 and L1 in cerebellar neurons during postnatal development is of particular interest. The levels of MeCP2 are highest in neurons, and the cerebellum has the highest neuronal density of all the different brain regions (Marzban et al., 2015). Cerebellar abnormalities are associated with autism (Fernández et al., 2019), cognitive impairment (Schmahmann, 2019), motor problems, and defects in memory function (Ferrari et al., 2018). Some of these abnormalities are present in RTT and L1 syndrome.

4. 6. L1-MECP2 INTERACTION INCREASES DURING NEURONAL DIFFERENTIATION

The expression levels of MeCP2 increase during neuronal development (Jung et al., 2003; Liu et al., 2017). MeCP2 has been shown to regulate neural cell differentiation in zebrafish (H. Gao et al., 2015) and in mice, where its deficiency alters gene expression and delays the cell maturation of hippocampal neurons (Smrt et al., 2007). In addition, human neural stem cells from patients with Rett syndrome present neuronal maturation defects (K.-Y. Kim et al., 2011), indicating that MeCP2 is vital for neural differentiation and maturation (H. Gao et al., 2015). In neural precursor cells, L1 was found to inhibit proliferation and enhance neural differentiation (Dihné et al., 2003). Due to the overlap in neural functions regulated by MeCP2 and L1 during differentiation and maturation, I studied the cellular distribution of MeCP2 and L1 using

immunostainings in neural stem cells before and after differentiation into neurons. I could observe stronger staining of MeCP2 in the nucleus during differentiation, and the MeCP2-staining pattern transitioned between uniform nuclear staining to an increasingly punctate nuclear staining, as it is shown in the literature (Kishi & Macklis, 2004). The signal of L1 located in the cytoplasm and increased during differentiation. The results showed that L1 and MeCP2 co-localized significantly more in differentiated neural stem cells than in neural stem cells before differentiation, suggesting the interaction between L1 and MeCP2 could be of importance during neuronal differentiation.

Post-translational modifications determine the cellular localization of L1 and MeCP2. L1 requires SUMOylation in order to be cleaved by myelin basic protein and for generation of L1-70 (Lutz, Loers, et al., 2014). Ubiquitination facilitates lysosomal degradation of L1 and could control the re-appearance of L1 at the cell surface influencing neurite outgrowth and cell adhesion. Additionally, phosphorylation of L1 prevents its binding to AP-2 and clathrin-mediated internalization of L1 (Schaefer et al., 2002). Phosphorylation of MeCP2 has been shown to be decisive for its subcellular localization, and its interaction with other proteins and DNA (Gonzales et al., 2012). Different phosphorylated forms of MeCP2 have been identified to localize in different cellular compartments, and their abundance varies at different stages of neural development, indicating that MeCP2 is translocated from the cytoplasm to the nucleus as the brain matures, and phosphorylation determines the cellular localization of MeCP2 (Liu et al., 2017). There are different phosphorylated forms of MeCP2: phosphorylated at serine 80 (pS80 MeCP2), at serine292 (pS292 MeCP2), and at serine 421 (pS421 MeCP2). pS421 and p292 are located in the cytoplasm, while pS80 MeCP2 and most of the total MeCP2 is located in the nucleus (Liu et al., 2017).

On the second postnatal day, when the levels of L1-70 rise (Lutz, 2013), the levels of pS421 MeCP2 are higher in the cytoplasm. L1-70 levels start decreasing on the sixth postnatal day, concomitant with a decrease in the levels of MeCP2 pS421 as shown in Figure 4.2. The results of the immunostaining in NSCs, together with the findings described in the literature, suggest that L1 fragments in the cytoplasm might interact with pS421 MeCP2 during differentiation.

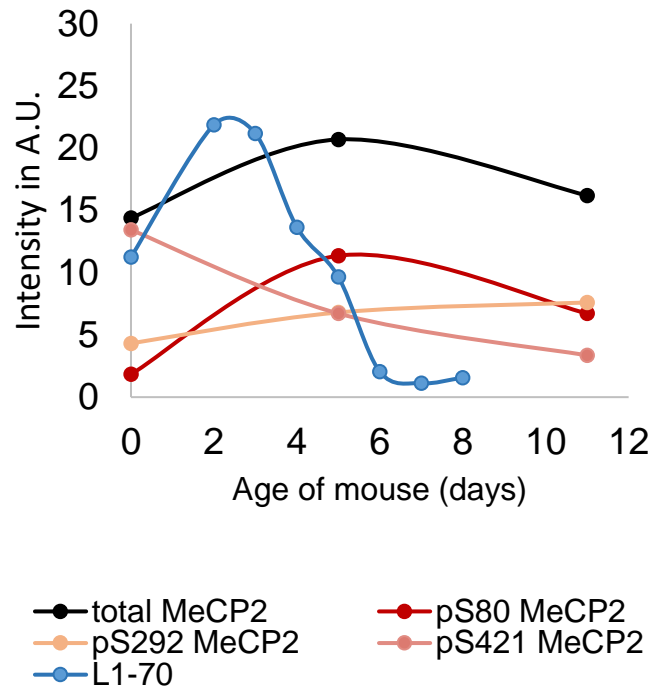


Figure 4. 2. Levels of L1-70, total MeCP2, and MeCP2 phosphorylated forms during development. Graph depicts data collected from the literature about L1-70 (Lutz, 2013) and MeCP2 (Liu et al., 2017). As the L1 data was from mouse brains, but the MeCP2 data was obtained from rat brains, the timeline has been adjusted with a 10%-time delay for the MeCP2 data.

Interestingly, pS421 MeCP2 is selectively found in the brain, and it has been found to regulate the transcription of Brain Derived Neurotrophic Factor (BDNF) (Zhou et al., 2006), which is vital for dendritic growth and spine maturation. Regulation of BDNF by MeCP2 is considered one of the mechanisms by which deficits present in organisms with MeCP2 disease-causing mutations are produced. Furthermore, similarly to the defective MeCP2 phenotype, L1-deficient mice show abnormal dendritic architecture, suggesting a role for L1 in dendritic neurogenesis (Demyanenko et al., 1999), and reduced density of dendritic spines in the cerebellum (Kraus, Kleene, Henis, et al., 2018), indicating L1 could a role in the formation of synaptic contacts. In addition, examination and comparison of transcriptome data from the literature studying transcripts expressed in the cerebellum of L1-deficient mice (Tapanes-Castillo et al., 2010) and MeCP2-deficient mice (Raman et al., 2018) compared to wild-type littermates, indicates that BDNF is one of the common dysregulated genes in MeCP2- and L1-

deficient mice, together with Wnt7a and Hes5 (Table 4.2). However, the exact mechanism by which MeCP2 regulates BDNF expression is still being discussed. Two opposing views have been integrated into a “dual operation” model by which MeCP2 can both repress and activate BDNF expression (W. Li & Pozzo-Miller, 2014): since in absence of membrane depolarization MeCP2 is bound to the BDNF promoter and prevents its transcription (Zhou et al., 2006); although, BDNF protein expression is lower in the brain of MeCP2 knockout mice (Chang et al., 2006), and neuronal activity-dependent phosphorylation of MeCP2 at serine 421 induces BDNF transcription (Zhou et al., 2006). However, in absence of neuronal activity in maturing neurons, the levels of BDNF transcripts are more abundant in MeCP2-deficient neurons (W. G. Chen et al., 2003).

The dysregulation of BDNF found in both MeCP2-deficient and L1-deficient mice, together with the synaptic deficits observed in these mice, suggests that the interaction between MeCP2 and L1 could influence the regulation of BDNF (Fig. 4.3).

Table 4. 2. Genes dysregulated in both cerebella of L1- and MeCP2-deficient mice compared to cerebella of their wild-type littermates. *Comparison of transcriptome data from the literature (Raman et al., 2018; Tapanes-Castillo et al., 2010). Gene ID on left column, phenotype name on top row. logFC: binary logarithm of the fold change. Red/green colour scale depicting the difference between low (red) and high (green) transcription levels in L1 or MeCP2-deficient mouse cerebella, compared to wild-type cerebella.*

	L1	MeCP2
Gene	logFC	logFC
Bdnf	-0.264	-0.726
Cdc7	-0.195	0.240
Col3a1	0.214	-0.544
Hes5	-0.259	-0.452
Pik3r1	-0.188	0.182
Wnt7a	-0.283	-0.215

Additionally, I performed immunostainings to examine the distribution of MeCP2 and L1 in the mouse brain. Images of stainings of 12-day-old L1 wild-type mice showed punctuate fluorescent signals of L1 co-localising with punctate MeCP2 in the nucleus of hippocampal neurons. The distribution of MeCP2 in hippocampal neurons is characterized by diffuse nuclear staining during development, and progressive punctate staining till its localization in heterochromatic regions (Kishi & Macklis, 2004; Liu et al., 2017), with the punctate MeCP2 staining being the most frequent in the adult brain. The signal of MeCP2 co-localized with L1 observed was punctate, but not yet located in heterochromatic regions of the chromatin as it would appear in mature neurons, indicating that the MeCP2-L1 interaction could be important during neuronal maturation.

4. 7. MECP2 INFLUENCES THE GENERATION OF L1-70

Several studies have found alterations in the expression of myelin-related genes in MeCP2-deficient cells and in some brain regions of and MeCP2-deficient mice (Jin et al., 2017; Vora et al., 2010). Additionally, cultured oligodendrocytes exhibited an increase in the expression of myelin genes, including myelin basic protein (MBP) after MeCP2 knockdown (KhorshidAhmad et al., 2016; Moore, 2011; Sharma et al., 2015; Vora et al., 2010), and the increase in gene expression was coupled with increased protein levels (Sharma et al., 2015). There is evidence showing that regulation of MBP by MeCP2 is a downstream consequence of the influence MeCP2 has on regulating BDNF gene expression (Chang et al., 2006; W. G. Chen et al., 2003), since MeCP2 impacts BDNF-induced endogenous myelin repair mechanisms, which in turn control the expression of MBP (Acosta et al., 2013; KhorshidAhmad et al., 2016).

Myelin basic protein is a serine protease relevant for L1 functions, because a particular MBP isoform (exon II-containing MBP, 21.5 kDa isoform) together with a part of dynamin I, cleaves L1 to generate L1-70. MBP is expressed endogenously in cultured cerebellar neurons and released into the cell culture supernatant as MBP-dynamin I fusion protein (Lutz, Loers, et al., 2014). My Western Blots with cortical neuron lysates indicate that this fusion protein is also expressed by cortical neurons. Knowing that MeCP2 can influence MBP expression, I decided to perform experiments in order to examine the effects of MeCP2 knockdown on the amount of L1-70. In experiments knocking-down MeCP2 using adeno-associated viruses carrying shRNAs, I could find a significantly increased amount of L1-70 in cortical neurons and cerebellar granule cells, indicating that MeCP2 can indirectly influence the proteolytic processing of L1 and the generation of L1-70, possibly due to changes in MBP expression.

Interestingly, MeCP2 is being studied in the context of the demyelinating disease multiple sclerosis due to its influence on BDNF, and downstream on myelination, showing its potential for novel therapeutic approaches to promote remyelination or myelin repair (KhorshidAhmad et al., 2016). The 21.5 kDa exon II-containing MBP isoform is downregulated in the adult central nervous system, and abundant during development (myelination), but samples of patients with multiple sclerosis show high levels of exon II-containing MBP isoform, possibly due to recapitulation of ontogenic events during myelin repair (Capello et al., 1997). Particularly the 21.5 kDa MBP is increased in the injured spinal cords of mice transduced by L1-encoding adeno-associated virus (AAV) (Jian Chen et al., 2007).

L1 is vital for myelination and the maintenance of myelin sheaths in the central and peripheral nervous system, enhancing remyelination after nerve injury and the recovery of motor functions (Barbin et al., 2004; Jian Chen et al., 2007). Specifically L1-70 has been shown to

enhance Schwann cell process formation, migration and myelination, and in utero injection of AAV encoding MBP into MBP-deficient (shiverer) mice, correlates with increased levels of L1-70 and normalizes myelination after injury and (Lutz et al., 2016), while the in utero injection of shiverer mice with inactive MBP, not proteolytically active to cleave L1, does not. These findings suggest that L1-70 could be an important player in the pathogenesis of demyelinating diseases like multiple sclerosis, and therefore a valuable target for therapeutic interventions. In addition, the influence that the levels of MeCP2 have in the regulation of L1-70 via MBP could be important for understanding the deficits present in patients with Rett syndrome.

Although an increased amount in MBP transcripts in MeCP2-deficient cells or regions of MeCP2-deficient mouse brains have been already described in other studies (Jin et al., 2017; Sharma et al., 2015; Vora et al., 2010), the increased amount of exon II-containing MBP after MeCP2 knockdown was not confirmed during this thesis, and could be considered a limitation in this work. I sought to determine the concentration of exon II-containing MBP mRNA in cerebellar granule cells using qPCR, however, the design of specific primers for this isoform is not possible due to overlap in the sequences of the different MBP isoforms, making impossible to distinguish the transcripts of this particular isoform.

4. 8. MeCP2 EXPRESSION INFLUENCES L1-DEPENDENT NEURITE OUTGROWTH

The influence of MBP in L1-functions due to the generation of L1-70 is important for L1-functions in neurite outgrowth, neuronal survival, neural migration, formation and maintenance of myelin, and synaptic activity and plasticity.

Considering both the fact that MeCP2 interacts with L1, and in addition influences MBP and therefore the generation of L1-70, L1-functions could be influenced by MeCP2 expression (Fig. 4.3). In order to study the influence of MeCP2 in L1-dependent neurite outgrowth, neurite outgrowth was measured in cerebellar granule cells from L1 wild-type mice, and L1^{RA} mutated mice (mutation in MBP cleavage site) after MeCP2 knockdown or overexpression. MeCP2 knocked-down and MeCP2 overexpressing cultured cerebellar neurons showed longer neurites than the controls, but in contrast, L1^{RA} mutant neurons not containing L1-70 did not show increased neurite outgrowth after MeCP2 knockdown. These results suggest that the increased neurite length could be caused by the higher amount of L1-70, which promotes neurite outgrowth (Lutz, Loers, et al., 2014).

This result is consistent with neurite outgrowth being enhanced by the higher amount of L1-70; however, it does not explain why MeCP2 overexpression caused increased neurite

outgrowth. Studies in MeCP2 mouse models with different MeCP2 loss-of-function mutations, have shown that each mutation produces particular behavioural deficits, emphasizing the different phenotypes in RTT (R. Z. Chen et al., 2001; Guy et al., 2001; Jentarra et al., 2010; Shahbazian, 2002). The cellular morphology in the different MeCP2 mutant mice varies greatly across different MeCP2 mutations (N. P. Belichenko et al., 2008; P. V. Belichenko et al., 2009; Rietveld et al., 2015; Robinson et al., 2012; I.-T. J. Wang et al., 2013). Moreover, it differs depending on cellular subtype and developmental time point, making comparisons across studies difficult (N. P. Belichenko et al., 2008; P. V. Belichenko et al., 2009; I.-T. J. Wang et al., 2013).

Regarding neurite outgrowth and dendritic complexity, most studies describe reduced neurite length and dendritic complexity in MeCP2-deficient cells or loss-of-function mutations, however these results have been generally obtained in pyramidal neurons (Rietveld et al., 2015; Sampathkumar et al., 2016; Zhou et al., 2006) or stem cells (Bu et al., 2017; Yoo et al., 2017). On the other hand, dorsal root ganglion neurons (DRGs) of Rett syndrome rat model and MeCP2 knocked-down DRGs showed increased neurite length when compared to wild-type DRGs (Bhattacharjee et al., 2017), and this increase was accompanied by the up-regulation of genes involved in actin polymerization. It is possible that MeCP2 knockdown has the same effect in cerebellar granule cells and DRGs since both cell types have important excitatory synaptic functions that rely on glutamate and NMDA receptors, and glutamate influences actin cytoskeleton dynamics (Basu & Lamprecht, 2018).

4. 9. NEURONAL MORPHOLOGY AND MECP2

In addition, studies performing measurements of neurite morphology observed after overexpression of MeCP2 and MeCP2 gain-of-function mutations *in vitro*, obtained very heterogeneous results, showing an increase (Jugloff et al., 2005; Larimore et al., 2009), no change (Chapleau et al., 2009) or decrease (Zhou et al., 2006) in neurite length and complexity. Although MeCP2 dosage alterations are considered an important component of the neurological disorder similarities between MeCP2-loss-of-function and gain-of-function mutations, it is possible that the mechanisms regulating neurite length differ in these contexts, and in MeCP2 knockdown and MeCP2 overexpression. It can only be hypothesized that the increased neurite outgrowth observed in MeCP2 knocked-down neurons could arise as a compensatory mechanism of the cells driven by L1 in response to the decrease of MeCP2 in this cell type, especially since the effect is mild, and L1 overexpression has been shown to normalize neuritogenesis in Rett syndrome-derived neural precursor cells (Yoo et al., 2017).

Both reduced dendritic outgrowth and soma size are thought to be contributors to the microcephaly phenotype of patients with RTT, and reduced soma size has been reported in RTT-post mortem tissue (Bauman et al., 1995). The changes in soma size have been shown to be consistent across cell types and MeCP2 loss-of-function mutations, even persisting throughout development (I.-T. J. Wang et al., 2013). Soma size is therefore considered a robust and reliable marker for evaluating MeCP2 function in studies of MeCP2 loss-of-function mutations (I.-T. J. Wang et al., 2013). I decided to measure the soma size of cerebellar granule cells from L1 wild-type mice, and L1^{RA} mutated mice (mutation in MBP cleavage site) after MeCP2 knockdown or overexpression, and obtained: MeCP2 knocked-down wild-type and L1^{RA} cerebellar neurons showed a decrease in soma size when compared to wild-type cerebellar neurons transduced with scrambled virus, or cerebellar neurons over expressing MeCP2. However, the soma size of MeCP2 overexpressing cerebellar neurons was only slightly smaller than the soma of MeCP2 wild-type neurons transduced with scrambled virus.

The molecular mechanisms by which MeCP2 loss-of-function mutations cause a reduction of neuronal soma size are not completely understood. On the other hand, the observation of a reduced soma size in MeCP2-deficient cells and in cells carrying MeCP2 loss-of-function mutations, is consistent in the literature (R. Z. Chen et al., 2001, 2001; Robinson et al., 2012; Taneja et al., 2009), and in agreement with the results I obtained.

Studies observing the soma size in MeCP2 overexpressing cells have found generally no difference (Jugloff et al., 2005; I.-T. J. Wang et al., 2013), or a reduction (Zhou et al., 2006). In my results I found a slight decrease in soma size in MeCP2 overexpressing cerebellar neurons when compared cerebellar neurons transduced with scramble sequence.

4. 10. L1-MECP2 INTERACTION: IMPLICATIONS FOR NEUROLOGICAL DISORDERS

The mTOR pathway is considered a primary regulator of cell size (Tumaneng et al., 2012), and dysregulation or dysfunction of the mTOR pathway was found in studies on cells from mice deficient in MeCP2 (Tropea et al., 2009) and from mice carrying MeCP2 loss-of-function mutations, as well as in RTT patients (Olson et al., 2018). The decreased cell size phenotype could be rescued in cerebellar neurons after supplementation of the cells with IGF-1 (Rangasamy et al., 2016), suggesting that the effects of a lack or dysfunction of MeCP2 in neuronal morphology can be the consequence of a dysregulation in the mTOR pathway.

Furthermore, research performed on samples from humans suffering from autism spectrum disorders found a dysregulation of the mTOR pathway (Jianling Chen et al., 2014), which is

important for neurobiological functions going beyond soma size, and affecting cell survival, growth (Brunet et al., 1999) and synaptic plasticity (Peineau et al., 2007). In addition, MeCP2-deficient cerebellar neurons showed increased neuronal cell death when exposed to excitotoxicity and hypoxia when compared to wild-type neurons, (Russell et al., 2007), suggesting a role for MeCP2 in neuronal death produced by glutamate-enhanced excitatory neurotransmission. Interestingly, enhancing the generation of the L1-70 fragment provided neuroprotection against glutamate toxicity in cerebellar neurons (Lutz, Loers, et al., 2014). These facts emphasize the role of MeCP2 and L1 function in neuronal injury and cell-death triggered by excitotoxicity, and indicate that the interaction between L1-70 and MeCP2 might play a role in the neuronal survival of cerebellar neurons.

Additional neuroprotective mechanisms link L1 and MeCP2. Foetal alcohol syndrome is a common and preventable cause of mental retardation, caused by prenatal ethanol exposure, resulting in birth defects and behavioural abnormalities (Arevalo et al., 2008). Studies suggest that ethanol can cause foetal alcohol syndrome by disrupting L1 function, because L1 syndrome and foetal alcohol syndrome present several common abnormalities, and ethanol can bind to L1 (Arevalo et al., 2008) inhibiting L1-mediated cell adhesion (Ramanathan et al., 1996) and neurite outgrowth (Bearer et al., 1999). However, the sensitivity of L1 to ethanol is reduced by the uncoupling of L1 at its intracellular domain from ankyrin and the spectrin-actin cytoskeleton (Dou et al., 2018). In this context it is interesting to observe that the expression of MeCP2 is increased by alcohol exposure (Liyanage et al., 2015; Repunte-Canonigo et al., 2014), and that mice with truncated MeCP2 experience increased sensitivity to ethanol when compared to wild-type mice. These findings jointly indicate that the interaction between MeCP2 and L1 via its intracellular domain could contribute to the detachment of L1 molecules from ankyrin, reducing the sensitivity of L1 to ethanol, and contributing to the mechanisms underlying foetal alcohol syndrome.

Gene expression analysis showed that mitochondrial dysfunction plays a role in the phenotype of MeCP2-deficient mice (Kriaucionis et al., 2006; Shulyakova et al., 2017). MeCP2-deficient cells present dysregulated expression patterns of genes important for mitochondrial function, which initially produce mitochondrial hyperpolarization (Galloway & Yoon, 2012), but eventually facilitate overproduction of radical oxygen species, which produce malfunction of the mitochondria and cause depolarization (Shulyakova et al., 2017). After the cleavage of L1 by myelin basic protein, the fragment L1-70 is not only imported into the nucleus, but into mitochondria (Kraus, Kleene, Braren, et al., 2018), where it regulates complex I activity and the mitochondrial membrane potential. In fact, the mitochondria from L1-deficient cerebellar neurons presented a reduction in membrane potential when compared to wild-type mitochondria. These findings suggest that the interaction between L1 and MeCP2 could be

important for correct mitochondrial function, and therapies that target different aspects of mitochondrial function could be beneficial for patients with RTT and L1-syndrome.

4. 11. L1 AND ITS NUCLEAR BINDING PARTNERS: RELATIONSHIPS AND GENE REGULATORY FUNCTIONS

The RE1-Silencing Transcription factor (REST) is highly expressed under conditions of low L1 expression, and vice versa, suggesting that L1 is repressed by REST (Menzel et al., 2016). In addition, MeCP2 inhibits the expression of REST by binding to the REST promoter (Abuhatzira et al., 2007); these findings suggest an influence of MeCP2 on the expression of L1 via regulation of REST (Fig. 4.3). REST has also been shown to regulate the transition of pluripotent cells to NSCs progenitors and to neurons *in vitro* (Ballas et al., 2005). REST recruits histone deacetylases (HDACs) and Sin3A, removing acetyl groups from the core histones, making the genes be tightly packed and inaccessible for the transcriptional machinery (Thiel et al., 2015).

Interestingly, NonO and SFPQ also participate in the silencing of gene expression recruiting HDAC/Sin3A (X. Dong et al., 2005; Mathur et al., 2001). These findings together involve L1, NonO, SFPQ and MeCP2 in REST-influenced gene regulation (Fig. 4.3).

Different studies showed that MeCP2 interacts with Heterochromatin protein 1 (HP1 γ) via its chromoshadow domain (Fujita et al., 2003), and interferes with HP1 γ chromatin binding activity, contributing to chromatin unfolding and reorganization, possibly preparing chromatin for subsequent transcriptional regulation (Brink et al., 2013). In this thesis, I could show that L1 and MeCP2 interact in the cytoplasm and nucleus of neurons. Additional findings by our group have shown that L1 also binds to the chromoshadow domain of HP1 γ , via the pentapeptide motif (PxVxL), which is present in the intracellular domain of L1 (Wolters, 2009; Castillo, personal communication), and in many HP1 γ binding partners (Thiru et al., 2004). These findings raise the question whether the L1 nuclear fragments could play a role in chromatin remodelling in conjunction with MeCP2 and HP1 γ .

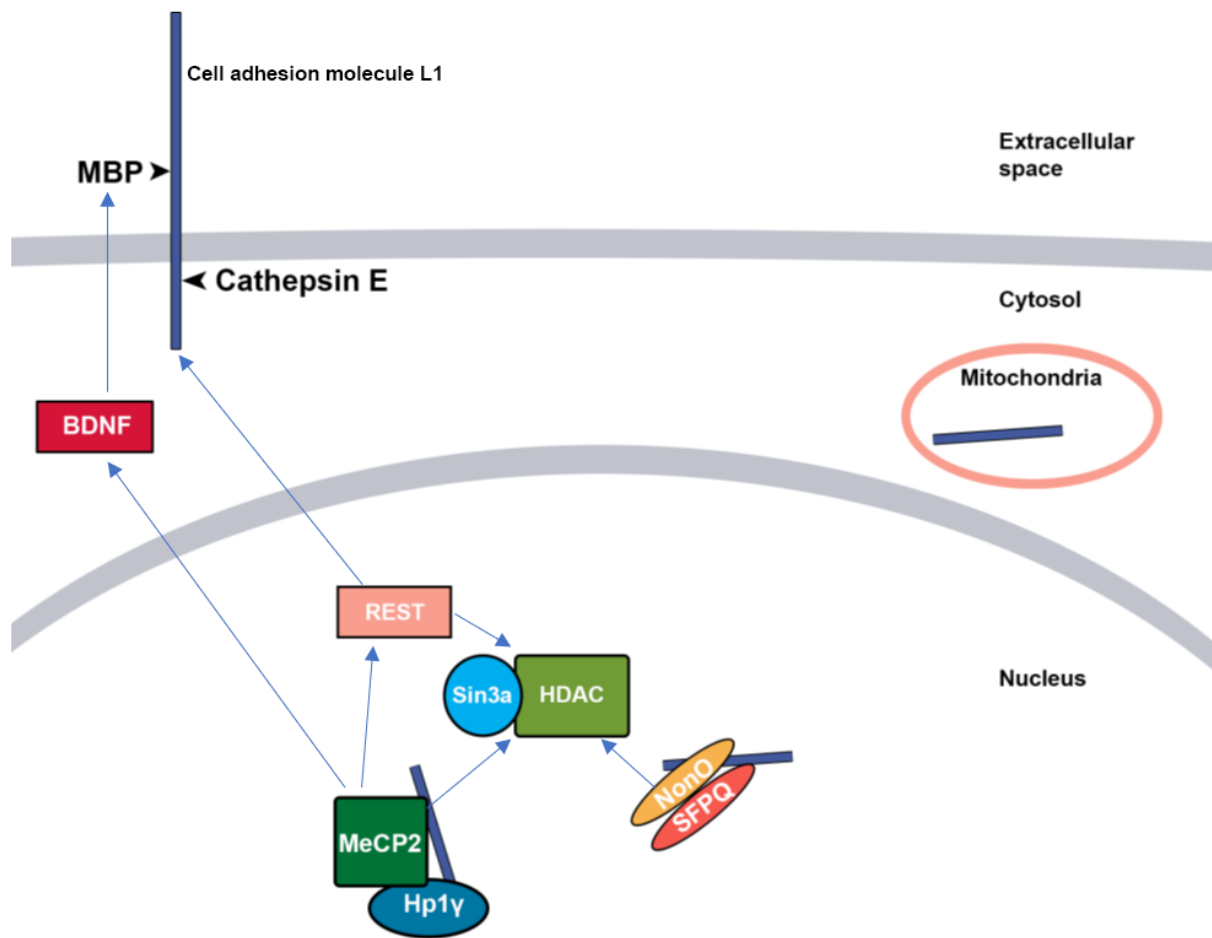


Figure 4. 3. Model for the relationships of L1 and its nuclear binding partners in the cellular context. Figure showing full-length L1 at the plasma membrane (Cell adhesion molecule L1), where it is cleaved by myelin basic protein (MBP) to generate L1-70, and by Cathepsin E to generate L1-30. L1-70 and L1-30 are internalized, and imported into the nucleus, however L1-70 can also be found in mitochondria. Both L1 fragments could interact via L1 cytoplasmic domain with the nuclear proteins MeCP2, NonO, SFPQ and HP1 γ . MeCP2 regulates the expression of REST, which regulate the expression of full-length L1. MeCP2 affects BDNF, which alters MBP expression, influencing the generation of L1-70. The interaction of L1-70 and L1-30 with the nuclear binding partners, could affect their functions of gene regulation via recruitment of Sin3a and HDAC, as well as chromatin remodeling and organization.

4. 12. CONCLUSIONS

During this work, the interaction of L1 with NonO, SFPQ, and MeCP2 has been confirmed. These interactions were mediated by the intracellular domain of L1, and they were enhanced upon stimulation of L1-signalling and mimicking of L1 homophilic interaction, indicating that these interactions could play a role in L1-signalling, neuronal migration, myelination, neurite outgrowth, and neuronal survival.

Using *in vitro* produced proteins for co-immunoprecipitation, I could show that MeCP2 interacts with the L1 fragments L1-70 and L1-30.

Examining the distribution of the binding partners and L1 *in vivo* by immunostainings, I could find co-localization of MeCP2 and L1 in the hippocampus of early postnatal mice. Moreover, L1 and MeCP2 co-localized in murine neural stem cells, and the co-localization of L1 and MeCP2 increased during neuronal differentiation, suggesting their interaction could play a role in this process.

In addition, I found that knockdown of MeCP2 leads to upregulation of L1 processing and generation of L1-70, triggering L1-dependent neurite outgrowth, indicating this effect could be caused by the already described upregulation of MBP by MeCP2.

5. SUMMARY/ ZUSAMMENFASSUNG

This work shows that the cell adhesion molecule L1 interacts with the nuclear proteins MeCP2, NonO and SFPQ via its intracellular domain.

The interaction between L1 and NonO/SFPQ is shown using ELISA and co-immunoprecipitation, and verified *in vitro* using proximity ligation assay in cerebellar granule cells. Stimulation of L1-signalling which leads to cleavage and generation of the L1 fragments L1-70 and L1-30 and their internalization and import into the nucleus, increased the number of positive signals in the proximity ligation assay. This indicates for the first time that L1 interacts with NonO and SFPQ in the cellular context, and that this interaction is enhanced via L1-signalling. In addition, immunostainings of NonO and L1 in mouse brain tissue slices showed joint localization of these proteins in regions of the cerebellum and the hippocampus.

The interaction between L1 and MeCP2 was confirmed using ELISA, BIND assay and co-immunoprecipitation. In addition, proximity ligation assay experiments using cerebellar granule cells showed close proximity (<40 nm) of L1 and MeCP2. An increase in the signal after stimulation of L1-signalling was observed. Furthermore, the interaction between MeCP2 and *in vitro* expressed L1 fragments L1-70 and L1-30 was confirmed using co-immunoprecipitation. Stainings in neural stem cells showed co-localization of L1 and MeCP2 in the cytoplasm, which increased with differentiation. Besides, stainings in mouse brain tissue slices from early postnatal mice showed that L1 and MeCP2 co-localize in the nucleus of hippocampal neurons, indicating that L1 and MeCP2 interact *in vivo*.

In order to study the functional consequences of the interaction between L1 and MeCP2 on L1-dependent neural functions, knockdown of MeCP2 was performed in cerebellar granule cells and cortical neurons, and in the mouse cerebellum. Western Blots of cerebellar granule cells and cortical neurons after MeCP2 knockdown showed that both cell types had increased levels of L1-70, possibly due to the effect of MeCP2 on the expression of MBP (protease which cleaves full-length L1 to generate L1-70). Thus, MeCP2 may play a role in regulating L1-mediated cellular functions. Moreover, increased neurite outgrowth was found in wild-type cerebellar granule cells after MeCP2 knockdown, but when studying cerebellar granule cells mutated in the MBP cleavage site after MeCP2 knockdown, neurite outgrowth was not increased. These results indicate that MeCP2 might modulate L1-dependent neurite outgrowth.

The novel nuclear L1-binding partners NonO, SFPQ and MeCP2 have important functions in gene regulation, chromatin structure remodelling, DNA repair, RNA processing, cell differentiation, cell growth and maintenance pathways, mitochondrial function, and synaptic

transmission. The interaction of L1 with these proteins reveals that proteolytic processing equips L1 with multiple functions, which could play a role in the pathogenesis of many neuronal diseases.

Diese Arbeit zeigt, dass das Zelladhäsionsmolekül L1 über seine intrazelluläre Domäne mit den Kernproteinen MeCP2, NonO und SFPQ interagiert.

Die Wechselwirkung zwischen L1 und NonO / SFPQ wurde unter Verwendung von ELISA und Ko-Immunpräzipitation mittels biochemischer Methoden bestätigt und *in vitro* in Körnerzellen des Kleinhirns unter Verwendung eines Proximity Ligation Assays gezeigt. Die Stimulierung der L1-Signalübertragung, die zur Spaltung und Erzeugung der L1-Fragmente L1-70 und L1-30 sowie deren Internalisierung und Import in den Kern führt, erhöhte die Anzahl positiver Signale im Proximity Ligation Assay. Dies zeigt erstmals, dass L1 im zellulären Kontext mit NonO und SFPQ interagiert und dass diese Interaktion durch L1-Signaltransduktion verstärkt wird. Zusätzlich zeigten Immunfärbungen von NonO und L1 in Hirngewebeschnitten von Mäusen eine gemeinsame Lokalisierung dieser Proteine in Regionen des Kleinhirns und des Hippocampus.

Die Wechselwirkung zwischen L1 und MeCP2 wurde ebenfalls unter Verwendung von ELISA, BIND-Assay und Co-Immunpräzipitation bestätigt. Zusätzlich zeigten Proximity Ligation Assay-Experimente unter Verwendung von Kleinhirn-Körnerzellen eine enge Nähe (<40 nm) von L1 und MeCP2. Ein Anstieg des Signals nach Stimulation des L1-Signaltransduktion wurde beobachtet. Darüber hinaus wurde die Wechselwirkung zwischen MeCP2 und *in vitro* exprimierten L1-Fragmenten L1-70 und L1-30 unter Verwendung von Ko-Immunpräzipitation bestätigt. Färbungen in neuronalen Stammzellen zeigten eine Ko-Lokalisation von L1 und MeCP2 im Zytoplasma, die mit der Differenzierung zunahm. Außerdem zeigten Färbungen in Maus-Hirngewebeschnitten von frühen postnatalen Mäusen, dass L1 und MeCP2 im Kern von Hippocampus-Neuronen co-lokalisiert sind, was darauf hinweist, dass L1 und MeCP2 *in vivo* interagieren.

Um die funktionellen Konsequenzen der Wechselwirkung zwischen L1 und MeCP2 auf L1-abhängige neuronale Funktionen zu untersuchen, wurde ein MeCP2 Knockdown in Kleinhirnkörnerzellen und kortikalen Neuronen sowie im Kleinhirn von Mäusen realisiert. Western-blots von Kleinhirnkörnerzellen und kortikalen Neuronen nach MeCP2-Knockdown zeigten, dass beide Zelltypen erhöhte L1-70-Werte hatten, möglicherweise aufgrund der Wirkung von MeCP2 auf die Expression von MBP (Protease, die L1 spaltet, um L1-70 zu erzeugen). Somit kann MeCP2 eine Rolle bei der Regulierung von L1-vermittelten

Zellfunktionen spielen. Darüber hinaus wurde ein erhöhtes Neuritenwachstum in Wildtyp-Kleinhirnkörnerzellen nach MeCP2-Knockdown gefunden. Im Gegensatz dazu war das Neuritenwachstum von Kleinhirnkörnerzellen, die L1 mit mutierter MBP-Spaltstelle exprimierten nicht erhöht. Diese Ergebnisse deuten darauf hin, dass MeCP2 das L1-abhängige Neuritenwachstum modulieren könnte.

Die neuen nukleären L1-Bindungspartner NonO, SFPQ und MeCP2 haben wichtige Funktionen bei der Genregulation, dem Umbau der Chromatinstruktur, der DNA-Reparatur, der RNA-Verarbeitung, der Zelldifferenzierung, den Zellwachstums und Zell-reparaturwegen, der Mitochondrienfunktion und der synaptischen Übertragung. Die Wechselwirkung von L1 mit diesen Proteinen zeigt, dass die proteolytische Spaltung L1 mit mehreren Funktionen ausstattet, die eine Rolle bei der Pathogenese vieler neuronaler Erkrankungen spielen könnten.

6. ABBREVIATIONS

A.U. – arbitrary units

aa – amino acids

AAV – Adeno-associated virus

amp – ampicillin

ANOVA – analysis of variance

APS – ammonium persulfate

BCA – bicinchoninic acid

BDNF – Brain Derived Neurotrophic Factor

BLAST - Basic Local Alignment Search Tool

bp – base pairs

BSA – bovine serum albumin

CA3 – cornu Ammonis 3

CAMs – cell adhesion molecules

cDNA – complementary deoxyribonucleic acid

CDS – coding sequence

CHL1 – close homolog of L1

CHL1-ICD – intracellular domain of close homolog of L1

CRASH – corpus callosum hypoplasia, retardation, adducted thumbs, spastic paraplegia, and hydrocephalus

Cy2, 3 and 5 – cyanine fluorescent dyes 2, 3 and 5

DAPI – 4',6-diamidino-2- phenylindole

DBHS – Drosophila human behaviour splicing proteins

dGTP – Deoxyguanosine triphosphate

ddH₂O – double distilled water

DMEM – Dulbecco's Modified Eagle Medium

DMSO – dimethyl sulfoxide

DNA – deoxyribonucleic acid

dsDNA – double stranded deoxyribonucleic acid

DTT – dithiothreitol

E – embryonic day

ECL – enhanced chemiluminescence

EDTA – ethylenediaminetetraacetic acid

EGTA – ethylene glycoltetraacetic acid

ELISA – enzyme-linked immunosorbent assay

ERM – ezrin-radixin-moesin

FNIII – Fibronectin type III domain

FBS – foetal bovine serum

Fc – fragment crystallizable (of an immunoglobulin)

Fig/Figs – figure/ figures

gDNA – genomic deoxyribonucleic acid

GFP – green fluorescent protein

h – hour or hours

HBSS – Hanks' Balanced Salt Solution

HDAC – Histone deacetylase

HEK293 – human embryonic kidney 293 cells

HEPES – 4-(2-hydroxyethyl)-1-piperazineethanesulfonic acid

HP1 γ – Heterochromatin protein 1

HRP – horseradish peroxidase

IF – immunofluorescent staining

Ig – immunoglobulin

IgCAMs – cell adhesion molecules from the immunoglobulin superfamily

IHC – immunohistochemistry

IP – immunoprecipitation

IPTG – Isopropyl β -D-1-thiogalactopyranoside

L1 – neural cell adhesion molecule L1

L1^{-ly} – L1-deficient mice

L1^{+ly} – L1 wild-type mice

L1^{-/+} – L1 heterozygous mice

L1-Fc – extracellular domain of cell adhesion molecule L1 conjugated with Fc fragment of human immunoglobulin G

L1-ICD – intracellular domain of the neural cell adhesion molecule L1

LB – lysogeny broth media

MBP – myelin basic protein

MeCP2 – methyl-CpG-binding protein 2

MeCP2- α – MeCP2 isoform, also called MeCP2B or MeCP-E1

MeCP2- β – MeCP2 isoform, MeCP2A or MeCP2-E2

min – minute or minutes

mRNA – messenger ribonucleic acid

MOI – multiplicity of infection

NCAM – neural cell adhesion molecule

ng - nanograms

nt - nucleotide

NonO – Non-POU domain-containing octamer-binding protein

NP-40 – nonyl phenoxypolyethoxylethanol

NSC – neural stem cell

OD – optical density

OD₆₀₀ – optical density at 600 nm

OPD – orthophenylene diamine

p – postnatal day

PBS – phosphate-buffered saline

PCR – polymerase chain reaction

PLL – poly-L-lysine

PSPC1 – Paraspeckle Component 1

PVDF – polyvinylidene difluoride

PWV – peak wavelength shift

REST – RE1-Silencing Transcription factor

RNA - ribonucleic acid

RNase – ribonuclease

RTT – Rett syndrome

s – second or seconds

SD – Standard deviation

SDS – sodium dodecyl sulphate

SDS-PAGE – sodium dodecyl sulphate-polyacrylamide gel electrophoresis

SEM – Standard error of the mean

SFPQ – Splicing Factor Proline and Glutamine Rich

SIN3A – Paired amphipathic helix protein Sin3a

SNP – single nucleotide polymorphism

TBS – Tris-buffered saline solution

TBS-T – Tris-buffered saline solution containing Tween-20

TEMED – Tetramethyl ethylenediamine

T_m - Primer Melting Temperature

u – unit

V – volts

vol – volume

w – weight

WB – Western Blot

7. BIBLIOGRAPHY

- Aaron, J. S., Taylor, A. B., & Chew, T.-L. (2018). Image co-localization – co-occurrence versus correlation. *Journal of Cell Science*, 131(3), jcs211847. <https://doi.org/10.1242/jcs.211847>
- Abuhatzira, L., Makedonski, K., Kaufman, Y., Razin, A., & Shemer, R. (2007). MeCP2 Deficiency in the Brain Decreases BDNF Levels by REST/CoREST-Mediated Repression and Increases TRKB Production. *Epigenetics*, 2(4), 214–222. <https://doi.org/10.4161/epi.2.4.5212>
- Acosta, C. M. R., Cortes, C., MacPhee, H., & Namaka, M. P. (2013). Exploring the role of nerve growth factor in multiple sclerosis: Implications in myelin repair. *CNS & Neurological Disorders Drug Targets*, 12(8), 1242–1256. <https://doi.org/10.2174/18715273113129990087>
- Adams, V. H., McBryant, S. J., Wade, P. A., Woodcock, C. L., & Hansen, J. C. (2007). Intrinsic disorder and autonomous domain function in the multifunctional nuclear protein, MeCP2. *The Journal of Biological Chemistry*, 282(20), 15057–15064. <https://doi.org/10.1074/jbc.M700855200>
- Altevogt, P., Doberstein, K., & Fogel, M. (2016). L1CAM in human cancer: L1CAM in human cancer. *International Journal of Cancer*, 138(7), 1565–1576. <https://doi.org/10.1002/ijc.29658>
- Appel, F., Holm, J., Conscience, J.-F., von Bohlen, F., Halbach, Faissner, A., James, P., & Schachner, M. (1995). Identification of the border between fibronectin type III homologous repeats 2 and 3 of the neural cell adhesion molecule L1 as a neurite outgrowth promoting and signal transducing domain. *Journal of Neurobiology*, 28(3), 297–312. <https://doi.org/10.1002/neu.480280304>
- Arevalo, E., Shanmugasundararaj, S., Wilkemeyer, M. F., Dou, X., Chen, S., Charness, M. E., & Miller, K. W. (2008). An alcohol binding site on the neural cell adhesion molecule L1. *Proceedings of the National Academy of Sciences*, 105(1), 371–375. <https://doi.org/10.1073/pnas.0707815105>
- Ausió, J., Paz, A. M. de, & Esteller, M. (2014). MeCP2: The long trip from a chromatin protein to neurological disorders. *Trends in Molecular Medicine*, 20(9), 487–498. <https://doi.org/10.1016/j.molmed.2014.03.004>
- Azemi, E., Lagenaur, C. F., & Cui, X. T. (2011). The surface immobilization of the neural adhesion molecule L1 on neural probes and its effect on neuronal density and gliosis at the probe/tissue interface. *Biomaterials*, 32(3), 681–692. <https://doi.org/10.1016/j.biomaterials.2010.09.033>
- Balaian, L. B., Moehler, T., & Montgomery, A. M. (2000). The human neural cell adhesion molecule L1 functions as a costimulatory molecule in T cell activation. *European Journal of Immunology*, 30(3), 938–943. [https://doi.org/10.1002/1521-4141\(200003\)30:3<938::AID-IMMU938>3.0.CO;2-Q](https://doi.org/10.1002/1521-4141(200003)30:3<938::AID-IMMU938>3.0.CO;2-Q)
- Baldovino, S., Moliner, A. M., Taruscio, D., Daina, E., & Roccatello, D. (2016). Rare Diseases in Europe: From a Wide to a Local Perspective. *The Israel Medical Association Journal: IMAJ*, 18(6), 359–363.
- Ballas, N., Grunseich, C., Lu, D. D., Speh, J. C., & Mandel, G. (2005). REST and Its Corepressors Mediate Plasticity of Neuronal Gene Chromatin throughout Neurogenesis. *Cell*, 121(4), 645–657. <https://doi.org/10.1016/j.cell.2005.03.013>
- Barbin, G., Aigrot, M. S., Charles, P., Foucher, A., Grumet, M., Schachner, M., Zalc, B., & Lubetzki, C. (2004). Axonal cell-adhesion molecule L₁ in CNS myelination. *Neuron Glia Biology*, 1(1), 65–72. <https://doi.org/10.1017/S1740925X04000092>
- Basu, S., & Lamprecht, R. (2018). The Role of Actin Cytoskeleton in Dendritic Spines in the Maintenance of Long-Term Memory. *Frontiers in Molecular Neuroscience*, 11, 143. <https://doi.org/10.3389/fnmol.2018.00143>
- Bauman, M. L., Kemper, T. L., & Arin, D. M. (1995). Pervasive neuroanatomic abnormalities of the brain in three cases of Rett's syndrome. *Neurology*, 45(8), 1581–1586. <https://doi.org/10.1212/wnl.45.8.1581>

- Bearer, C. F., Swick, A. R., O’Riordan, M. A., & Cheng, G. (1999). Ethanol inhibits L1-mediated neurite outgrowth in postnatal rat cerebellar granule cells. *The Journal of Biological Chemistry*, *274*(19), 13264–13270. <https://doi.org/10.1074/jbc.274.19.13264>
- Bedogni, F., Rossi, R. L., Galli, F., Cobolli Gigli, C., Gandaglia, A., Kilstrup-Nielsen, C., & Landsberger, N. (2014). Rett syndrome and the urge of novel approaches to study MeCP2 functions and mechanisms of action. *Neuroscience and Biobehavioral Reviews*, *46 Pt 2*, 187–201. <https://doi.org/10.1016/j.neubiorev.2014.01.011>
- Belichenko, N. P., Belichenko, P. V., Li, H. H., Mobley, W. C., & Francke, U. (2008). Comparative study of brain morphology in *Mecp2* mutant mouse models of Rett syndrome. *The Journal of Comparative Neurology*, *508*(1), 184–195. <https://doi.org/10.1002/cne.21673>
- Belichenko, P. V., Wright, E. E., Belichenko, N. P., Masliah, E., Li, H. H., Mobley, W. C., & Francke, U. (2009). Widespread changes in dendritic and axonal morphology in *Mecp2*-mutant mouse models of rett syndrome: Evidence for disruption of neuronal networks. *The Journal of Comparative Neurology*, *514*(3), 240–258. <https://doi.org/10.1002/cne.22009>
- Bennett, V., & Baines, A. J. (2001). Spectrin and Ankyrin-Based Pathways: Metazoan Inventions for Integrating Cells Into Tissues. *Physiological Reviews*, *81*(3), 1353–1392. <https://doi.org/10.1152/physrev.2001.81.3.1353>
- Bhattacharjee, A., Mu, Y., Winter, M. K., Knapp, J. R., Eggimann, L. S., Gunewardena, S. S., Kobayashi, K., Kato, S., Krizsan-Agbas, D., & Smith, P. G. (2017). Neuronal cytoskeletal gene dysregulation and mechanical hypersensitivity in a rat model of Rett syndrome. *Proceedings of the National Academy of Sciences*, *114*(33), E6952–E6961. <https://doi.org/10.1073/pnas.1618210114>
- Bienvenu, T., & Chelly, J. (2006). Molecular genetics of Rett syndrome: When DNA methylation goes unrecognized. *Nature Reviews. Genetics*, *7*(6), 415–426. <https://doi.org/10.1038/nrg1878>
- Brink, M. C., Piebes, D. G. E., de Groote, M. L., Luijsterburg, M. S., Casas-Delucchi, C. S., van Driel, R., Rots, M. G., Cardoso, M. C., & Verschure, P. J. (2013). A Role for MeCP2 in Switching Gene Activity via Chromatin Unfolding and HP1c Displacement. *PLOS ONE*, *8*(7), 14.
- Brown, K., Selfridge, J., Lager, S., Connelly, J., De Sousa, D., Kerr, A., Webb, S., Guy, J., Merusi, C., Koerner, M. V., & Bird, A. (2016). The molecular basis of variable phenotypic severity among common missense mutations causing Rett syndrome. *Human Molecular Genetics*, *25*(3), 558–570. <https://doi.org/10.1093/hmg/ddv496>
- Brücke, T., Sofic, E., Killian, W., Rett, A., & Riederer, P. (1987). Reduced concentrations and increased metabolism of biogenic amines in a single case of Rett-syndrome: A postmortem brain study. *Journal of Neural Transmission*, *68*(3–4), 315–324. <https://doi.org/10.1007/bf02098506>
- Brümmendorf, T., Kenwrick, S., & Rathjen, F. G. (1998). Neural cell recognition molecule L1: From cell biology to human hereditary brain malformations. *Current Opinion in Neurobiology*, *8*(1), 87–97. [https://doi.org/10.1016/S0959-4388\(98\)80012-3](https://doi.org/10.1016/S0959-4388(98)80012-3)
- Brunet, A., Bonni, A., Zigmond, M. J., Lin, M. Z., Juo, P., Hu, L. S., Anderson, M. J., Arden, K. C., Blenis, J., & Greenberg, M. E. (1999). Akt Promotes Cell Survival by Phosphorylating and Inhibiting a Forkhead Transcription Factor. *Cell*, *96*(6), 857–868. [https://doi.org/10.1016/S0092-8674\(00\)80595-4](https://doi.org/10.1016/S0092-8674(00)80595-4)
- Bu, Q., Wang, A., Hamzah, H., Waldman, A., Jiang, K., Dong, Q., Li, R., Kim, J., Turner, D., & Chang, Q. (2017). CREB Signaling Is Involved in Rett Syndrome Pathogenesis. *The Journal of Neuroscience*, *37*(13), 3671–3685. <https://doi.org/10.1523/JNEUROSCI.3735-16.2017>
- Capello, E., Voskuhl, R. R., McFarland, H. F., & Raine, C. S. (1997). Multiple sclerosis: Re-expression of a developmental gene in chronic lesions correlates with remyelination. *Annals of Neurology*, *41*(6), 797–805. <https://doi.org/10.1002/ana.410410616>
- Carlston, C. M., Bleyl, S. B., Andrews, A., Meyers, L., Brown, S., Bayrak-Toydemir, P., Bale, J. F., & Botto, L. D. (2019). Expanding the genetic and clinical spectrum of the NONO-

- associated X-linked intellectual disability syndrome. *American Journal of Medical Genetics Part A*, 179(5), 792–796. <https://doi.org/10.1002/ajmg.a.61091>
- Castellani, V. (2002). Cis and trans interactions of L1 with neuropilin-1 control axonal responses to semaphorin 3A. *The EMBO Journal*, 21(23), 6348–6357. <https://doi.org/10.1093/emboj/cdf645>
- Chahrouh, M., Jung, S. Y., Shaw, C., Zhou, X., Wong, S. T. C., Qin, J., & Zoghbi, H. Y. (2008). MeCP2, a Key Contributor to Neurological Disease, Activates and Represses Transcription. *Science*, 320(5880), 1224–1229. <https://doi.org/10.1126/science.1153252>
- Chang, Q., Khare, G., Dani, V., Nelson, S., & Jaenisch, R. (2006). The Disease Progression of Mecp2 Mutant Mice Is Affected by the Level of BDNF Expression. *Neuron*, 49(3), 341–348. <https://doi.org/10.1016/j.neuron.2005.12.027>
- Chapleau, C. A., Calfa, G. D., Lane, M. C., Albertson, A. J., Larimore, J. L., Kudo, S., Armstrong, D. L., Percy, A. K., & Pozzo-Miller, L. (2009). Dendritic spine pathologies in hippocampal pyramidal neurons from Rett syndrome brain and after expression of Rett-associated MECP2 mutations. *Neurobiology of Disease*, 35(2), 219–233. <https://doi.org/10.1016/j.nbd.2009.05.001>
- Chen, Jian, Wu, J., Apostolova, I., Skup, M., Irintchev, A., Kügler, S., & Schachner, M. (2007). Adeno-associated virus-mediated L1 expression promotes functional recovery after spinal cord injury. *Brain*, 130(4), 954–969. <https://doi.org/10.1093/brain/awm049>
- Chen, Jianling, Alberts, I., & Li, X. (2014). Dysregulation of the IGF-1/PI3K/AKT/mTOR signaling pathway in autism spectrum disorders. *International Journal of Developmental Neuroscience*, 35(C), 35–41. <https://doi.org/10.1016/j.ijdevneu.2014.03.006>
- Chen, R. Z., Akbarian, S., Tudor, M., & Jaenisch, R. (2001). Deficiency of methyl-CpG binding protein-2 in CNS neurons results in a Rett-like phenotype in mice. *Nature Genetics*, 27(3), 327–331. <https://doi.org/10.1038/85906>
- Chen, S., Mantei, N., Dong, L., & Schachner, M. (1999). Prevention of neuronal cell death by neural adhesion molecules L1 and CHL1. *Journal of Neurobiology*, 38(3), 12.
- Chen, W. G., Chang, Q., Lin, Y., Meissner, A., West, A. E., Griffith, E. C., Jaenisch, R., & Greenberg, M. E. (2003). Derepression of BDNF transcription involves calcium-dependent phosphorylation of MeCP2. *Science (New York, N.Y.)*, 302(5646), 885–889. <https://doi.org/10.1126/science.1086446>
- Cheung, A. Y. L. (2013). *DECIPHERING X-CHROMOSOME INACTIVATION AND THE ROLE OF MECP2E1 IN RETT SYNDROME PATIENT INDUCED PLURIPOTENT STEM CELLS*. University of Toronto.
- Clemson, C. M., Hutchinson, J. N., Sara, S. A., Ensminger, A. W., Fox, A. H., Chess, A., & Lawrence, J. B. (2009). An architectural role for a nuclear noncoding RNA: NEAT1 RNA is essential for the structure of paraspeckles. *Molecular Cell*, 33(6), 717–726. <https://doi.org/10.1016/j.molcel.2009.01.026>
- Cooper, M. A. (2002). Optical biosensors in drug discovery. *Nature Reviews Drug Discovery*, 1(7), 515–528. <https://doi.org/10.1038/nrd838>
- Cunningham, B. T., Li, P., Schulz, S., Lin, B., Baird, C., Gerstenmaier, J., Genick, C., Wang, F., Fine, E., & Laing, L. (2004). Label-Free Assays on the BIND System. *Journal of Biomolecular Screening*, 9(6), 481–490. <https://doi.org/10.1177/1087057104267604>
- Dahme, M., Bartsch, U., Martini, R., Anliker, B., Schachner, M., & Mantei, N. (1997). Disruption of the mouse L1 gene leads to malformations of the nervous system. *Nature Genetics*, 17(3), 346–349. <https://doi.org/10.1038/ng1197-346>
- Dastidar, S. G., Bardai, F. H., Ma, C., Price, V., Rawat, V., Verma, P., Narayanan, V., & D’Mello, S. R. (2012). Isoform-Specific Toxicity of Mecp2 in Postmitotic Neurons: Suppression of Neurotoxicity by FoxG1. *Journal of Neuroscience*, 32(8), 2846–2855. <https://doi.org/10.1523/JNEUROSCI.5841-11.2012>
- Daubner, G. M., Cléry, A., & Allain, F. H.-T. (2013). RRM-RNA recognition: NMR or crystallography...and new findings. *Current Opinion in Structural Biology*, 23(1), 100–108. <https://doi.org/10.1016/j.sbi.2012.11.006>

- Della Ragione, F., Vacca, M., Fioriniello, S., Pepe, G., & D'Esposito, M. (2016). MECP2, a multi-talented modulator of chromatin architecture. *Briefings in Functional Genomics*, *elw023*. <https://doi.org/10.1093/bfgp/elw023>
- Demyanenko, G. P., Shibata, Y., & Maness, P. F. (2001). Altered distribution of dopaminergic neurons in the brain of L1 null mice. *Developmental Brain Research*, *126*(1), 21–30. [https://doi.org/10.1016/S0165-3806\(00\)00129-2](https://doi.org/10.1016/S0165-3806(00)00129-2)
- Demyanenko, G. P., Tsai, A. Y., & Maness, P. F. (1999). Abnormalities in Neuronal Process Extension, Hippocampal Development, and the Ventricular System of L1 Knockout Mice. *The Journal of Neuroscience*, *19*(12), 4907–4920. <https://doi.org/10.1523/JNEUROSCI.19-12-04907.1999>
- Dickson, T. C., Mintz, C. D., Benson, D. L., & Salton, S. R. J. (2002). Functional binding interaction identified between the axonal CAM L1 and members of the ERM family. *The Journal of Cell Biology*, *157*(7), 1105–1112. <https://doi.org/10.1083/jcb.200111076>
- Dihné, M., Bernreuther, C., Sibbe, M., Paulus, W., & Schachner, M. (2003). A New Role for the Cell Adhesion Molecule L1 in Neural Precursor Cell Proliferation, Differentiation, and Transmitter-Specific Subtype Generation. *The Journal of Neuroscience*, *23*(16), 6638–6650. <https://doi.org/10.1523/JNEUROSCI.23-16-06638.2003>
- Dong, B., Horowitz, D. S., Kobayashi, R., & Krainer, A. R. (1993). Purification and cDNA cloning of HeLa cell p54nrb, a nuclear protein with two RNA recognition motifs and extensive homology to human splicing factor PSF and Drosophila NONA/BJ6. *Nucleic Acids Research*, *21*(17), 4085–4092. <https://doi.org/10.1093/nar/21.17.4085>
- Dong, X., Shylnova, O., Challis, J. R. G., & Lye, S. J. (2005). Identification and characterization of the protein-associated splicing factor as a negative co-regulator of the progesterone receptor. *The Journal of Biological Chemistry*, *280*(14), 13329–13340. <https://doi.org/10.1074/jbc.M409187200>
- Dou, X., Menkari, C., Mitsuyama, R., Foroud, T., Wetherill, L., Hammond, P., Suttie, M., Chen, X., Chen, S.-Y., Charness, M. E., & the Collaborative Initiative on Fetal Alcohol Spectrum Disorders. (2018). L1 coupling to ankyrin and the spectrin-actin cytoskeleton modulates ethanol inhibition of L1 adhesion and ethanol teratogenesis. *The FASEB Journal*, *32*(3), 1364–1374. <https://doi.org/10.1096/fj.201700970>
- Dunn, K. W., Kamocka, M. M., & McDonald, J. H. (2011). A practical guide to evaluating colocalization in biological microscopy. *American Journal of Physiology-Cell Physiology*, *300*(4), C723–C742. <https://doi.org/10.1152/ajpcell.00462.2010>
- Ehrhart, F., Coort, S. L. M., Cirillo, E., Smeets, E., Evelo, C. T., & Curfs, L. M. G. (2016). Rett syndrome – biological pathways leading from MECP2 to disorder phenotypes. *Orphanet Journal of Rare Diseases*, *11*(1), 158. <https://doi.org/10.1186/s13023-016-0545-5>
- Fernández, M., Sierra-Arregui, T., & Peñagarikano, O. (2019). The Cerebellum and Autism: More than Motor Control. In S. Palermo & R. Morese (Eds.), *Behavioral Neuroscience*. IntechOpen. <https://doi.org/10.5772/intechopen.85897>
- Ferrari, C., Cattaneo, Z., Oldrati, V., Casiraghi, L., Castelli, F., D'Angelo, E., & Vecchi, T. (2018). TMS Over the Cerebellum Interferes with Short-term Memory of Visual Sequences. *Scientific Reports*, *8*(1), 6722. <https://doi.org/10.1038/s41598-018-25151-y>
- Fox, A. H., Lam, Y. W., Leung, A. K. L., Lyon, C. E., Andersen, J., Mann, M., & Lamond, A. I. (2002). Paraspeckles: A Novel Nuclear Domain. *Current Biology*, *13*.
- Fransen, E. (1998). L1 knockout mice show dilated ventricles, vermis hypoplasia and impaired exploration patterns. *Human Molecular Genetics*, *7*(6), 999–1009. <https://doi.org/10.1093/hmg/7.6.999>
- Fujita, N., Watanabe, S., Ichimura, T., Tsuruzoe, S., Shinkai, Y., Tachibana, M., Chiba, T., & Nakao, M. (2003). Methyl-CpG Binding Domain 1 (MBD1) Interacts with the Suv39h1-HP1 Heterochromatic Complex for DNA Methylation-based Transcriptional Repression. *Journal of Biological Chemistry*, *278*(26), 24132–24138. <https://doi.org/10.1074/jbc.M302283200>

- Furukawa, M. T., Sakamoto, H., & Inoue, K. (2015). Interaction and colocalization of HERMES/RBPMS with NonO, PSF, and G3BP1 in neuronal cytoplasmic RNP granules in mouse retinal line cells. *Genes to Cells: Devoted to Molecular & Cellular Mechanisms*, 20(4), 257–266. <https://doi.org/10.1111/gtc.12224>
- Galloway, C. A., & Yoon, Y. (2012). What comes first, misshape or dysfunction? The view from metabolic excess. *The Journal of General Physiology*, 139(6), 455–463. <https://doi.org/10.1085/jgp.201210771>
- Gao, H., Bu, Y., Wu, Q., Wang, X., Chang, N., Lei, L., Chen, S., Liu, D., Zhu, X., Hu, K., & Xiong, J.-W. (2015). Mecp2 regulates neural cell differentiation by suppressing the Id1 to Her2 axis in zebrafish. *Journal of Cell Science*, 128(12), 2340–2350. <https://doi.org/10.1242/jcs.167874>
- Gao, X., Kong, L., Lu, X., Zhang, G., Chi, L., Jiang, Y., Wu, Y., Yan, C., Duerksen-Hughes, P., Zhu, X., & Yang, J. (2014). Paraspeckle protein 1 (PSPC1) is involved in the cisplatin induced DNA damage response—Role in G1/S checkpoint. *PloS One*, 9(5), e97174. <https://doi.org/10.1371/journal.pone.0097174>
- Ghosh, R. P., Horowitz-Scherer, R. A., Nikitina, T., Shlyakhtenko, L. S., & Woodcock, C. L. (2010). MeCP2 Binds Cooperatively to Its Substrate and Competes with Histone H1 for Chromatin Binding Sites. *Molecular and Cellular Biology*, 30(19), 4656–4670. <https://doi.org/10.1128/MCB.00379-10>
- Glascocock, J. J., Osman, E. Y., Coady, T. H., Rose, F. F., Shababi, M., & Lorson, C. L. (2011). Delivery of Therapeutic Agents Through Intracerebroventricular (ICV) and Intravenous (IV) Injection in Mice. *Journal of Visualized Experiments*, 56, 2968. <https://doi.org/10.3791/2968>
- Gonzales, M. L., Adams, S., Dunaway, K. W., & LaSalle, J. M. (2012). Phosphorylation of Distinct Sites in MeCP2 Modifies Cofactor Associations and the Dynamics of Transcriptional Regulation. *Molecular and Cellular Biology*, 32(14), 2894–2903. <https://doi.org/10.1128/MCB.06728-11>
- Guseva, D., Angelov, D. N., Irintchev, A., & Schachner, M. (2009). Ablation of adhesion molecule L1 in mice favours Schwann cell proliferation and functional recovery after peripheral nerve injury. *Brain*, 132(8), 2180–2195. <https://doi.org/10.1093/brain/awp160>
- Gutwein, P., Mechttersheimer, S., Riedle, S., Stoeck, A., Gast, D., Joumaa, S., Zentgraf, H., Fogel, M., & Altevogt, D. P. (2003). ADAM10-mediated cleavage of L1 adhesion molecule at the cell surface and in released membrane vesicles. *The FASEB Journal*, 17(2), 292–294. <https://doi.org/10.1096/fj.02-0430fje>
- Guy, J., Hendrich, B., Holmes, M., Martin, J. E., & Bird, A. (2001). A mouse Mecp2-null mutation causes neurological symptoms that mimic Rett syndrome. *Nature Genetics*, 27(3), 322–326. <https://doi.org/10.1038/85899>
- Ha, K., Takeda, Y., & Dynan, W. S. (2011). Sequences in PSF/SFPQ mediate radioresistance and recruitment of PSF/SFPQ-containing complexes to DNA damage sites in human cells. *DNA Repair*, 10(3), 252–259. <https://doi.org/10.1016/j.dnarep.2010.11.009>
- Haeussler, M., Schönig, K., Eckert, H., Eschstruth, A., Mianné, J., Renaud, J.-B., Schneider-Maunoury, S., Shkumatava, A., Teboul, L., Kent, J., Joly, J.-S., & Concordet, J.-P. (2016). Evaluation of off-target and on-target scoring algorithms and integration into the guide RNA selection tool CRISPOR. *Genome Biology*, 17(1), 148. <https://doi.org/10.1186/s13059-016-1012-2>
- Hansen, J. C., Ghosh, R. P., & Woodcock, C. L. (2010). Binding of the Rett syndrome protein, MeCP2, to methylated and unmethylated DNA and chromatin. *IUBMB Life*, 62(10), 732–738. <https://doi.org/10.1002/iub.386>
- Holm, J., Appel, F., & Schachner, M. (1995). Several extracellular domains of the neural cell adhesion molecule L1 are involved in homophilic interactions. *Journal of Neuroscience Research*, 42(1), 9–20. <https://doi.org/10.1002/jnr.490420103>
- Huang, J., Casas Garcia, G. P., Perugini, M. A., Fox, A. H., Bond, C. S., & Lee, M. (2018). Crystal structure of a SFPQ/PSPC1 heterodimer provides insights into preferential

- heterodimerization of human DBHS family proteins. *Journal of Biological Chemistry*, 293(17), 6593–6602. <https://doi.org/10.1074/jbc.RA117.001451>
- Huang, Z. J. (2006). Subcellular organization of GABAergic synapses: Role of ankyrins and L1 cell adhesion molecules. *Nature Neuroscience*, 9(2), 163–166. <https://doi.org/10.1038/nn1638>
- Huda, F., Konno, A., Matsuzaki, Y., Goenawan, H., Miyake, K., Shimada, T., & Hirai, H. (2014). Distinct transduction profiles in the CNS via three injection routes of AAV9 and the application to generation of a neurodegenerative mouse model. *Molecular Therapy - Methods & Clinical Development*, 1, 14032. <https://doi.org/10.1038/mtm.2014.32>
- Hutchinson, A. N., Deng, J. V., Aryal, D. K., Wetsel, W. C., & West, A. E. (2012). Differential regulation of MeCP2 phosphorylation in the CNS by dopamine and serotonin. *Neuropsychopharmacology: Official Publication of the American College of Neuropsychopharmacology*, 37(2), 321–337. <https://doi.org/10.1038/npp.2011.190>
- Itoh, K., Cheng, L., Kamei, Y., Fushiki, S., Kamiguchi, H., Gutwein, P., Stoeck, A., Arnold, B., Altevogt, P., & Lemmon, V. (2004). Brain development in mice lacking L1–L1 homophilic adhesion. *The Journal of Cell Biology*, 165(1), 145–154. <https://doi.org/10.1083/jcb.200312107>
- Itoh, M., Tahimic, C. G. T., Ide, S., Otsuki, A., Sasaoka, T., Noguchi, S., Oshimura, M., Goto, Y., & Kurimasa, A. (2012). Methyl CpG-binding protein isoform MeCP2_e2 is dispensable for Rett syndrome phenotypes but essential for embryo viability and placenta development. *The Journal of Biological Chemistry*, 287(17), 13859–13867. <https://doi.org/10.1074/jbc.M111.309864>
- Jaafar, L., Li, Z., Li, S., & Dynan, W. S. (2017). SFPQ•NONO and XLF function separately and together to promote DNA double-strand break repair via canonical nonhomologous end joining. *Nucleic Acids Research*, 45(4), 1848–1859. <https://doi.org/10.1093/nar/gkw1209>
- Jakeman, L. B., Chen, Y., Lucin, K. M., & McTigue, D. M. (2006). Mice lacking L1 cell adhesion molecule have deficits in locomotion and exhibit enhanced corticospinal tract sprouting following mild contusion injury to the spinal cord. *European Journal of Neuroscience*, 23(8), 1997–2011. <https://doi.org/10.1111/j.1460-9568.2006.04721.x>
- Jentarra, G. M., Olfers, S. L., Rice, S. G., Srivastava, N., Homanics, G. E., Blue, M., Naidu, S., & Narayanan, V. (2010). Abnormalities of cell packing density and dendritic complexity in the MeCP2 A140V mouse model of Rett syndrome/X-linked mental retardation. *BMC Neuroscience*, 11(1), 19. <https://doi.org/10.1186/1471-2202-11-19>
- Jiang, Y. J., Brand, M., Heisenberg, C. P., Beuchle, D., Furutani-Seiki, M., Kelsh, R. N., Warga, R. M., Granato, M., Haffter, P., Hammerschmidt, M., Kane, D. A., Mullins, M. C., Odenthal, J., van Eeden, F. J., & Nüsslein-Volhard, C. (1996). Mutations affecting neurogenesis and brain morphology in the zebrafish, *Danio rerio*. *Development (Cambridge, England)*, 123, 205–216.
- Jin, X.-R., Chen, X.-S., & Xiao, L. (2017). MeCP2 Deficiency in Neuroglia: New Progress in the Pathogenesis of Rett Syndrome. *Frontiers in Molecular Neuroscience*, 10, 316. <https://doi.org/10.3389/fnmol.2017.00316>
- Jordan, C., Li, H. H., Kwan, H. C., & Francke, U. (2007). Cerebellar gene expression profiles of mouse models for Rett syndrome reveal novel MeCP2 targets. *BMC Medical Genetics*, 8(1), 36. <https://doi.org/10.1186/1471-2350-8-36>
- Jouet, M., Rosenthal, A., Armstrong, G., MacFarlane, J., Stevenson, R., Paterson, J., Metzenberg, A., Ionasescu, V., Temple, K., & Kenrick, S. (1994). X-linked spastic paraplegia (SPG1), MASA syndrome and X-linked hydrocephalus result from mutations in the L1 gene. *Nature Genetics*, 7(3), 402–407. <https://doi.org/10.1038/ng0794-402>
- Jugloff, D. G. M., Jung, B. P., Purushotham, D., Logan, R., & Eubanks, J. H. (2005). Increased dendritic complexity and axonal length in cultured mouse cortical neurons overexpressing methyl-CpG-binding protein MeCP2. *Neurobiology of Disease*, 19(1–2), 18–27. <https://doi.org/10.1016/j.nbd.2004.11.002>

- Jung, B. P., Jugloff, D. G. M., Zhang, G., Logan, R., Brown, S., & Eubanks, J. H. (2003). The expression of methyl CpG binding factor MeCP2 correlates with cellular differentiation in the developing rat brain and in cultured cells. *Journal of Neurobiology*, *55*(1), 86–96. <https://doi.org/10.1002/neu.10201>
- Kalus, I., Schnegelsberg, B., Seidah, N. G., Kleene, R., & Schachner, M. (2003). The Proprotein Convertase PC5A and a Metalloprotease Are Involved in the Proteolytic Processing of the Neural Adhesion Molecule L1. *Journal of Biological Chemistry*, *278*(12), 10381–10388. <https://doi.org/10.1074/jbc.M208351200>
- Kamiguchi, H., Long, K. E., Pendergast, M., Schaefer, A. W., Rapoport, I., Kirchhausen, T., & Lemmon, V. (1998). The Neural Cell Adhesion Molecule L1 Interacts with the AP-2 Adaptor and Is Endocytosed via the Clathrin-Mediated Pathway. *The Journal of Neuroscience*, *18*(14), 5311–5321. <https://doi.org/10.1523/JNEUROSCI.18-14-05311.1998>
- Kanai, Y., Dohmae, N., & Hirokawa, N. (2004). Kinesin Transports RNA: Isolation and Characterization of an RNA-Transporting Granule. *Neuron*, *43*, 513–525.
- KhorshidAhmad, T., Acosta, C., Cortes, C., Lakowski, T. M., Gangadaran, S., & Namaka, M. (2016). Transcriptional Regulation of Brain-Derived Neurotrophic Factor (BDNF) by Methyl CpG Binding Protein 2 (MeCP2): A Novel Mechanism for Re-Myelination and/or Myelin Repair Involved in the Treatment of Multiple Sclerosis (MS). *Molecular Neurobiology*, *53*(2), 1092–1107. <https://doi.org/10.1007/s12035-014-9074-1>
- Kiefel, H., Bondong, S., Hazin, J., Ridinger, J., Schirmer, U., Riedle, S., & Altevogt, P. (2012). L1CAM: A major driver for tumor cell invasion and motility. *Cell Adhesion & Migration*, *6*(4), 374–384. <https://doi.org/10.4161/cam.20832>
- Kilkenny, C., Browne, W., Cutchill, I., Emerson, M., & Altman, D. (2010). Improving Bioscience Research Reporting: The ARRIVE Guidelines for Reporting Animal Research. *PLoS Biology*, *8*(6), e1000412. <https://doi.org/10.1371/journal.pbio.1000412>
- Kim, J.-Y., Grunke, S. D., Levites, Y., Golde, T. E., & Jankowsky, J. L. (2014). Intracerebroventricular Viral Injection of the Neonatal Mouse Brain for Persistent and Widespread Neuronal Transduction. *Journal of Visualized Experiments*, *91*, 51863. <https://doi.org/10.3791/51863>
- Kim, K.-Y., Hysolli, E., & Park, I.-H. (2011). Neuronal maturation defect in induced pluripotent stem cells from patients with Rett syndrome. *Proceedings of the National Academy of Sciences*, *108*(34), 14169–14174. <https://doi.org/10.1073/pnas.1018979108>
- Kishi, N., & Macklis, J. D. (2004). MECP2 is progressively expressed in post-migratory neurons and is involved in neuronal maturation rather than cell fate decisions. *Molecular and Cellular Neuroscience*, *27*(3), 306–321. <https://doi.org/10.1016/j.mcn.2004.07.006>
- Kleene, R., Yang, H., Kutsche, M., & Schachner, M. (2001). The Neural Recognition Molecule L1 Is a Sialic Acid-binding Lectin for CD24, Which Induces Promotion and Inhibition of Neurite Outgrowth. *Journal of Biological Chemistry*, *276*(24), 21656–21663. <https://doi.org/10.1074/jbc.M101790200>
- Knott, G. J., Bond, C. S., & Fox, A. H. (2016). The DBHS proteins SFPQ, NONO and PSPC1: A multipurpose molecular scaffold. *Nucleic Acids Research*, *44*(9), 3989–4004. <https://doi.org/10.1093/nar/gkw271>
- Kraus, K., Kleene, R., Braren, I., Loers, G., Lutz, D., & Schachner, M. (2018). A fragment of adhesion molecule L1 is imported into mitochondria, and regulates mitochondrial metabolism and trafficking. *Journal of Cell Science*, *131*(9), jcs210500. <https://doi.org/10.1242/jcs.210500>
- Kraus, K., Kleene, R., Henis, M., Braren, I., Kataria, H., Sharaf, A., Loers, G., Schachner, M., & Lutz, D. (2018). A Fragment of Adhesion Molecule L1 Binds to Nuclear Receptors to Regulate Synaptic Plasticity and Motor Coordination. *Molecular Neurobiology*, *55*(9), 7164–7178. <https://doi.org/10.1007/s12035-018-0901-7>
- Kriaucionis, S. (2004). The major form of MeCP2 has a novel N-terminus generated by alternative splicing. *Nucleic Acids Research*, *32*(5), 1818–1823. <https://doi.org/10.1093/nar/gkh349>

- Kriaucionis, S., Paterson, A., Curtis, J., Guy, J., MacLeod, N., & Bird, A. (2006). Gene Expression Analysis Exposes Mitochondrial Abnormalities in a Mouse Model of Rett Syndrome. *Molecular and Cellular Biology*, 26(13), 5033–5042. <https://doi.org/10.1128/MCB.01665-05>
- Kuhn, T. B., Stoeckli, E. T., Condrau, M. A., Rathjen, F. G., & Sonderegger, P. (1991). Neurite outgrowth on immobilized axonin-1 is mediated by a heterophilic interaction with L1(G4). *The Journal of Cell Biology*, 115(4), 1113–1126. <https://doi.org/10.1083/jcb.115.4.1113>
- Lagenaur, C., & Lemmon, V. (1987). An L1-like molecule, the 8D9 antigen, is a potent substrate for neurite extension. *Proceedings of the National Academy of Sciences of the United States of America*, 84(21), 7753–7757. <https://doi.org/10.1073/pnas.84.21.7753>
- Larimore, J. L., Chapleau, C. A., Kudo, S., Theibert, A., Percy, A. K., & Pozzo-Miller, L. (2009). Bdnf overexpression in hippocampal neurons prevents dendritic atrophy caused by Rett-associated MECP2 mutations. *Neurobiology of Disease*, 34(2), 199–211. <https://doi.org/10.1016/j.nbd.2008.12.011>
- Lekman, A., Witt-Engerström, I., Gottfries, J., Hagberg, B. A., Percy, A. K., & Svennerholm, L. (1989). Rett syndrome: Biogenic amines and metabolites in postmortem brain. *Pediatric Neurology*, 5(6), 357–362. [https://doi.org/10.1016/0887-8994\(89\)90049-0](https://doi.org/10.1016/0887-8994(89)90049-0)
- Li, S., Li, Z., Shu, F.-J., Xiong, H., Phillips, A. C., & Dynan, W. S. (2014). Double-strand break repair deficiency in NONO knockout murine embryonic fibroblasts and compensation by spontaneous upregulation of the PSPC1 paralog. *Nucleic Acids Research*, 42(15), 9771–9780. <https://doi.org/10.1093/nar/gku650>
- Li, W., & Pozzo-Miller, L. (2014). BDNF deregulation in Rett syndrome. *Neuropharmacology*, 76, 737–746. <https://doi.org/10.1016/j.neuropharm.2013.03.024>
- Li, Y., Wang, H., Muffat, J., Cheng, A. W., Orlando, D. A., Lovén, J., Kwok, S.-M., Feldman, D. A., Bateup, H. S., Gao, Q., Hockemeyer, D., Mitalipova, M., Lewis, C. A., Vander Heiden, M. G., Sur, M., Young, R. A., & Jaenisch, R. (2013). Global transcriptional and translational repression in human-embryonic-stem-cell-derived Rett syndrome neurons. *Cell Stem Cell*, 13(4), 446–458. <https://doi.org/10.1016/j.stem.2013.09.001>
- Lieberoth, A., Splittstoesser, F., Katagihallimath, N., Jakovcevski, I., Loers, G., Ranscht, B., Karagogeos, D., Schachner, M., & Kleene, R. (2009). Lewis(x) and alpha2,3-sialyl glycans and their receptors TAG-1, Contactin, and L1 mediate CD24-dependent neurite outgrowth. *The Journal of Neuroscience: The Official Journal of the Society for Neuroscience*, 29(20), 6677–6690. <https://doi.org/10.1523/JNEUROSCI.4361-08.2009>
- Liu, F., Ni, J.-J., & Sun, F.-Y. (2017). Expression of Phospho-MeCP2s in the Developing Rat Brain and Function of Postnatal MeCP2 in Cerebellar Neural Cell Development. *Neuroscience Bulletin*, 33(1), 1–16. <https://doi.org/10.1007/s12264-016-0086-x>
- Livide, G., Patriarchi, T., Amenduni, M., Amabile, S., Yasui, D., Calcagno, E., Lo Rizzo, C., De Falco, G., Ulivieri, C., Ariani, F., Mari, F., Mencarelli, M. A., Hell, J. W., Renieri, A., & Meloni, I. (2015). GluD1 is a common altered player in neuronal differentiation from both MECP2-mutated and CDKL5-mutated iPS cells. *European Journal of Human Genetics*, 23(2), 195–201. <https://doi.org/10.1038/ejhg.2014.81>
- Liyanage, V. R. B., Zachariah, R. M., Davie, J. R., & Rastegar, M. (2015). Ethanol deregulates Mecp2/MeCP2 in differentiating neural stem cells via interplay between 5-methylcytosine and 5-hydroxymethylcytosine at the Mecp2 regulatory elements. *Experimental Neurology*, 265, 102–117. <https://doi.org/10.1016/j.expneurol.2015.01.006>
- Loers, G., Chen, S., Grumet, M., & Schachner, M. (2005). Signal transduction pathways implicated in neural recognition molecule L1 triggered neuroprotection and neuritogenesis: L1-mediated neuroprotection and neuritogenesis. *Journal of Neurochemistry*, 92(6), 1463–1476. <https://doi.org/10.1111/j.1471-4159.2004.02983.x>

- Long, S. W., Ooi, J. Y. Y., Yau, P. M., & Jones, P. L. (2011). A brain-derived MeCP2 complex supports a role for MeCP2 in RNA processing. *Bioscience Reports*, *31*(5), 333–343. <https://doi.org/10.1042/BSR20100124>
- Lu, H., Ash, R. T., He, L., Kee, S. E., Wang, W., Yu, D., Hao, S., Meng, X., Ure, K., Ito-Ishida, A., Tang, B., Sun, Y., Ji, D., Tang, J., Arenkiel, B. R., Smirnakis, S. M., & Zoghbi, H. Y. (2016). Loss and Gain of MeCP2 Cause Similar Hippocampal Circuit Dysfunction that Is Rescued by Deep Brain Stimulation in a Rett Syndrome Mouse Model. *Neuron*, *91*(4), 739–747. <https://doi.org/10.1016/j.neuron.2016.07.018>
- Lutz, D. (2013). *Novel Proteolytic Fragments of the Cell Adhesion Molecule L1, Their Intracellular Trafficking and Functional Roles in the Nervous System of Mus Musculus (Linnaeus, 1758)*. University of Hamburg.
- Lutz, D., Kataria, H., Kleene, R., Loers, G., Chaudhary, H., Guseva, D., Wu, B., Jakovcevski, I., & Schachner, M. (2016). Myelin Basic Protein Cleaves Cell Adhesion Molecule L1 and Improves Regeneration After Injury. *Molecular Neurobiology*, *53*(5), 3360–3376. <https://doi.org/10.1007/s12035-015-9277-0>
- Lutz, D., Loers, G., Kleene, R., Oezen, I., Kataria, H., Katagihallimath, N., Braren, I., Harauz, G., & Schachner, M. (2014). Myelin Basic Protein Cleaves Cell Adhesion Molecule L1 and Promotes Neuritogenesis and Cell Survival. *Journal of Biological Chemistry*, *289*(19), 13503–13518. <https://doi.org/10.1074/jbc.M113.530238>
- Lutz, D., Sharaf, A., Drexler, D., Kataria, H., Wolters-Eisfeld, G., Brunne, B., Kleene, R., Loers, G., Frotscher, M., & Schachner, M. (2017). Proteolytic cleavage of transmembrane cell adhesion molecule L1 by extracellular matrix molecule Reelin is important for mouse brain development. *Scientific Reports*, *7*(1), 15268. <https://doi.org/10.1038/s41598-017-15311-x>
- Lutz, D., Wolters-Eisfeld, G., Joshi, G., Djogo, N., Jakovcevski, I., Schachner, M., & Kleene, R. (2012). Generation and Nuclear Translocation of Sumoylated Transmembrane Fragment of Cell Adhesion Molecule L1. *Journal of Biological Chemistry*, *287*(21), 17161–17175. <https://doi.org/10.1074/jbc.M112.346759>
- Lutz, D., Wolters-Eisfeld, G., Schachner, M., & Kleene, R. (2014). Cathepsin E generates a sumoylated intracellular fragment of the cell adhesion molecule L1 to promote neuronal and Schwann cell migration as well as myelination. *Journal of Neurochemistry*, *128*(5), 713–724. <https://doi.org/10.1111/jnc.12473>
- Lyst, M. J., Ekiert, R., Ebert, D. H., Merusi, C., Nowak, J., Selfridge, J., Guy, J., Kastan, N. R., Robinson, N. D., de Lima Alves, F., Rappsilber, J., Greenberg, M. E., & Bird, A. (2013). Rett syndrome mutations abolish the interaction of MeCP2 with the NCoR/SMRT co-repressor. *Nature Neuroscience*, *16*(7), 898–902. <https://doi.org/10.1038/nn.3434>
- Makovets, S. (Ed.). (2013). *DNA electrophoresis: Methods and protocols*. Humana Press/Springer.
- Maness, P. F., & Schachner, M. (2007). Neural recognition molecules of the immunoglobulin superfamily: Signaling transducers of axon guidance and neuronal migration. *Nature Neuroscience*, *10*(1), 19–26. <https://doi.org/10.1038/nn1827>
- Martínez de Paz, A., Khajavi, L., Martin, H., Claveria-Gimeno, R., Tom Dieck, S., Cheema, M. S., Sanchez-Mut, J. V., Moksa, M. M., Carles, A., Brodie, N. I., Sheikh, T. I., Freeman, M. E., Petrotchenko, E. V., Borchers, C. H., Schuman, E. M., Zytnicki, M., Velazquez-Campoy, A., Abian, O., Hirst, M., ... Ausió, J. (2019). MeCP2-E1 isoform is a dynamically expressed, weakly DNA-bound protein with different protein and DNA interactions compared to MeCP2-E2. *Epigenetics & Chromatin*, *12*(1), 63. <https://doi.org/10.1186/s13072-019-0298-1>
- Marzban, H., Del Bigio, M. R., Alizadeh, J., Ghavami, S., Zachariah, R. M., & Rastegar, M. (2015). Cellular commitment in the developing cerebellum. *Frontiers in Cellular Neuroscience*, *8*. <https://doi.org/10.3389/fncel.2014.00450>
- Matarazzo, V., Cohen, D., Palmer, A. M., Simpson, P. J., Khokhar, B., Pan, S.-J., & Ronnett, G. V. (2004). The transcriptional repressor *Mecp2* regulates terminal neuronal differentiation. *Molecular and Cellular Neuroscience*, *27*(1), 44–58. <https://doi.org/10.1016/j.mcn.2004.05.005>

- Mathur, M., Tucker, P. W., & Samuels, H. H. (2001). PSF is a novel corepressor that mediates its effect through Sin3A and the DNA binding domain of nuclear hormone receptors. *Molecular and Cellular Biology*, *21*(7), 2298–2311. <https://doi.org/10.1128/MCB.21.7.2298-2311.2001>
- Mechtersheimer, S., Gutwein, P., Agmon-Levin, N., Stoeck, A., Oleszewski, M., Riedle, S., Postina, R., Fahrenholz, F., Fogel, M., Lemmon, V., & Altevogt, P. (2001). Ectodomain shedding of L1 adhesion molecule promotes cell migration by autocrine binding to integrins. *The Journal of Cell Biology*, *155*(4), 661–674. <https://doi.org/10.1083/jcb.200101099>
- Menzel, L., Paterka, M., Bittner, S., White, R., Bobkiewicz, W., van Horssen, J., Schachner, M., Witsch, E., Kuhlmann, T., Zipp, F., & Schäfer, M. K. E. (2016). Down-regulation of neuronal L1 cell adhesion molecule expression alleviates inflammatory neuronal injury. *Acta Neuropathologica*, *132*(5), 703–720. <https://doi.org/10.1007/s00401-016-1607-4>
- Mircsof, D., Langouët, M., Rio, M., Moutton, S., Siquier-Pernet, K., Bole-Feysot, C., Cagnard, N., Nitschke, P., Gaspar, L., Žnidarič, M., Alibeu, O., Fritz, A.-K., Wolfer, D. P., Schröter, A., Bosshard, G., Rudin, M., Koester, C., Crestani, F., Seebeck, P., ... Colleaux, L. (2015). Mutations in NONO lead to syndromic intellectual disability and inhibitory synaptic defects. *Nature Neuroscience*, *18*(12), 1731–1736. <https://doi.org/10.1038/nn.4169>
- Miyake, K., & Nagai, K. (2007). Phosphorylation of methyl-CpG binding protein 2 (MeCP2) regulates the intracellular localization during neuronal cell differentiation. *Neurochemistry International*, *50*(1), 264–270. <https://doi.org/10.1016/j.neuint.2006.08.018>
- Mnatzakanian, G. N., Lohi, H., Munteanu, I., Alfred, S. E., Yamada, T., MacLeod, P. J. M., Jones, J. R., Scherer, S. W., Schanen, N. C., Friez, M. J., Vincent, J. B., & Minassian, B. A. (2004). A previously unidentified MECP2 open reading frame defines a new protein isoform relevant to Rett syndrome. *Nature Genetics*, *36*(4), 339–341. <https://doi.org/10.1038/ng1327>
- Moore, D. (2011). *Novel Role of MeCP2 in Developing Oligodendrocytes and Myelination* [Master Thesis]. Virginia Commonwealth University.
- Nakamura, Y., Lee, S., Haddox, C. L., Weaver, E. J., & Lemmon, V. P. (2010). Role of the cytoplasmic domain of the L1 cell adhesion molecule in brain development. *The Journal of Comparative Neurology*, *518*(7), 1113–1132. <https://doi.org/10.1002/cne.22267>
- Nan, X., Campoy, F. J., & Bird, A. (1997). MeCP2 Is a Transcriptional Repressor with Abundant Binding Sites in Genomic Chromatin. *Cell*, *88*(4), 471–481. [https://doi.org/10.1016/S0092-8674\(00\)81887-5](https://doi.org/10.1016/S0092-8674(00)81887-5)
- Nayeem, N., Silletti, S., Yang, X.-M., Lemmon, V. P., Reisfeld, R. A., Stallcup, W. B., & Montgomery, A. M. P. (1999). A potential role for the plasmin(ogen) system in the posttranslational cleavage of the neural cell adhesion molecule L1. *Journal of Cell Science*, *112*, 11.
- Nolte, C., Moos, M., & Schachner, M. (1999). Immunolocalization of the neural cell adhesion molecule L1 in epithelia of rodents. *Cell and Tissue Research*, *298*(2), 261–273. <https://doi.org/10.1007/s004419900063>
- Olson, C. O., Pejhan, S., Kroft, D., Sheikholeslami, K., Fuss, D., Buist, M., Ali Sher, A., Del Bigio, M. R., Sztainberg, Y., Siu, V. M., Ang, L. C., Sabourin-Felix, M., Moss, T., & Rastegar, M. (2018). MECP2 Mutation Interrupts Nucleolin–mTOR–P70S6K Signaling in Rett Syndrome Patients. *Frontiers in Genetics*, *9*, 635. <https://doi.org/10.3389/fgene.2018.00635>
- Olson, C. O., Zachariah, R. M., Ezeonwuka, C. D., Liyanage, V. R. B., & Rastegar, M. (2014). Brain Region-Specific Expression of MeCP2 Isoforms Correlates with DNA Methylation within Mecp2 Regulatory Elements. *PLoS ONE*, *9*(3), e90645. <https://doi.org/10.1371/journal.pone.0090645>

- Ong, S. A., Tan, J. J., Tew, W. L., & Chen, K.-S. (2011). Rasd1 modulates the coactivator function of NonO in the cyclic AMP pathway. *PLoS One*, 6(9), e24401. <https://doi.org/10.1371/journal.pone.0024401>
- Passini, M. A., & Wolfe, J. H. (2001). Widespread Gene Delivery and Structure-Specific Patterns of Expression in the Brain after Intraventricular Injections of Neonatal Mice with an Adeno-Associated Virus Vector. *Journal of Virology*, 75(24), 12382–12392. <https://doi.org/10.1128/JVI.75.24.12382-12392.2001>
- Peineau, S., Taghibiglou, C., Bradley, C., Wong, T. P., Liu, L., Lu, J., Lo, E., Wu, D., Saule, E., Bouschet, T., Matthews, P., Isaac, J. T. R., Bortolotto, Z. A., Wang, Y. T., & Collingridge, G. L. (2007). LTP Inhibits LTD in the Hippocampus via Regulation of GSK3 β . *Neuron*, 53(5), 703–717. <https://doi.org/10.1016/j.neuron.2007.01.029>
- Percy, A. K. (2011). Rett Syndrome: Exploring the Autism Link. *Archives of Neurology*, 68(8), 985. <https://doi.org/10.1001/archneurol.2011.149>
- Raman, A. T., Pohodich, A. E., Wan, Y.-W., Yalamanchili, H. K., Lowry, W. E., Zoghbi, H. Y., & Liu, Z. (2018). Apparent bias toward long gene misregulation in MeCP2 syndromes disappears after controlling for baseline variations. *Nature Communications*, 9(1), 3225. <https://doi.org/10.1038/s41467-018-05627-1>
- Ramanathan, R., Wilkemeyer, M. F., Mittal, B., Perides, G., & Charness, M. E. (1996). Alcohol inhibits cell-cell adhesion mediated by human L1. *The Journal of Cell Biology*, 133(2), 381–390. <https://doi.org/10.1083/jcb.133.2.381>
- Rangasamy, S., Olfers, S., Gerald, B., Hilbert, A., Svejda, S., & Narayanan, V. (2016). Reduced neuronal size and mTOR pathway activity in the Mecp2 A140V Rett syndrome mouse model. *F1000Research*, 5, 2269. <https://doi.org/10.12688/f1000research.8156.1>
- Rathjen, F. G., & Schachner, M. (1984). Immunocytological and biochemical characterization of a new neuronal cell surface component (Li antigen) which is involved in cell adhesion. *The EMBO Journal*, 10.
- Reinstein, E., Tzur, S., Cohen, R., Bormans, C., & Behar, D. M. (2016). Intellectual disability and non-compact cardiomyopathy with a de novo NONO mutation identified by exome sequencing. *European Journal of Human Genetics*, 24(11), 1635–1638. <https://doi.org/10.1038/ejhg.2016.72>
- Remy, S., Chenouard, V., Tesson, L., Usal, C., Ménoret, S., Brusselle, L., Heslan, J.-M., Nguyen, T. H., Bellien, J., Merot, J., De Cian, A., Giovannangeli, C., Concordet, J.-P., & Anegon, I. (2017). Generation of gene-edited rats by delivery of CRISPR/Cas9 protein and donor DNA into intact zygotes using electroporation. *Scientific Reports*, 7(1), 16554. <https://doi.org/10.1038/s41598-017-16328-y>
- Repunte-Canonigo, V., Chen, J., Lefebvre, C., Kawamura, T., Kreifeldt, M., Basson, O., Roberts, A. J., & Sanna, P. P. (2014). MeCP2 regulates ethanol sensitivity and intake: MeCP2 regulates ethanol. *Addiction Biology*, 19(5), 791–799. <https://doi.org/10.1111/adb.12047>
- Richter, M. (2002). *Identification and Characterization of Intracellular Binding Partners of the CHL1 (Close Homologue of L1) Neural Cell Recognition Molecule*. Fakultät für Biologie der Universität Bielefeld.
- Riedle, S., Kiefel, H., Gast, D., Bondong, S., Wolterink, S., Gutwein, P., & Altevogt, P. (2009). Nuclear translocation and signalling of L1-CAM in human carcinoma cells requires ADAM10 and presenilin/ γ -secretase activity. *Biochemical Journal*, 420(3), 391–402. <https://doi.org/10.1042/BJ20081625>
- Rietveld, L., Stuss, D. P., McPhee, D., & Delaney, K. R. (2015). Genotype-specific effects of Mecp2 loss-of-function on morphology of Layer V pyramidal neurons in heterozygous female Rett syndrome model mice. *Frontiers in Cellular Neuroscience*, 9. <https://doi.org/10.3389/fncel.2015.00145>
- Robinson, L., Guy, J., McKay, L., Brockett, E., Spike, R. C., Selfridge, J., Sousa, D. D., Merusi, C., Riedel, G., Bird, A., & Cobb, S. R. (2012). Morphological and functional reversal of phenotypes in a mouse model of Rett syndrome. *Brain*, 135, 12.

- Rolf, B., Kutsche, M., & Bartsch, U. (2001). Severe hydrocephalus in L1-deficient mice. *Brain Research*, 891(1–2), 247–252. [https://doi.org/10.1016/S0006-8993\(00\)03219-4](https://doi.org/10.1016/S0006-8993(00)03219-4)
- Russell, J. C., Blue, M. E., Johnston, M. V., Naidu, S., & Hossain, M. A. (2007). Enhanced cell death in MeCP2 null cerebellar granule neurons exposed to excitotoxicity and hypoxia. *Neuroscience*, 150(3), 563–574. <https://doi.org/10.1016/j.neuroscience.2007.09.076>
- Sadoul, K., Sadoul, R., Faissner, A., & Schachner, M. (1988). Biochemical Characterization of Different Molecular Forms of the Neural Cell Adhesion Molecule L1. *Journal of Neurochemistry*, 50(2), 510–521. <https://doi.org/10.1111/j.1471-4159.1988.tb02941.x>
- Samaco, R. C., & Neul, J. L. (2011). Complexities of Rett Syndrome and MeCP2. *Journal of Neuroscience*, 31(22), 7951–7959. <https://doi.org/10.1523/JNEUROSCI.0169-11.2011>
- Samatov, T. R., Wicklein, D., & Tonevitsky, A. G. (2016). L1CAM: Cell adhesion and more. *Progress in Histochemistry and Cytochemistry*, 51(2), 25–32. <https://doi.org/10.1016/j.proghi.2016.05.001>
- Sampathkumar, C., Wu, Y.-J., Vadhvani, M., Trimbuch, T., Eickholt, B., & Rosenmund, C. (2016). Loss of MeCP2 disrupts cell autonomous and autocrine BDNF signaling in mouse glutamatergic neurons. *eLife*, 5, e19374. <https://doi.org/10.7554/eLife.19374>
- Schaefer, A. W., Kamei, Y., Kamiguchi, H., Wong, E. V., Rapoport, I., Kirchhausen, T., Beach, C. M., Landreth, G., Lemmon, S. K., & Lemmon, V. (2002). L1 endocytosis is controlled by a phosphorylation-dephosphorylation cycle stimulated by outside-in signaling by L1. *The Journal of Cell Biology*, 157(7), 1223–1232. <https://doi.org/10.1083/jcb.200203024>
- Schäfer, M. K. E., & Frotscher, M. (2012). Role of L1CAM for axon sprouting and branching. *Cell and Tissue Research*, 349(1), 39–48. <https://doi.org/10.1007/s00441-012-1345-4>
- Schäfer, M. K. E., Schmitz, B., & Diestel, S. (2010). L1CAM ubiquitination facilitates its lysosomal degradation. *FEBS Letters*, 584(21), 4475–4480. <https://doi.org/10.1016/j.febslet.2010.10.011>
- Schmahmann, J. D. (2019). The cerebellum and cognition. *Neuroscience Letters*, 688, 62–75. <https://doi.org/10.1016/j.neulet.2018.07.005>
- Shahbazian, M. D. (2002). Insight into Rett syndrome: MeCP2 levels display tissue- and cell-specific differences and correlate with neuronal maturation. *Human Molecular Genetics*, 11(2), 115–124. <https://doi.org/10.1093/hmg/11.2.115>
- Sharma, K., Singh, J., Pillai, P. P., & Frost, E. E. (2015). Involvement of MeCP2 in Regulation of Myelin-Related Gene Expression in Cultured Rat Oligodendrocytes. *Journal of Molecular Neuroscience*, 57(2), 176–184. <https://doi.org/10.1007/s12031-015-0597-3>
- Shav-Tal, Y., & Zipori, D. (2002). PSF and p54(nrb)/NonO--multi-functional nuclear proteins. *FEBS Letters*, 531(2), 109–114. [https://doi.org/10.1016/s0014-5793\(02\)03447-6](https://doi.org/10.1016/s0014-5793(02)03447-6)
- Shulyakova, N., Andrezza, A. C., Mills, L. R., & Eubanks, J. H. (2017). Mitochondrial Dysfunction in the Pathogenesis of Rett Syndrome: Implications for Mitochondria-Targeted Therapies. *Frontiers in Cellular Neuroscience*, 11. <https://doi.org/10.3389/fncel.2017.00058>
- Skene, P. J., Illingworth, R. S., Webb, S., Kerr, A. R. W., James, K. D., Turner, D. J., Andrews, R., & Bird, A. P. (2010). Neuronal MeCP2 Is Expressed at Near Histone-Octamer Levels and Globally Alters the Chromatin State. *Molecular Cell*, 37(4), 457–468. <https://doi.org/10.1016/j.molcel.2010.01.030>
- Smrt, R. D., Eaves-Egenes, J., Barkho, B. Z., Santistevan, N. J., Zhao, C., Aimone, J. B., Gage, F. H., & Zhao, X. (2007). Mecp2 deficiency leads to delayed maturation and altered gene expression in hippocampal neurons. *Neurobiology of Disease*, 27(1), 77–89. <https://doi.org/10.1016/j.nbd.2007.04.005>
- Stefanelli, G., Gandaglia, A., Costa, M., Cheema, M. S., Di Marino, D., Barbiero, I., Kilstrup-Nielsen, C., Ausió, J., & Landsberger, N. (2016). Brain phosphorylation of MeCP2 at serine 164 is developmentally regulated and globally alters its chromatin association. *Scientific Reports*, 6(1), 28295. <https://doi.org/10.1038/srep28295>
- Sury, M. D., McShane, E., Hernandez-Miranda, L. R., Birchmeier, C., & Selbach, M. (2015). Quantitative Proteomics Reveals Dynamic Interaction of c-Jun N-terminal Kinase

- (JNK) with RNA Transport Granule Proteins Splicing Factor Proline- and Glutamine-rich (Sfpq) and Non-POU Domain-containing Octamer-binding Protein (Nono) during Neuronal Differentiation. *Molecular & Cellular Proteomics*, 14(1), 50–65. <https://doi.org/10.1074/mcp.M114.039370>
- Taneja, P., Ogier, M., Brooks-Harris, G., Schmid, D. A., Katz, D. M., & Nelson, S. B. (2009). Pathophysiology of Locus Ceruleus Neurons in a Mouse Model of Rett Syndrome. *Journal of Neuroscience*, 29(39), 12187–12195. <https://doi.org/10.1523/JNEUROSCI.3156-09.2009>
- Tapanes-Castillo, A., Weaver, E. J., Smith, R. P., Kamei, Y., Caspary, T., Hamilton-Nelson, K. L., Slifer, S. H., Martin, E. R., Bixby, J. L., & Lemmon, V. P. (2010). A modifier locus on chromosome 5 contributes to L1 cell adhesion molecule X-linked hydrocephalus in mice. *Neurogenetics*, 11(1), 53–71. <https://doi.org/10.1007/s10048-009-0203-3>
- Taxman, D. J., Moore, C. B., Guthrie, E. H., & Huang, M. T.-H. (2010). Short Hairpin RNA (shRNA): Design, Delivery, and Assessment of Gene Knockdown. In M. Sioud (Ed.), *RNA Therapeutics* (Vol. 629, pp. 139–156). Humana Press. https://doi.org/10.1007/978-1-60761-657-3_10
- The Human Protein Atlas: WWW.PROTEINATLAS.ORG*. (2020, February). The Human Protein Atlas. WWW.PROTEINATLAS.ORG
- Thiel, G., Ekici, M., & Rössler, O. G. (2015). RE-1 silencing transcription factor (REST): A regulator of neuronal development and neuronal/endocrine function. *Cell and Tissue Research*, 359(1), 99–109. <https://doi.org/10.1007/s00441-014-1963-0>
- Thiru, A., Nietlispach, D., Mott, H. R., Okuwaki, M., Lyon, D., Nielsen, P. R., Hirshberg, M., Verreault, A., Murzina, N. V., & Laue, E. D. (2004). Structural basis of HP1/PXVXL motif peptide interactions and HP1 localisation to heterochromatin. *The EMBO Journal*, 23(3), 489–499. <https://doi.org/10.1038/sj.emboj.7600088>
- Thomas-Jinu, S., Gordon, P. M., Fielding, T., Taylor, R., Smith, B. N., Snowden, V., Blanc, E., Vance, C., Topp, S., Wong, C.-H., Bielen, H., Williams, K. L., McCann, E. P., Nicholson, G. A., Pan-Vazquez, A., Fox, A. H., Bond, C. S., Talbot, W. S., Blair, I. P., ... Houart, C. (2017). Non-nuclear Pool of Splicing Factor SFPQ Regulates Axonal Transcripts Required for Normal Motor Development. *Neuron*, 94(2), 322-336.e5. <https://doi.org/10.1016/j.neuron.2017.03.026>
- Tropea, D., Giacometti, E., Wilson, N. R., Beard, C., McCurry, C., Fu, D. D., Flannery, R., Jaenisch, R., & Sur, M. (2009). Partial reversal of Rett Syndrome-like symptoms in MeCP2 mutant mice. *Proceedings of the National Academy of Sciences*, 106(6), 2029–2034. <https://doi.org/10.1073/pnas.0812394106>
- Tudor, M., Akbarian, S., Chen, R. Z., & Jaenisch, R. (2002). Transcriptional profiling of a mouse model for Rett syndrome reveals subtle transcriptional changes in the brain. *PNAS*, 99(24), 6.
- Tumaneng, K., Russell, R. C., & Guan, K.-L. (2012). Organ size control by Hippo and TOR pathways. *Current Biology: CB*, 22(9), R368-379. <https://doi.org/10.1016/j.cub.2012.03.003>
- Vora, P., Mina, R., Namaka, M., & Frost, E. E. (2010). A novel transcriptional regulator of myelin gene expression: Implications for neurodevelopmental disorders. *NeuroReport*, 21(14), 917–921. <https://doi.org/10.1097/WNR.0b013e32833da500>
- Wachowiak, R., Fiegel, H. C., Kaifi, J. T., Quaas, A., Krickhahn, A., Schurr, P. G., Erttmann, R., Schachner, M., Kluth, D., Sauter, G., & Izbicki, J. R. (2007). L1 Is Associated With Favorable Outcome in Neuroblastomas in Contrast to Adult Tumors. *Annals of Surgical Oncology*, 14(12), 3575–3580. <https://doi.org/10.1245/s10434-007-9608-0>
- Wai Wong, C., Dye, D. E., & Coombe, D. R. (2012). The Role of Immunoglobulin Superfamily Cell Adhesion Molecules in Cancer Metastasis. *International Journal of Cell Biology*, 2012, 1–9. <https://doi.org/10.1155/2012/340296>
- Wang, C., Wang, C.-M., Clark, K. R., & Sferra, T. J. (2003). Recombinant AAV serotype 1 transduction efficiency and tropism in the murine brain. *Gene Therapy*, 10(17), 1528–1534. <https://doi.org/10.1038/sj.gt.3302011>

- Wang, I.-T. J., Reyes, A.-R. S., & Zhou, Z. (2013). Neuronal morphology in MeCP2 mouse models is intrinsically variable and depends on age, cell type, and Mecp2 mutation. *Neurobiology of Disease*, *58*, 3–12. <https://doi.org/10.1016/j.nbd.2013.04.020>
- Wei, C. H., & Ryu, S. E. (2012). Homophilic interaction of the L1 family of cell adhesion molecules. *Experimental & Molecular Medicine*, *44*(7), 413. <https://doi.org/10.3858/emm.2012.44.7.050>
- Wilfinger, W. W., Mackey, K., & Chomczynski, P. (1997). Effect of pH and Ionic Strength on the Spectrophotometric Assessment of Nucleic Acid Purity. *BioTechniques*, *22*(3), 474–481. <https://doi.org/10.2144/97223st01>
- Wolters, G. (2009). *Untersuchungen neuer Funktionen der intrazellulären Domäne des Zelladhäsionsmoleküls L1 im Gehirn von Mus musculus (Linnaeus, 1758)*. University of Hamburg.
- Won, Y., Choi, H., Kim, I. S., & Mun, J. Y. (2017). Structural Study on Apoptosis of Chronic Eosinophilic Leukemia Cells by Interaction of S100A8 with Splicing Factor, Proline and Glutamine-Rich. *Applied Microscopy*, *47*(4), 233–237. <https://doi.org/10.9729/AM.2017.47.4.233>
- Yamasaki, M., Thompson, P., & Lemmon, V. (1997). CRASH Syndrome: Mutations in L1CAM Correlate with Severity of the Disease. *Neuropediatrics*, *28*(03), 175–178. <https://doi.org/10.1055/s-2007-973696>
- Yang, Y., Kucukkal, T. G., Li, J., Alexov, E., & Cao, W. (2016). Binding Analysis of Methyl-CpG Binding Domain of MeCP2 and Rett Syndrome Mutations. *ACS Chemical Biology*, *11*(10), 2706–2715. <https://doi.org/10.1021/acscchembio.6b00450>
- Yoo, M., Carromeu, C., Kwon, O., Muotri, A., & Schachner, M. (2017). The L1 adhesion molecule normalizes neuritogenesis in Rett syndrome-derived neural precursor cells. *Biochemical and Biophysical Research Communications*, *494*(3–4), 504–510. <https://doi.org/10.1016/j.bbrc.2017.10.073>
- Young, J. I., Hong, E. P., Castle, J. C., Crespo-Barreto, J., Bowman, A. B., Rose, M. F., Kang, D., Richman, R., Johnson, J. M., Berget, S., & Zoghbi, H. Y. (2005). Regulation of RNA splicing by the methylation-dependent transcriptional repressor methyl-CpG binding protein 2. *Proceedings of the National Academy of Sciences of the United States of America*, *102*(49), 17551–17558. <https://doi.org/10.1073/pnas.0507856102>
- Zachariah, R. M., & Rastegar, M. (2012). Linking Epigenetics to Human Disease and Rett Syndrome: The Emerging Novel and Challenging Concepts in MeCP2 Research. *Neural Plasticity*, *2012*, 1–10. <https://doi.org/10.1155/2012/415825>
- Zhang, W., Feng, G., Wang, L., Teng, F., Wang, L., Li, W., Zhang, Y., & Zhou, Q. (2018). MeCP2 deficiency promotes cell reprogramming by stimulating IGF1/AKT/mTOR signaling and activating ribosomal protein-mediated cell cycle gene translation. *Journal of Molecular Cell Biology*, *10*(6), 515–526. <https://doi.org/10.1093/jmcb/mjy018>
- Zhou, Z., Hong, E. J., Cohen, S., Zhao, W.-N., Ho, H.-Y. H., Schmidt, L., Chen, W. G., Lin, Y., Savner, E., Griffith, E. C., Hu, L., Steen, J. A. J., Weitz, C. J., & Greenberg, M. E. (2006). Brain-specific phosphorylation of MeCP2 regulates activity-dependent Bdnf transcription, dendritic growth, and spine maturation. *Neuron*, *52*(2), 255–269. <https://doi.org/10.1016/j.neuron.2006.09.037>

8. ACKNOWLEDGEMENTS

I want to first of all, sincerely thank Prof. Dr. Melitta Schachner, for the great opportunity she gave me to do my PhD in her research group, for supervising my work with interest, and for her advices in how to present and discuss findings.

I would also like to extend my deepest gratitude to Prof. Dr. Bartsch, Prof. Dr. Kneussel, Prof. Dr. Kuhl, for agreeing to be my Thesis Committee, and for giving me nice ideas I could apply in my project. Special thanks to Prof. Dr. Bartsch for his help in providing neural stem cells I could use in my experiments, and I am also thankful to Sabine Helbing for the technical assistance with these cells.

I want to thank Dr. Ralf Kleene for his support, for sharing his knowledge of L1 and its functions, for his willingness to help the PhD students in publishing results, and for correcting my thesis.

I am extremely grateful to Dr. Gabriele Loers for all the numerous occasions she gave me advice when I needed it. I also thank her for her availability and active willingness to help and solve problems, and for correcting my thesis. She has given me great support.

I am also very grateful to Ute Bork for the technical assistance, for her nice personality, and importantly for saving me when the battery of my car was empty.

I would like to thank all my fellow PhD students, who created a great environment to work and enjoy doing it. I am grateful I could be a part of such a great team.

I thank Dr. Sabine Hoffmeister-Ullerich, for organizing the amazing Molecular Biology Graduate Program, which gave me great opportunities to network and learn. I also thank her for her advice and help.

Special thanks to Johanna Kostka, Prof. Dr. Lutz, and Dr. Mary Muhia, for their assistance in my experiments and their advice.

In addition, I am grateful to Dr. Guido Hermey for his help with microscopy, and for letting me use his nice microscope.

Finally, I would like to thank my wonderful parents, brother, and boyfriend. I cannot thank you enough for all the support, love, and encouragement you have been giving me.

9. CURRICULUM VITAE

“Lebenslauf wurde aus datenschutzrechtlichen Gründen entfernt”.

10. APPENDIX: VECTOR MAPS

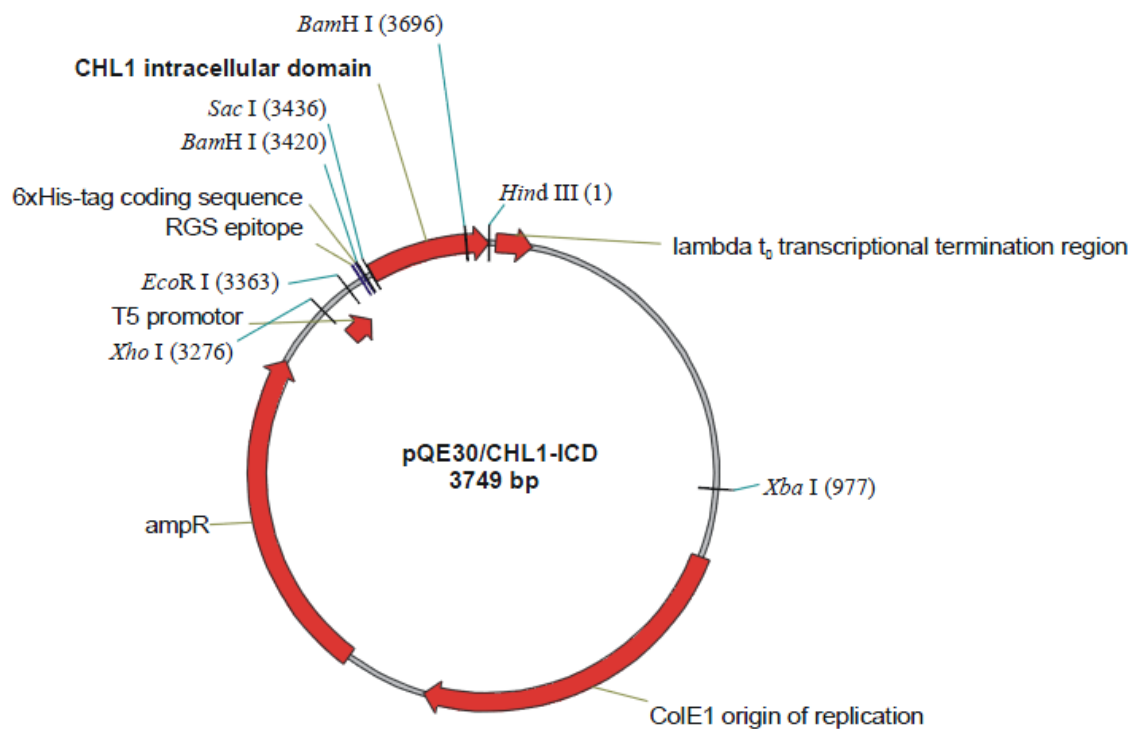


Figure. 10.1. pQE-30 carrying CHL1-ICD (Qiagen).

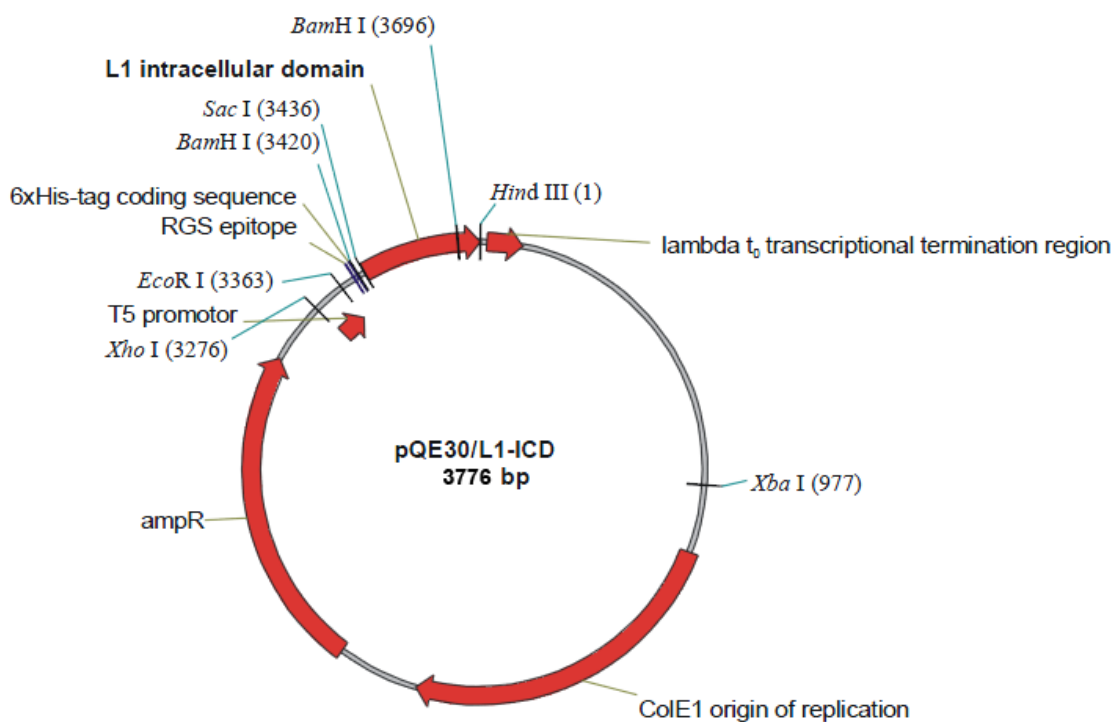


Figure. 10. 2. pQE-30 carrying L1-ICD (Qiagen).

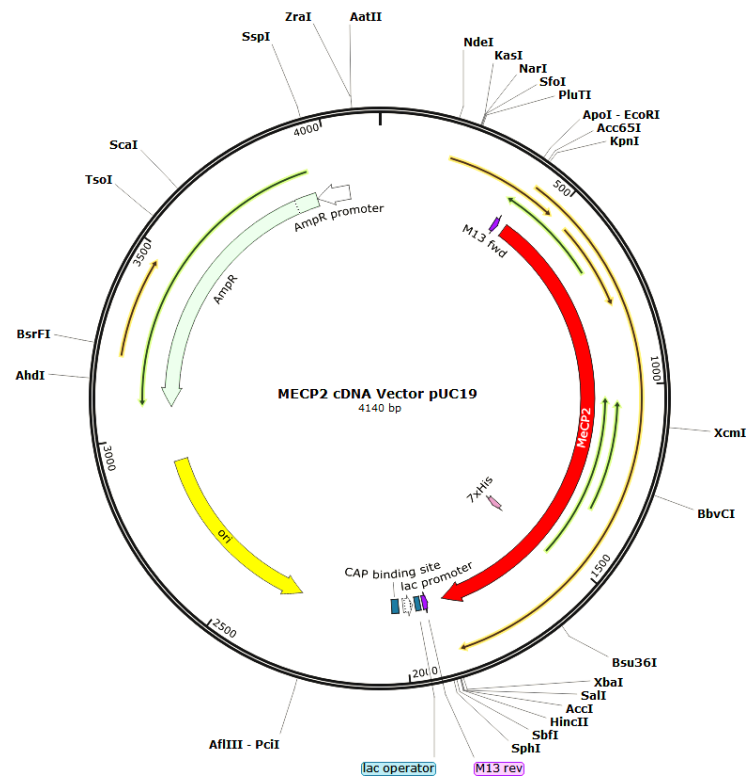


Figure. 10. 3. MECP2 cDNA ORF Clone in Cloning Vector pUC19 Vector (SinoBiological).

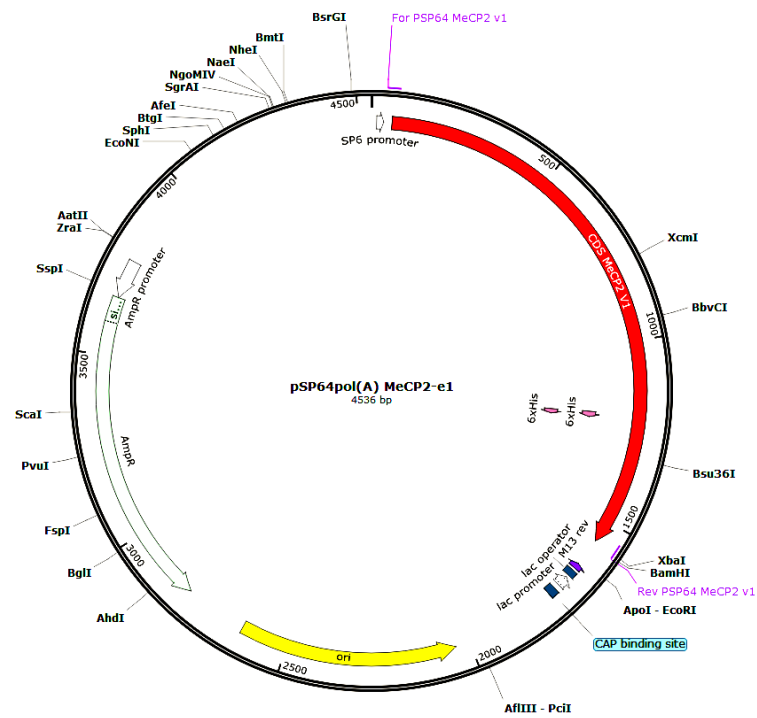


Figure. 10.4 pSP64 Poly(A) Vector carrying MeCP2- α (Promega).

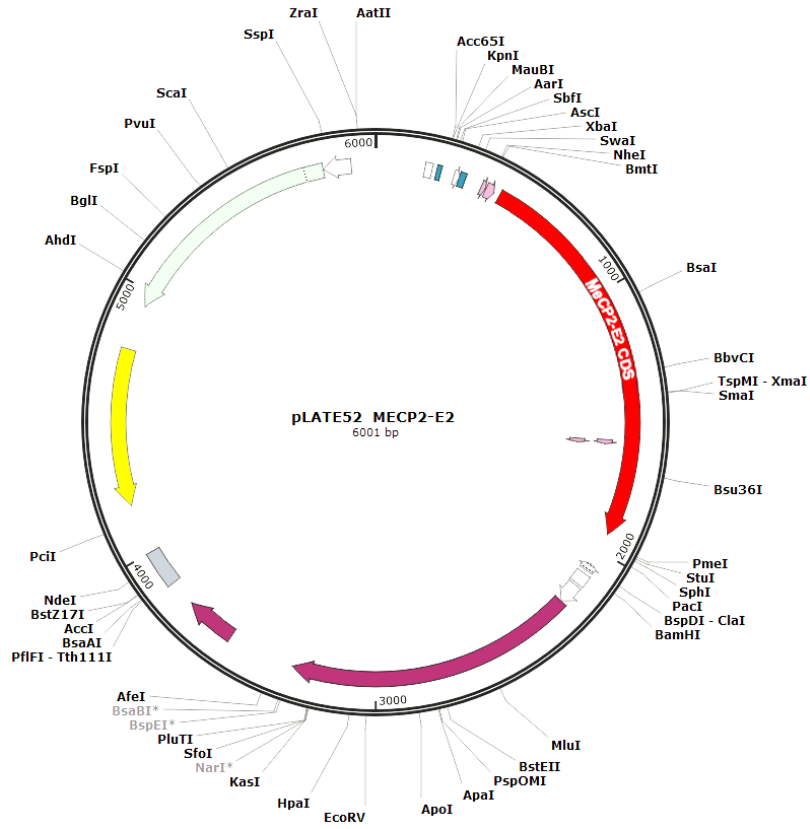


Figure. 10.5. SP64 Poly(A) Vector carrying MeCP2-- β (Promega).

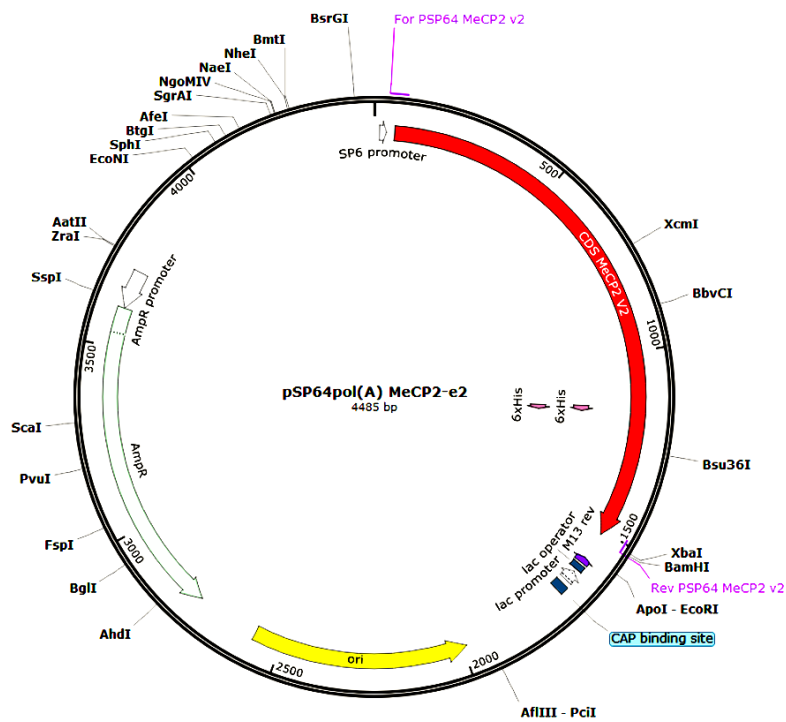


Figure. 10.6. pLATE52 carrying MeCP2- β (Thermo-Fisher Scientific).

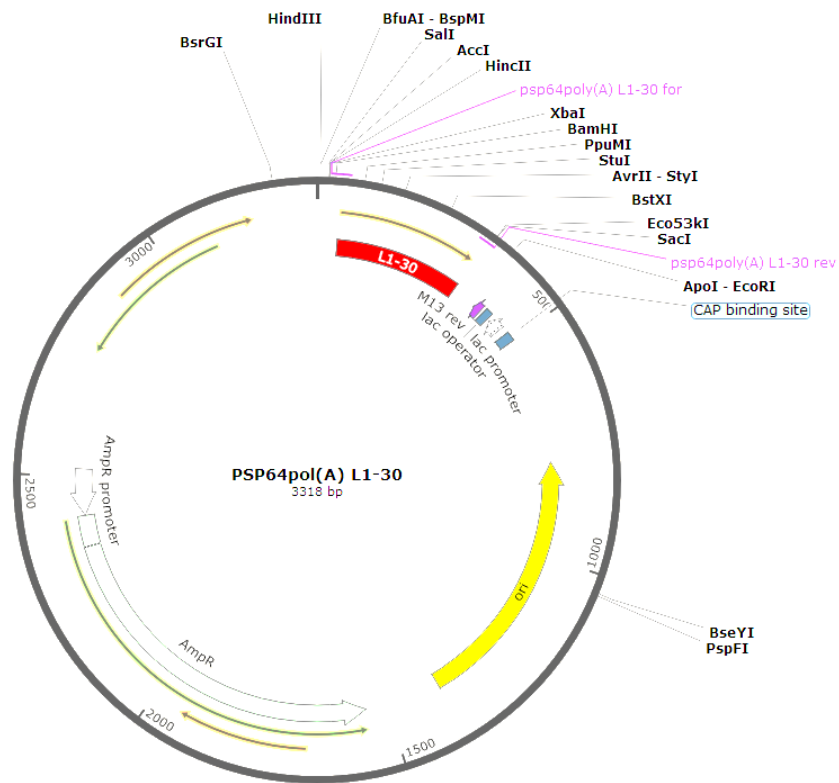


Figure. 10. 7. SP64 Poly(A) Vector carrying L1-30 (Promega).

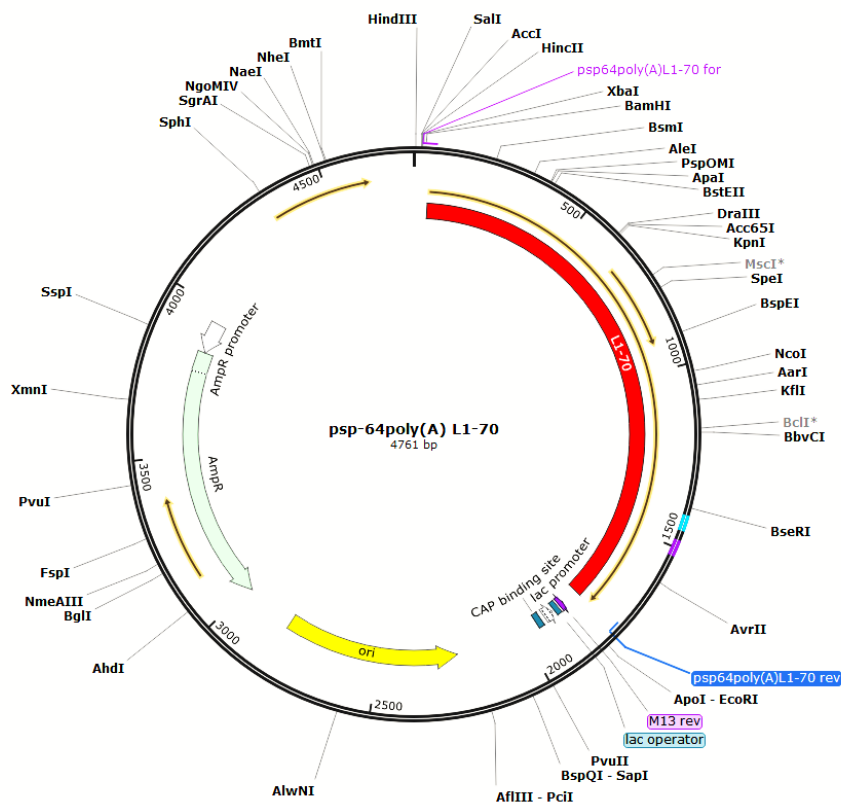


Figure. 10. 8. pSP64 Poly(A) Vector carrying L1-70 (Promega).

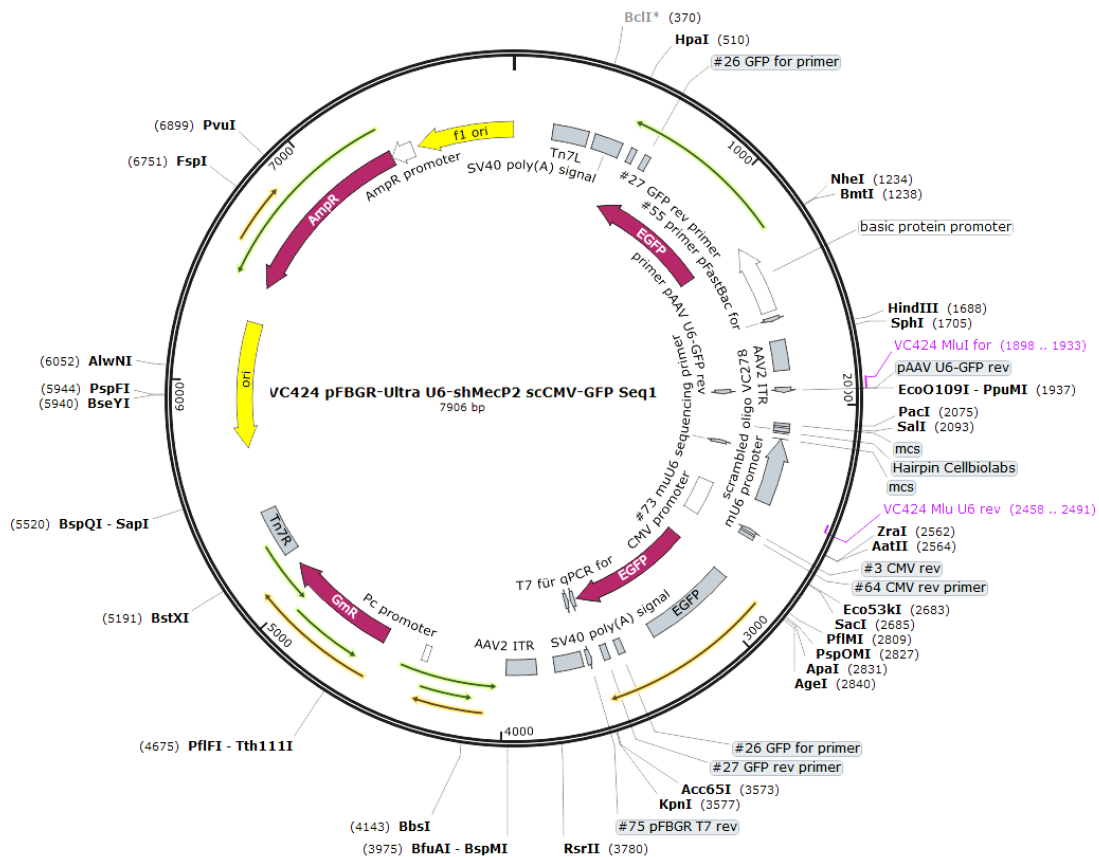


Figure. 10. 9. Viral vector AAV1-scCMV-GFP U6-shMecP2.

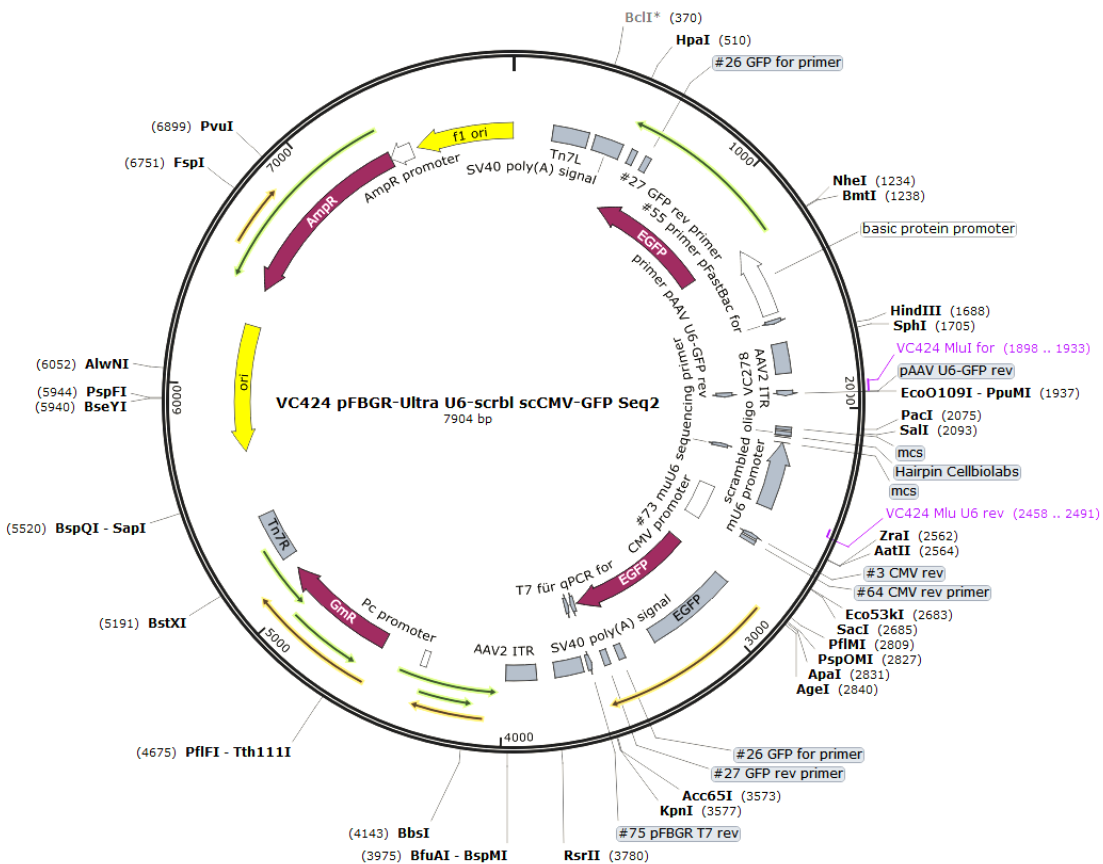


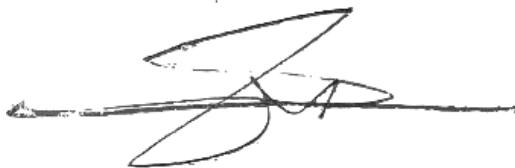
Figure. 10. 10. AAV1-scCMV-GFP U6-scrbl.

11. EIDESSTATTLICHE ERKLÄRUNG

Ich versichere ausdrücklich, dass ich die Arbeit selbständig und ohne fremde Hilfe verfasst, andere als die von mir angegebenen Quellen und Hilfsmittel nicht benutzt und die aus den benutzten Werken wörtlich oder inhaltlich entnommenen Stellen einzeln nach Ausgabe (Auflage und Jahr des Erscheinens), Band und Seite des benutzten Werkes kenntlich gemacht habe.

Ferner versichere ich, dass ich die Dissertation bisher nicht einem Fachvertreter an einer anderen Hochschule zur Überprüfung vorgelegt oder mich anderweitig um Zulassung zur Promotion beworben habe.

Ich erkläre mich einverstanden, dass meine Dissertation vom Dekanat der Medizinischen Fakultät mit einer gängigen Software zur Erkennung von Plagiaten überprüft werden kann.

A handwritten signature in black ink, consisting of several overlapping loops and a long horizontal stroke at the bottom.

Unterschrift:

